UNIVERSITY OF CALIFORNIA, SAN DIEGO

Transport and Transients in Buoyancy Driven Flows

A dissertation submitted in partial satisfaction of the requirements for the degree Doctor of Philosophy

in

Engineering Sciences (Mechanical Engineering)

by

Diogo Tomás Bolster

Committee in charge:

Professor Paul F. Linden, Chair
Professor Steven Buckley
Professor Chantal Darquenne
Professor Kim Prather
Professor Daniel Tartakovsky

2007

.

The dissertation of Diogo Tomás Bolster is approved, and it is acceptable in quality and form for publication on microfilm:

Chair

University of California, San Diego

2007

Dedicated to my wife Annie, my parents, Tom and Fatimá and my brothers Ferdia and André

I am no longer young enough to know everything.

It is a very sad thing that nowadays there is so little useless information.

Oscar Wilde

If the facts don't fit the theory, change the facts.

As far as the laws of mathematics refer to reality, they are not certain; and as far as they are certain, they do not refer to reality.

Albert Einstein

Be careful about reading health books. You may die of a misprint.

Clothes make the man. Naked people have little or no influence on society.

Mark Twain

TABLE OF CONTENTS

LIST OF FIGURES

LIST OF TABLES

ACKNOWLEDGMENTS

Many people helped me during my time at the U C San Diego and while words cannot sufficiently express my gratitude I would like to note my thanks to them here. First and foremost I would like to thank my wife Annie, who has been ridiculously patient and understanding over the last four years. Thanks for listening, even when you didn't understand and thanks for understanding, even when you probably shouldn't have....

Along those lines I would also like to thank my parents and my brothers for their patience and support all those years before I came to San Diego. Without them I would have never made it here in the first place.

I would like to give a big thank you to my academic advisor Paul Linden for his patience and support over the last three years. Without his insight, both into my research and my personal development, I do not believe I could have achieved all that I have. I would also like to give a special thanks to Daniel Tartakovsky, whose many discussions either during a bench press at the gym or over a coffee in his office, both inspired and guided me into areas I previously knew nothing about. Thanks also to Colm Caulfield, who was my advisor when I first started here at UCSD. Under his supervision is where I first learned many of the methods that I used during my PhD.

Thanks to my doctoral committee members for taking time out of their busy schedules and assisting me. I also owe much gratitude to many other staff members at UCSD including Stefan Lewelyn Smith, Costas Pozrikidis, Sutanu Sarkar, Jim Rotman and Keiko Nomura, who patiently listened and helped me with my many and never ending questions. Thanks also to all the professors with whom I took classes during my first year, even if you did occasionally get very close to breaking me.

Finally a big shout out to all my fellow students with whom I have shared this big adventure. You know who you are!

Financial support was generously provided by Joan and Irwin Jacobs, the UC Energy Institute and the California Energy Commission.

Chapter 4, in part, has been accepted for publication in the *Journal of Fluid Mechanics*, ('Contaminants in Ventilated Filling Boxes', 2007, D Bolster & PF Linden (Cambridge University Press)). Chapter 5, in part, will be submitted for publication to *Atmospheric Environment*, 2007, D Bolster & PF Linden (Elsevier Science). Chapter 6, in part, has been submitted for publication to *Energy & Buildings*, 2007, D Bolster & PF Linden (Elsevier Science). Chapter 7, in part, has been submitted for publication to *Building Services Engineering Research and Technology*, 2007, D Bolster & CP Caulfield (CIBSE). Chapter 8, in part, has been accepted for publication in *Advances in Water Resources*, ('Analytical Models of Contaminant Transport in Coastal Aquifers' 2007, D Bolster, DM Tartakovsky & M Dentz (Elsevier Science)). I was both the primary investigator and lead author of each of the papers described above.

VITA

1979	Born Dublin, Ireland
2002	BE UC Dublin, Ireland (Mechanical Engineering)
2005	M.Sc., UC San Diego (Mechanical Engineering)
2003–2007	Research Assistant, U. California, San Diego
2004-2005	Teaching Assistant, U. California, San Diego
2007	Ph.D., U. California, San Diego (Eng. Sciences)

SELECTED PUBLICATIONS

D Bolster and P. F. Linden, 2007: Contaminants in Ventilated Filling Boxes. *J. Fluid Mech.*, in-press.

D Bolster, D.M. Tartakovsky and M. Dentz, 2007: Analytical Models of Contaminant Transport in Coastal Aquifers. *Adv. Water Res.*, in-press.

FIELDS OF STUDY

Major Field: Fluid mechanics

Natural and low-energy building ventilation
Profs. Paul F. Linden and Colm P. Caulfield (U. Cambridge)

Transport in Porous Media
Profs. Paul F. Linden and Daniel Tartakovsky

ABSTRACT OF THE DISSERTATION

Transport and Transients in
Buoyancy Driven Flows

by

Diogo Tomás Bolster
Doctor of Philosophy in Engineering Sciences (Mechanical Engineering)
University of California, San Diego, 2007
Professor Paul F. Linden, Chair

Natural and forced displacement ventilation offer promising strategies for cooling buildings in an energy efficient manner. However, there is the issue of whether or not they can provide adequate indoor air quality. Here, we investigate this in two studies - one for passive and the other for particulate contaminants. The complex internal stratification of buoyancy, typical of displacement systems, affects the transport of contaminants in a non trivial manner. While on average traditional and modern low energy ventilation systems are comparable regarding efficiency of contaminant removal, we show that the detailed vertical distribution of contaminants tells quite a different story regarding personal exposure.

Further, most previous studies on natural displacement ventilation focus only on steady states, while most true buildings have continuously changing heat loads. Here, two projects on transients in natural displacement ventilation are presented. The first studies the influence of sudden changes in heat loads, while the second focuses on heat sources that vary in a periodic fashion. Many benefits of natural ventilation are observed, including that it is self controlling in a very favorable manner and that a well designed space is capable of handling even very large changes in heat load.

This thesis presents a separate investigation of contaminants in coastal aquifers. Due to buoyancy effects, saltwater from the ocean often intrudes into aquifers, which gives rise to a nontrivial flow pattern that is very different from that typical of inland aquifers. Using a simple mathematical model, we investigate the influence of these flow patterns on the transport of conservative contaminants in a coastal aquifer. We find that depending on the specific characteristics of the aquifer that the saltwater intrusion can play a significant role on transport. It forces contaminant towards the upper seaward boundary, thus causing elevated contaminant discharge into the surf zone at beach areas.

1

Thesis outline and scope

Unlike the work presented in most theses, due to certain unforeseen events during my studies at UCSD and my occasionally multitasking/distracted personality I have been lucky enough to work on a somewhat wide set of research projects, which are described in detail in this document. Fortunately, all of my projects can be tied together by the fact that they deal with transients in buoyancy driven flows and the transport of contaminants in such flows, whether that flow is in a building or in the subsurface. This thesis can roughly be broken into three sections as detailed in the list below:

1. Chapters 4-5 – Contaminants and Low Energy Ventilation Systems
2. Chapters 6-7 – Transients in Natural Ventilation due to Changes in Heat Loads
3. Chapter 8 –Transport of Contaminants in Coastal Groundwater Systems

Chapter 4 deals with the transport of passive contaminants through a space that is ventilated by means of a low energy system such as natural or displacement ventilation. A simple building geometry is considered and modelled using the principles developed by Linden et al. (1990). Theoretical and numerical

models are developed and compared with analogue laboratory experiments for validation. The models are then used to compare these low energy ventilation systems to traditional ventilation systems in terms of contaminant removal efficiency.

Chapter 5 is a direct extension of chapter 4 in that the same problem is considered with the exception that particulate rather than passive contaminants are considered. Particulate contaminants display very different and interesting dynamical behaviour to gravitational settling. The theoretical models for passive contaminants are extended to include this behaviour. Additionally, in place of small scale, full scale laboratory experiments are conducted. Again, the contaminant removal efficiency of the low energy and traditional ventilation systems are compared.

Chapter 6 studies the transient flow between steady states in a naturally ventilated space associated with a sudden change in internal heat load. Two numerical models are developed and compared to small scale laboratory experiments. The results of the theoretical models are used to identify some of the advantages and weaknesses associated with natural ventilation and in particular identify its elegant self controlling mechanism.

Chapter 7 is an extension of the work in chapter 6. Instead of considering heat sources which change suddenly in time, we look at heat sources that change periodically so as to reflect certain true life sources. Once again, numerical models are compared to small scale experiments for validation purposes. We identify several characteristic system flow rates and identify parameter regimes over which each of these flow rates is the appropriate one to choose.

Chapter 8 looks at the flow of groundwater in coastal aquifer systems. Using the simple, yet elegant Henry model formulation for coastal aquifer flows, we use asymptotic perturbation techniques to study the transport of contaminants in such coastal aquifers. So as to reflect the nature of true aquifers, we consider two different flow regimes, one where inertial effects are dominant and the other where dispersive effects are most important. We consider two pollution transport

Table 1.1: Scientific contribution arising from the present thesis.

Chapter	Journal/Conference proceeding	Status	Co-author
4	*Journal of Fluid Mechanics*	Accepted	P. F. Linden
5	*Atmospheric Environment*	To be Submitted	P. F. Linden
6	*Energy and Buildings*	Submitted	P. F. Linden A. Maillard
7	*BSERT Journal*	Submitted	C. P. Caulfield
8	*Advances in Water Resources*	In Press	D. M. Tartakovsky M. Dentz

problems. The first, a natural attenuation scenario, describes the flushing of a contaminant from a coastal aquifer by clean fresh water, while the second, a contaminant spill scenario, considers an isolated point source. The results of these theoretical models identify key dynamical differences between the transport of contaminants in inland compared to coastal aquifers and may assist in explaining certain unexplained coastal water contamination scenarios.

Most components of the thesis have been submitted for publication either as journal articles or as extended abstracts in a conference proceedings. Details are provided in Table 1.1. Each of chapters 4-8 are reprints of the documents submitted to journals with minor revisions so as to avoid excessive repetition.

2

Introduction and Motivation of Research Projects

In this thesis I present three general areas of research : (a) Natural Ventilation and Transients, (b) Contaminant Transport in Low Energy Ventilation Systems and (c) Contaminant Transport in Coastal Groundwater Systems. This chapter briefly introduces the problems and outlines the motivation for studying them.

2.1 Natural ventilation - Buildings and energy consumption

Santamouris (2005) states that for every 1% increase in population there is a 2% rise in energy consumption. The UN estimates that each year the world's population increases by 75 million people. The world already consumes vast amounts of energy, mostly produced from carbon based fuels (see figure 2.1) and of this energy a very large fraction is consumed by the developed world, with the United States alone using 25%. Few people would argue with Santamouris' observation that "energy consumption defines the quality of urban life...". The economies of developing countries such as China and India, which have enormous

populations, are growing rapidly and with this growth there is an increased demand for luxuries and an associated rise in demand for energy.

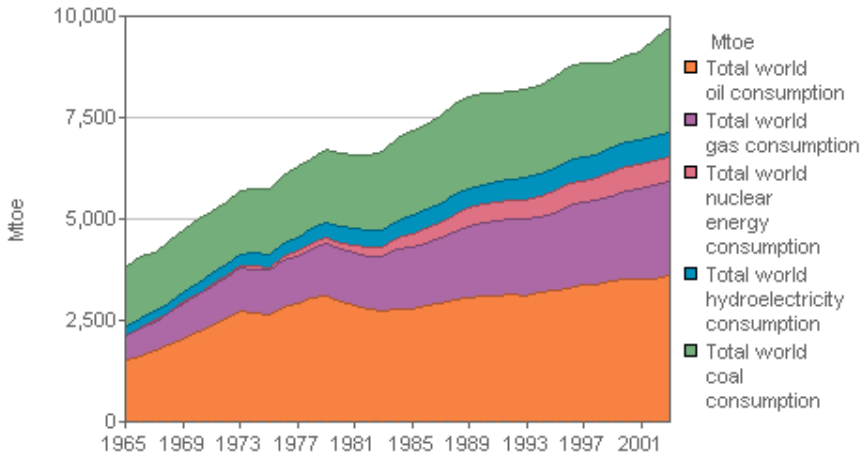

Figure 2.1: Global Energy Consumption by Fuel Type (www.eia.doe.gov)

Interestingly, while most of the media focus is on making cars more fuel efficient and reducing energy consumption by factories, the largest consumer of energy is actually buildings, which accounts for 40% of the global energy consumption and close to 50% of the world's anthropogenic CO_2 emissions (see figure 2.3). So whether your motivation is to reduce energy consumption to keep some money in your pockets, or to slow global warming by reducing CO_2 emissions, buildings are clearly an important area of focus.

In the United States, which is the world's largest consumer of energy and producer of CO_2, a significant fraction of the energy used by buildings is devoted to summer-time cooling by air conditioning systems. According to the Energy Information Administration, in 2003, close to 10% of the total annual energy consumption is devoted to this, costing an estimated $90 billion per year. It is estimated that $3.5 \times 10^9\,\mathrm{m}^2$ of commercial space are actively cooled by traditional air conditioners with an annual energy cost of approximately 250 TWh. (See Santamouris (2005))

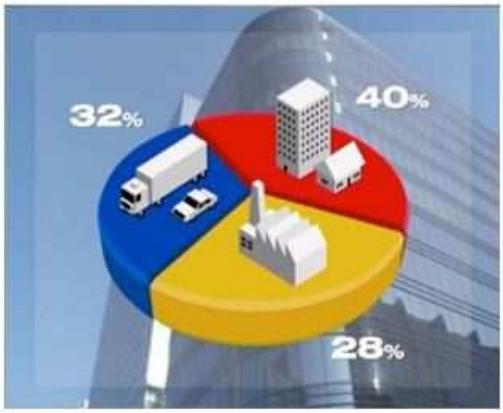

Figure 2.2: Fraction of Energy Used Per Sector - Transportation (Blue - 32%) , Industry (Yellow - 28% and Buildings (Red - 40%) (Tiempo climate newswatch - www.cru.uea.ac.uk)

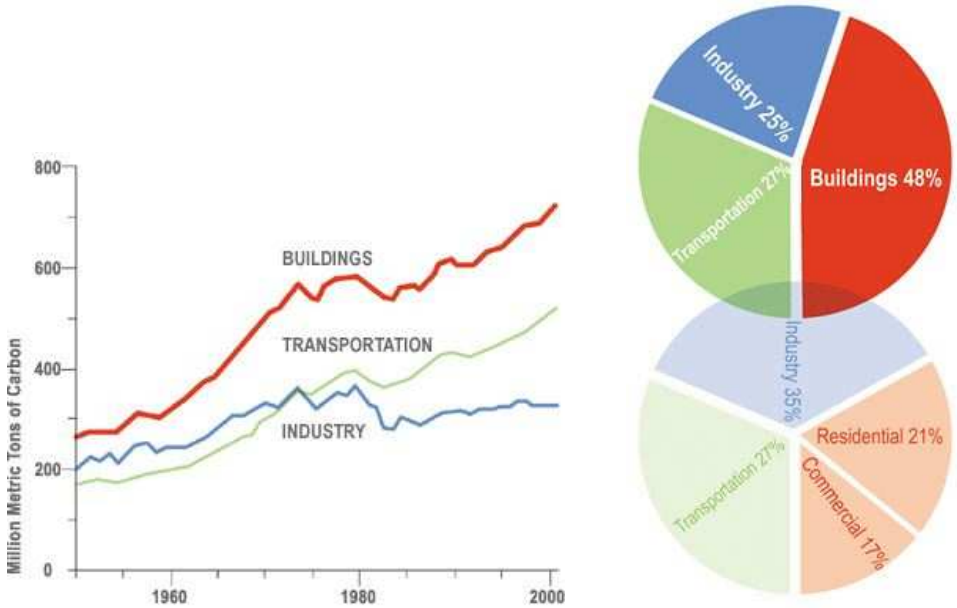

(a) (b)

Figure 2.3: (a) Quantity of Carbon Used Per Sector (b) Pie Chart of Carbon Usage Per Sector (www.architecture2030.org)

Natural ventilation aims to reduce this demand on energy and provide free cooling of buildings by exploiting natural phenomena such as stratification due to internal heat gains, wind forcing and solar radiation. Numerous methods are proposed (see Santamouris (2005) for details) and in all cases small naturally occurring pressure differences are exploited to drive a flow between the external and internal environment. In many cases across the world these schemes can provide adequate ventilation throughout most of the year and for times when they may not be adequate hybrid systems, which combine mechanical and natural cooling methods may be used.

Many low energy cooling systems, mechanical as well as natural, rely on the idea that continuously extracting the warmest air from a space will lead to the most efficient system and so exploit the natural stratification that will arise in a space with heat sources, always extracting hot air from the top of a space. The idea is to only cool the lower part of the room, where occupants are located, with a philosophy of 'Cool the occupants, not the Buildings'.

Most of the studies and theoretical models for natural ventilation to date only consider steady states, where heat sources within the ventilated space do not vary over time. This is obviously not a true reflection of the real world, where buildings experience changes in heat loads over a wide range of timescales - seasonal, diurnal, hourly and in some cases even on the order of minutes. While understanding the steady states of natural ventilation is clearly important for proper design, understanding the influence of time varying heat sources on natural ventilation is important in order to understand the true behavior of these systems. It also encourages better design methods through a deeper understanding of these systems. Consequently, chapters 6 and 7 are dedicated to this.

2.2 Contaminants in Buildings

Recent studies have shown that people spend substantial amounts of time indoors, in many cases an average of close to 90 %. As such it has become very important to understand the details of the indoor environment, in particular regarding human comfort, health, indoor air quality and energy consumption. This holds especially true considering that the United Nations Centre for Human Settlements estimates that 30% of buildings around the world are not adequately ventilated and as a result the indoor air is well below the minimum recommended health standards (Santamouris (2005)).

Hospitals, places we go to get better, are not as safe as we would like to think. Many people go in to treat one symptom and leave with some other secondary infection that they picked up while in the hospital. According to the Committee to Reduce Infection Deaths, infections contracted in hospitals are the 4th largest killer in the US. One in twenty patients contract an infection, which amounts to almost 2 million Americans a year and an estimated 103,000 of them die. While some of these infections occur due to lack of proper hygiene some will also occur due to transport of bacteria and viruses through the air and as such effective air quality strategies should be implemented to reduce this occurance of secondary infections.

Transport of smoke in buildings is another interesting and important area of study in the field of air quality control. On the smaller scale we have cigarette smoking and the controversial debate of passive smoking. If one person in a space is smoking, how much of that smoke are other people in that same space, or even adjacent spaces inhaling and how can we reduce this amount? On the larger scale we have fires in building. According to the Connecticut Medical Center website, 70% of all fire related deaths are not from burns, but rather from smoke inhalation caused by toxic gases produced as fires develop and spread. If we could design effective detection and emergency ventilation strategies, the number of fire-related

deaths could be reduced.

The recent contamination of several US buildings by letters containing anthrax has raised a large concern regarding the deliberate release of lethal toxins within a building. Other toxins, not released in malice, should also raise some concern, such as pollutants from industrial processes, outdoor pollution penetration and building material fumes (i.e. from paint, glue, etc.). This demonstrates the need to better understand the transport and fate of such toxins within buildings.

On a less morbid note, as mentioned in the previous section, energy consumption by ventilation systems must also be adequately considered. It is clearly important to develop energy efficient ventilation strategies. However, it is also important that these strategies provide an adequate, safe and uncontaminated environment for building occupants .

As discussed earlier, most low-energy ventilation systems rely on stratification in a space, extracting the hottest air so as to maximise cooling efficiency. This stratification can lead to a very different flow pattern compared to those associated with traditional mixing ventilation systems. In turn, these different flow patterns give rise to very different patterns of contaminant transport. It is widely believed that, by the same mechanism as they remove heat more efficiently, these low-energy ventilation systems also remove contaminants more effectively than traditional systems. However, this is currently only a belief and has not been extensively studied.

Additionally, when studying contaminant transport it is important to distinguish between different types of contaminants, which can very broadly be put into two categories - gaseous and particulate. Gaseous contaminants are usually considered as passive contaminants, because it is assumed that they exactly follow the main air stream movements in a space. Some of the more common gaseous contaminants that cause concern in buildings are : Carbon Monoxide (CO), Carbon Dioxide (CO_2), Nitrogen Oxides (NO_x), Ozone (O_3), SO_2 (Sulphur Dioxide), moisture, formaldahyde (HCHO), Radon gas and its progeny. Many of these

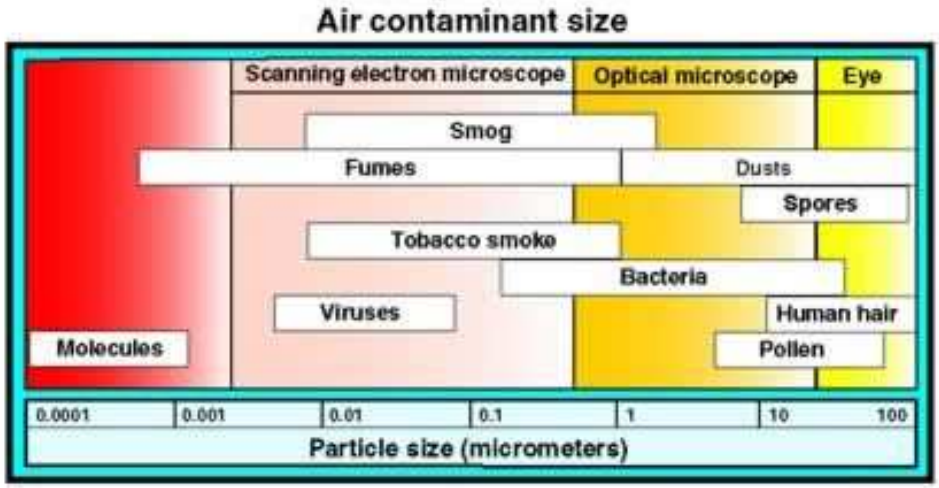

Figure 2.4: Types of Particulate Contaminants and Size Distribution

contaminants are combustion byproducts and due to the increased amount of automobiles and industrial plants there has been an increasing concern about the levels of these contaminants in the outdoor air. Evidence exists that city-dwellers can be more exposed to such pollutants indoors than outdoors (Blondeau et al. (2005)). Formaldehyde is used in many glues, paints and materials used in buildings and is released from these sources. Radon is released through the radioactive decay of naturally occurring radium-226 and subsequently decays to short lived radioactive decay products called progeny. All of the above mentioned contaminants can have adverse effects on a person's health, comfort and ability to work if their levels become too high.

Particulate contaminants tend not to be passive and do not follow the flow in a space exactly. However it is often assumed that their presence does not influence the flow. Particulate contaminants come in various sizes, shapes and types. Size is particularly important when studying particulate contaminants, because it determines their behaviour. Typically large particles only remain suspended in air for a short period whereas smaller particles can remain airborne for significant amounts of time. Also health effects that result from inhaling indoor aerosols are

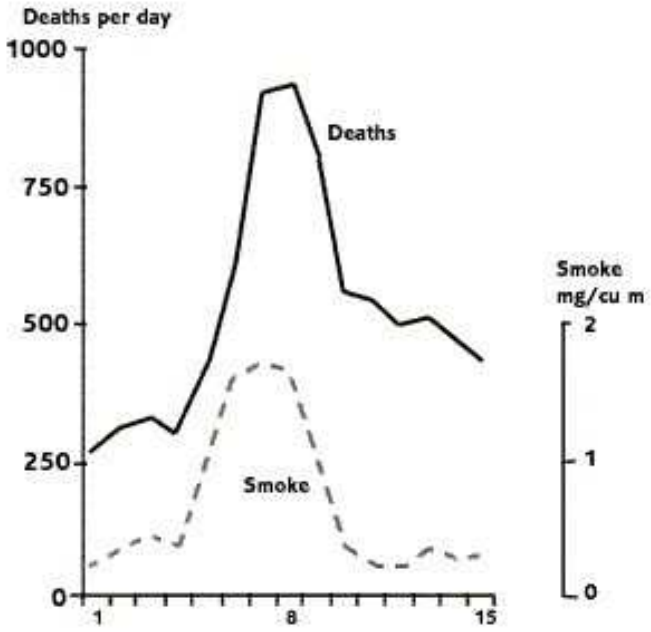

(a)

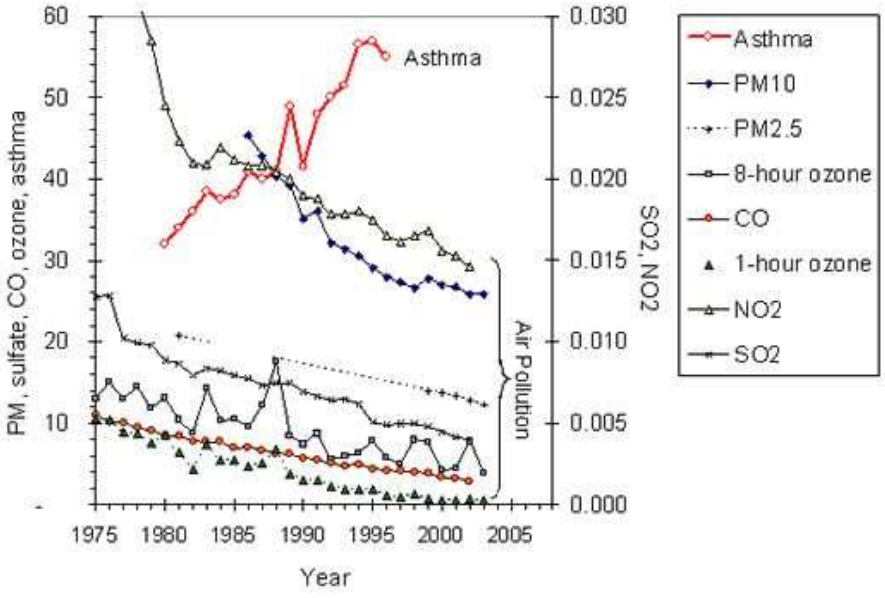

(b)

Figure 2.5: Influence of Contaminants on Health - (a) Deaths in London during the Great Smog of 1952 (b) Decrease in overall pollution towards finer particles - Increase in asthma (www.metoffice.gov.uk)

directly related to the particle diameters (Owen et al. (1992)). For example, even though pollution levels in the USA have decreased since the 1970s, respiratory diseases such as asthma are on the rise (see figure 2.5), which is believed to be a consequence of a greater production of finer particles - i.e. while the mass of pollutant particles is decreasing, the number of fine particles is increasing. It is also important to know particle size distributions for the efficient design of filters. Particulate contaminants are typically catagorized into the following groups:

(i)Bioaerosols: These aerosols contain particles of a living origin (animal or plant) and present a special hazard as allergens. Typical plant bioaerosols include pollen, spores and molds, the size of which tends to be large, causing their suspension times to be short. Animal aerosols come in the form of bacteria, viruses, hair, insect parts and dandruff, which range from small to large.

(ii)Mineral: These are non-organic aerosols that do not present the infection potential of bioaerosols, but can be still be harmful in that they might be carcinogenic or mutagenic. These particles include asbestos, carbons, clay and artificial fibers.

(iii)Combustion: These aerosols are produced by burning. Sources include cigarettes, cooking sources, heating plants, industrial plants and outdoor traffic. Most of these particles are in the respirable range and present a hazard in the form of carcinogens.

(iv)Home/Personal Care: These are mostly products such as deodorants, dusting aids and hair sprays. They tend to be produced in only small quantities of mass, but over short periods so the local concentration can be quite high. Many of the particles produced are in the breathing range.

(v) Radioactive: These aerosols are introduced again by radon when it attaches itself to other particles.

The study of particulate contaminants is more complicated than that of tracer gas contaminants. There are several effects such as deposition, tracking, resuspension and coagulation that must be accounted for.

In order to prevent damage to human health and optimize comfort conditions, both at work and at home, it is important to study and understand how both passive and particulate contaminants move within buildings. It is important to optimize current and design new ventilation strategies. It is useful to understand how these ventilation strategies work in order to design effective and efficient methods of detection of contaminants in order to detect and prevent any dangerous exposures of toxic levels to occupants in a building. In chapters 4 and 5 we consider the transport of passive and particulate contaminants in low energy ventilation systems respectively.

2.3 Contaminants in Coastal Aquifers

A large proportion of the world's population (about 70%) is located in regions close to the coast. In many of these regions the only readily accessible source of water are coastal aquifers, which due to the proximity of saline water are at great risk of salt contaminantion, making the water undrinkable and agriculturally unusable. Within the past few decades, the water quality in many of the coastal aquifers around the world (especially along the Mediterranean Sea) has rapidly degraded. Overexploitation of the groundwater basins, particularly due to agriculture and tourism, has resulted in the lowering of groundwater tables and increasing seawater intrusion into the aquifers. Many countries (such as Cyprus and Israel) have had to shut down hundreds of wells along the coastline that were used primarily for drinking water.

Facing a shortage of suitable drinking water, these countries have had either to look for alternative sources, such as imported water, or to implement costly technological solutions, such as desalination.

But as many well-publicized projects move forward to address salinity in the groundwater basin, another problem looms for residents: pollution by other contaminants, organic and inorganic. Until recently, countries have paid little at-

tention to this and other threats to the quality of the groundwater. The presence of even trace levels of certain contaminants in wastewaters is an issue of concern where such waters are reclaimed for potable and non-potable uses. The potential impacts of some of these compounds include abnormal physiological processes and reproductive impairment (e.g. endocrine disrupting chemicals), increased incidences of cancer and development of antibioticresistant bacteria. Hence, there is a need to identify and quantify the contaminants present and to understand their fate in the environment. As an example results from an E.U.-sponsored project entitled BOREMED show that boron contamination poses a potential threat to the future use of many groundwater basins along the Mediterranean for the supply of drinking and irrigation water.

While the major sources of water pollution may be urban and industrial effluent it is also a serious concern in pastoral areas where contamination by organic compounds (e.g. fertilizers and fecal matters) can adversely affect livestock water supplies.

Contaminated drinking water is a significant factor in the spread of infectious, water-related diseases. Lack of water for personal hygiene leads to the increased possibility of transmission of disease by a variety of faecal - oral routes. Both from a human and livestock point of view, reliance on polluted water supplies can lead to a high incidence of water-based diseases (bilharzia, river blindness, schistosomiasis, Guinea worm) and insect-vector, water-related diseases (trypanosomiasis, malaria, yellow fever, dengue and onchocerciasis). In considering the provision of additional water sources, therefore, their effect on the possible spread of disease must be taken into account. Groundwater is normally of high bacteriological quality since the soil usually affords the underlying aquifer a considerable degree of protection against contamination. Therefore understanding how it becomes contaminated and the fate of the contaminants is critical to maintaining clean and usable water supplies.

It is also important to point out that this is very much a global issue. It

appears to have so far received the most attention in Mediteranean (perhaps due to the increased salinity of that sea and large coastal population densities). However a simple internet search shows that awareness of this problem is rapidly increasing on all continents, from beach closures in North America due to contamination from groundwater sources, to contamination of vital water resources in Australia and Africa by coastal mining settlements, to the closing of important coastal water wells in the island nations of Eastern Asia. Chater 8 presents a theoretical investigation of contaminant transport in coastal aquifers.

3

An Introduction to the Fluid Dynamics of Low Energy Ventilation and Contaminant Transport Modelling

3.1 Abstract

Many studies have focused on developing simplified theoretical models for natural and other low energy ventilation methods (see the review by Linden (1999) for details). Typically, simple geometries with isolated heat sources are considered and the mixing dynamics are modelled using the plume theory of Morton et al. (1956) and the 'filling box model' of Baines and Turner (1969). Due to the complexity and nonlinearities of the modeling equation, the simplest models only consider steady states. However, elegant reduced numerical models such as those of Germeles (1975) can be used to study transient effects. Due to the simplified nature of these models experiments are usually conducted for validation purposes. In this chapter an introductory description and literature review of the theoretical, numerical and experimental tools for studying natural ventilation and contaminant

transport is given.

3.2 Modelling Isolated Heat Sources - Turbulent Convection from an Isolated Point

Many heat sources can be treated as isolated and the plume model for turbulent convection from an isolated point developed by Morton et al. (1956) may be used to model them. In this section we present the derivation of the integral conservation equations for an axisymetric turbulent plume. Consider the equations for axisymmetric, Boussinesq, steady flow with no diffusion and no swirl

$$u\frac{\partial u}{\partial r} + w\frac{\partial u}{\partial z} = -\frac{1}{\rho_o}p_r, \tag{3.1}$$

$$u\frac{\partial w}{\partial r} + w\frac{\partial w}{\partial z} = -\frac{1}{\rho_o}p_z - g\frac{\rho}{\rho_0}, \tag{3.2}$$

$$u\frac{\partial \rho}{r} + w\frac{\rho}{z} = 0, \tag{3.3}$$

$$\frac{1}{r}\frac{\partial}{\partial r}\Big(ru\Big) + \frac{\partial w}{\partial z}, \tag{3.4}$$

where $\mathbf{u} = (u, 0, w)$ is the velocity field in cylindrical coordinates (r, θ, z) and ρ is density.

Integrating 3.4 in the radial direction we obtain

$$\int_0^\infty r\frac{\partial w}{\partial z}dr = -\int_0^\infty \frac{\partial}{\partial r}\Big(ru\Big)dr. \tag{3.5}$$

If we now define the volume flux as

$$Q = 2\pi\int_0^\infty rqdr, \tag{3.6}$$

then equation (3.5) can be rewritten as

$$\frac{dQ}{dz} = 2\pi r u|_{\infty}. \tag{3.7}$$

The inflow term on the right hand side, $2\pi r u|_{\infty}$, comes about due to entrainment into the plume. It is not possible to calculate this inflow directly. However, Morton et al. (1956) introduced the concept of an entrainment velocity, where it is assumed that the velocity of the fluid being entrained into the plume is proportional to some characteristic vertical velocity in the plume, i.e.

$$2\pi r u|_{\infty} = b u_e, \qquad u_e = \alpha w, \tag{3.8}$$

where α is the entrainment constant. This entrainment assumption has been shown experimentally to work well and is very appealing due to its simple nature and relationship to a local velocity scale. The entrainment constant will take on different values, depending on the characteristic vertical velocity that is chosen. This is typically based on the assumed profile of the plume. While experiments show that plumes typically have Gaussian profiles, it is often easier from a theoretical perspective to assume a top hat profile - see figure 3.1. The characteristic vertical velocity will be different in each case and so α will take on different values.

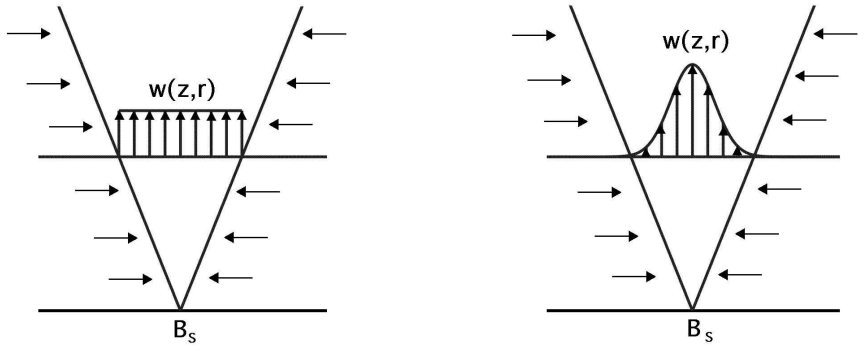

(a) (b)

Figure 3.1: Plume Velocity Profiles (a) Top Hat (b) Gaussian

In a similar fashion, equations 3.1-3.4 can be used to derive conserva-

tion equations for buoyancy, $B = 2\pi \int_0^\infty rwg\left(\frac{\rho_e - \rho}{\rho_0}\right)dr$ and momentum, $M = 2\pi \int_0^\infty w^2 dr$. These three equations combined are known as the plume equations and represent a closed set of equations describing the evolution of a turbulent plume. They can be written as

$$\frac{dQ}{dz} = 2\pi^{\frac{1}{2}} M^{\frac{1}{2}} \qquad M\frac{dM}{dz} = \frac{BQ}{M} \qquad \frac{dB}{dz} = \frac{g}{\rho_0}\frac{d\rho_e}{dz}Q \tag{3.9}$$

3.3 An Isolated Heat Source in a Confined Space - The Filling Box Model

The discussion of plumes in the previous section assumes that the environment is infinite. In this section we consider a plume rising from a point source in an enclosure of height H and horizontal area A, as depicted in figure 3.3. In this scenario the fluid in the plume will rise to the ceiling and then spread out horizontally as a gravity current. When the gravity current hits the side walls a downwards flow is established that forms a buoyant region at the top of the enclosure. This creates a circulation with some of the downwards advecting fluid being re-entrained into the plume. This circulation leads to a stable stratification in the enclosure. This process was first described by Baines and Turner (1969) and is known as the 'filling box'. In order to study this system the enclosure is divided into two regions, the plume and the ambient. Assuming that the plume evolves much more rapidly than the ambient (i.e. it behaves in a quasi-steady manner), equations (3.9) can be used to describe the plume. This assumption can be shown to be true as long as the fastest time scale of the ambient is much longer than the slowest of the plume, which is true if

$$\left(\frac{5}{6\epsilon}\right)^2 \frac{A}{\pi H^2} >> 1. \tag{3.10}$$

In order to study the flow in the background, two additional equations are required. These are conservation of volume and conservation of mass. Assuming

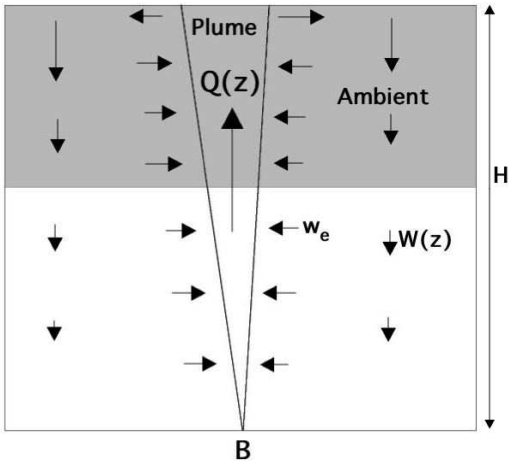

Figure 3.2: The Filling Box Model

that the plume occupies a much smaller cross sectional area than the area of the space (i.e. $\pi b^2 << A$), conservation of volumes is

$$Q(z) = w(z)A, \tag{3.11}$$

where $w(z)$ is the vertical velocity in the ambient flow. Conservation of mass, neglecting diffusion, due to high Reynolds and Peclet numbers, is

$$\frac{\partial \rho_e}{\partial t} - w\frac{\partial \rho_e}{\partial z} = 0. \tag{3.12}$$

Baines and Turner (1969) presented asymptotic long time solutions for the mean density, based on the idea that since the source buoyancy flux is constant, the mean density in the enclosure decreases linearly over time and that the ambient establishes a self similar stratification, $\rho_e(z) - ct$ for some constant c. This leads to the odd behaviour that the temperature in the box will ultimately increase to infinity (i.e. $\rho \to -\infty$) due to the fact that the buoyancy of the source is always constant. Real thermal sources of course do not display this behaviour due to their finite temperature and Caulfield and Woods (2002) accounted for this by including a non ideal source of buoyancy, which is merely a source with a finite mass flux

at the origin and showed that resolved this infinite limit by developing asymptotic solutions with a finite long time temperature.

3.4 Emptying Filling Boxes - A Model for Natural Ventilation

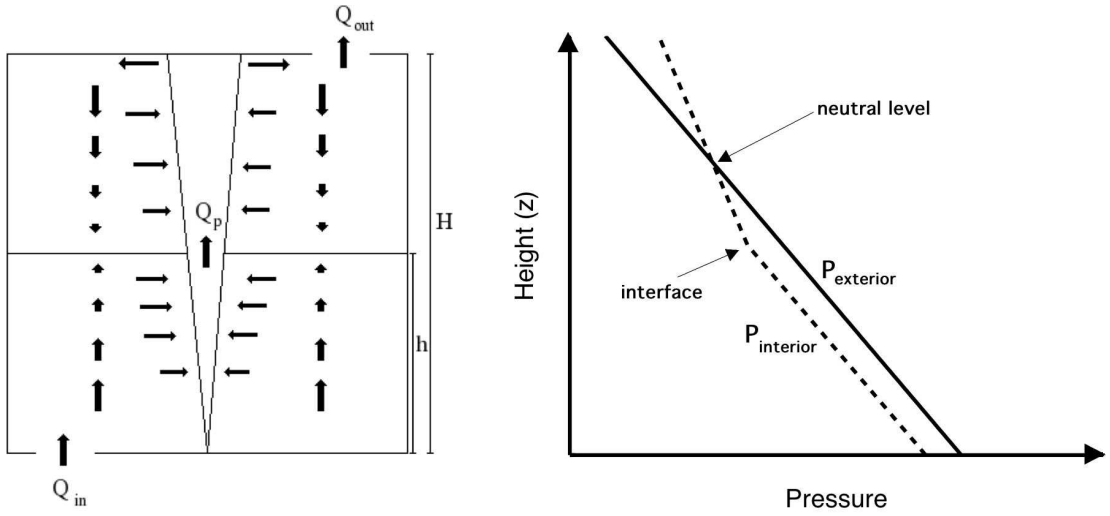

(a) (b)

Figure 3.3: (a) Two Layer Model for Natural Ventilation (b) Interior and Exterior Pressure Distributions

An application of plume theory in a confined space is the flow in naturally ventilated spaces, where an ambient stratification occurs. Linden et al. (1990) conducted the first such study. They considered the case of a steady flow in a single space with a single isolated heat source and openings to the exterior at low and high levels. The flow that arises depends on the location and sizes of these openings to the exterior. The heat source is modelled as a plume with source buoyancy flux B_s, located at the bottom of the room.

As in the filling box, the plume rises to the top of the room, spreads out and then descends back into the room, establishing a buoyant upper layer in the upper part of the room. Now there is a difference in density gradient between

the interior and exterior with less dense air inside. Hence there will be a pressure difference between the inside and outside as depicted in figure 3.3. This pressure difference causes an inflow of fresh fluid through the lower opening and an outflow of buoyant fluid through the upper opening. For a steady heat source, the flow in the room eventually reaches a steady state with fresh ambient fluid in the lower part of the room and buoyant fluid in the upper part. These layers are separated by an interface at height, h. The aim of a well designed naturally ventilated space is to have this interface sit above occupants of the space. Interestingly, the height of this interface is independent of the source buoyancy flux B. The physical reason for this is that B is the only system parameter with dimensions of time, which means that in a steady state it can not influence the height h. This means that a well designed natural ventilation system will work regardless of the strength of the heat source, which is a very appealing feature.

The buoyancy of the upper layer can be determined from the source buoyancy flux since the density of the upper layer must be equal to the density of the plume at the interface. Since the lower layer is unstratified, the buoyancy flux of the plume at the interface is equal source buoyancy flux as can be seen from 3.9. Therefore, the reduced gravity of the upper layer is

$$g'_u = \frac{B_s^{\frac{2}{3}}}{Ch^{\frac{5}{3}}}, \tag{3.13}$$

where $C = \frac{6}{5}\alpha\left(\frac{9}{10}\alpha\right)^{\frac{1}{3}}\pi^{\frac{2}{3}}$ is a constant based on the entrainment assumption.

The flowrate through the upper and lower vents can be calculated from the buoyancy of the upper layer, the interface height and an effective opening area

$$Q = A^*\sqrt{g'_u(H-h)}, \tag{3.14}$$

where

$$A^* = \frac{\sqrt{2}c_t c_b a_t a_b}{\sqrt{c_t^2 a_t^2 + c_b^2 a_b^2}}. \tag{3.15}$$

a_t and a_b are the areas of the upper and lower openings respectively and c_t and c_b are the respective coefficients of contraction.

Finally, the interface height, h, can be determined by noting that by conservation of volume, the volume flux in the plume at the interface must be equal to flow rate in and out of the room. Since the lower layer is unstratified we can use the solution to the plume equations in an unstratified medium. Therefore, the interface height can be determined from the nonlinear equation

$$\frac{A^*}{H^2} = C^{\frac{3}{2}} \left(\frac{\zeta^5}{1-\zeta} \right)^{\frac{1}{2}}, \tag{3.16}$$

where $\zeta = \frac{h}{H}$ is the dimensionless interface height.

As a final remark to this, it is interesting to note from (3.15) that when one opening is much smaller than the other

$$A^* \approx \sqrt{2} c_s a_s, \tag{3.17}$$

where the subscript s refers to the smaller opening. This suggests that the smaller of the two openings always controls the flow. From a practical perspective it means that by constricting the upper openings, occupants may open and close the lower openings at will without affecting the ventilation system significantly.

3.5 Germeles Algorithm

The system of equations (plume and background) described in the previous sections can be solved using a modification of a numerical method developed by Germeles (1975). The method relies on the discretization of the ambient density into a finite number of layers, n. As mentioned before it is assumed that the plume evolves far more rapidly than the ambient density field does. Therefore, for any given time step the plume equations are solved assuming a constant background density gradient. The plume equations are solved through the entire height of the

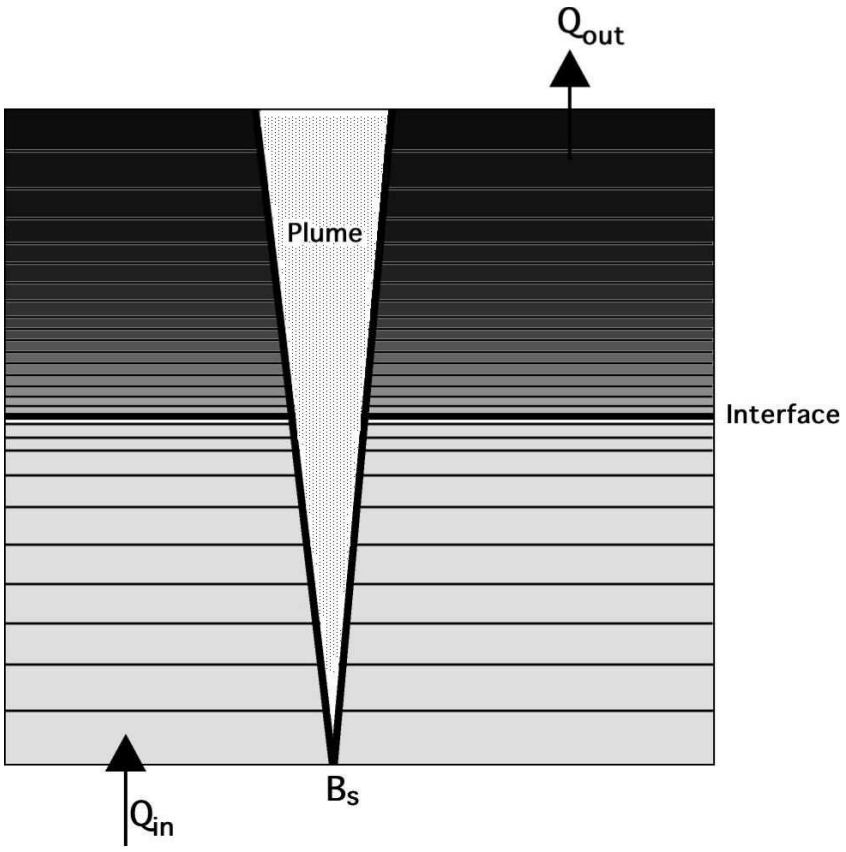

Figure 3.4: Image of Germeles Layers

room using the integration method of choice. The work presented in this thesis used either a 2nd order Euler or 4th order Runge-Kutta method.

The density layers in the background are then advected downwards with a velocity calculated using the discretized version of equation 3.11, i.e.

$$w(i) = \frac{Q(i) - Q_{top}}{A(i)} \tag{3.18}$$

where i represents each different layer ($1 < i < n$). During a given timestep of length Δt, each background layer will be advected downwards as follows

$$y_{new}(i) = y_{old}(i) - \Delta t w(i) \tag{3.19}$$

Note that layers lower down in the room will advect downwards more slowly than those above them. This process captures the entrainment of fluid from each layer by the rising plume. When the plume reaches the ceiling, a new layer is added at the top of the room, with an interface location given by:

$$y_{new}(n+1) = 1 - \Delta t \frac{Q(n) - Q_{top}}{A(n)} \tag{3.20}$$

and the density of this new layer is the density of the fluid at the top of the plume. This layer contains the volume of fluid arriving at the ceiling during the timestep which does not flow out through the upper opening. n represents the top layer in the box. A new layer of ambient fluid is also introduced at the bottom of the room with depth $Q_{in}\Delta t$.

The model is somewhat more complicated when the plume does not remain buoyant as it rises. Although the plume fluid undoubtedly overshoots its level of neutral buoyancy, for simplicity we assume that negligible entrainment occurs during this overshoot, and the plume fluid will intrude at its neutral height. As discussed in more detail in Bower (2005) this assumption is valid provided that the difference in buoyancy fluxes is sufficiently large.

Therefore below the level of zero buoyancy, the interfaces have velocities as before:

$$w(i) = \left(\frac{-Q(i) + Q_{top}}{A(i)} \right) \tag{3.21}$$

while above the level of zero buoyancy:

$$w(i) = \frac{Q_{top}}{a(i)} \tag{3.22}$$

Since there is no flow of the plume through these layers they simply drain upwards due to the outflow through the upper opening. Rather than introducing a new layer of fluid at the top of the box we introduce a new layer at the neutral buoyancy height.

3.6 Laboratory Experiments

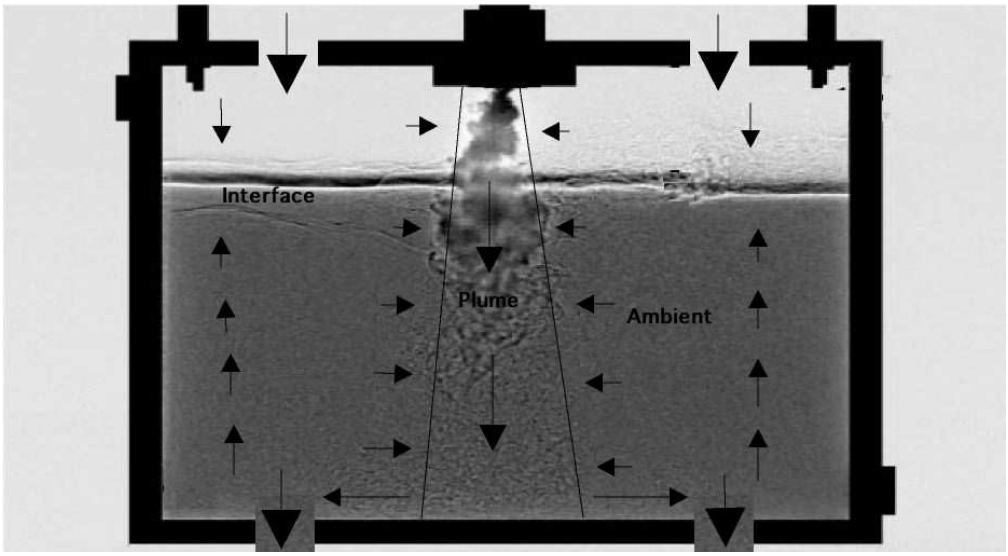

Figure 3.5: Small Scale Experimental Tank for Natural Ventilation Study

An additional manner of studying these flows is by physical experiments, either at full or small scale. While full scale experiments may seem the most useful, they can often be difficult and expensive to conduct. Therefore, small scale analogue laboratory experiments can provide a practical and insightful method for studying and understanding the full scale flows.

In the lab, at small scales, stack driven ventilation is more difficult to study than wind driven ventilation, because Reynolds numbers are orders smaller in the stack driven flows and as such it is difficult to obtain dynamic similarity over the scales. Therefore, water, in place of air, is typically chosen as the working fluid and salt, instead of heat, is used as the density altering scalar. By using water and salt, dynamic similarity over lab and full scales is maintained (Linden (1999)).

In order to understand this, let us consider the Reynolds and Peclet numbers, given respectively by

$$Re = \frac{g'^{1/2} H^{3/2}}{\nu}, \qquad Pe = \frac{g'^{1/2} H^{3/2}}{D}, \tag{3.23}$$

where ν is the kinematic viscosity, D is the coefficient of molecular or thermal diffusivity, H is a characteristic vertical length scale and $g' = g\frac{\Delta\rho}{\rho}$ is a characteristic reduced gravity. $(g'H)^{1/2}$ represents a characteristic velocity for a buoyancy-driven flow.

Table 3.1 shows typical values of all the above quantities in laboratory and full scale situations. It is worth noting that the length scales in the lab may be reduced by a factor of 10, while still maitaining adequate similarity. Typical values of these Reynolds and Peclet numbers are large and thus in ventilation flows inertial effects dominate viscous ones, except at the small scales.

These small-scale experiments offer many advantages. Visualization of the flow is easy as tracer dyes can be used to track the flow. Additionally, with the use of digital image processing fine details and structures of the flow can be observed and quantified.

Unfortunately, there are disadvantages associated with these small scale experiments. Neither radiative effects, nor conductive transport through boundaries can be captured when salt is used as the active scalar. Using temperature as the scalar may resolve these issues. However, such experiments prove difficult to conduct and as such have not been actively pursued in the research community.

Table 3.1: Typical values of Reynolds and Peclet Numbers for laboratory and full scale ventilation studies

	Laboratory scale [water]	Building scale [air]
g' [m/s^2]	0.35	0.15
H [m]	0.3	3.0
ν [m^2/s]	1.0×10^{-6}	1.5×10^{-5}
D [m^2/s]	2.5×10^{-9}	2.1×10^{-5}
Re	9.7×10^{4}	1.3×10^{5}
Pe	3.9×10^{7}	9.6×10^{4}

3.7 Contaminant Modelling

While there has been significant research in the field of contaminant modelling, most of it is based on single and multi zone models. In a single zone model it is assumed that the entire space (building) of interest is well mixed. This type of model is typically used for a single story building with no partitions, although it has been used inappropriately for large, complex buildings, where it is clearly not valid. With multi-zone models the building is broken into several zones, which interact with one another. Each of the zones is assumed to be well mixed.

This approximation of uniform and instantaneous mixing is very convenient and can often be justified for cases with strong internal air motion. However this assumption may not always be appropriate, say if pollutant emissions are from a localized source and air movement is weak. In such cases exposure to the contaminants may depend heavily on a person's location with a space. Ozkaynak et al. (1982) found that pollutant levels in a kitchen with the oven on depended heavily on the sampling location. Rodes et al. (1991a) discovered that personal sampling almost always reveals a higher exposure to contaminants that would be predicted from indoor air monitoring that assumes perfect mixing. Lambert et al. (1993) showed that the levels of suspended particles in a non smoking section of a restaurant were 40-65 % less than those in the smoking section.

In general, an efficient manner of air quality control is to remove the contaminant before it has time to mix throughout the space, which means extracting it from near the source, where the concentration will be highest. Therefore it is important to understand how the contaminant will disperse in the room. In most indoor environments the transport of the pollutant will be by advection, since the diffusion rate will be relatively small. An approximate diffusion timescale would be 5 days for a typical space, yet from experience we know that the actual dispersion rate is more on the order of minutes or hours than days.

Baughman et al. (1994) saw natural convection as an important mode of air motion in residences. They noted that there is a characteristic time scale associated with mixing, τ_{mix}. It is defined such that for $t << \tau_{mix}$ the pollutant concentration varies siginificantly throughout the room and for $t >> \tau_{mix}$ the pollutant concentration is basically uniform. There is also a time scale associated with the removal of the pollutant from indoor air, τ_{rem} (e.g. The inverse of the air-exchange rate). A final time scale τ_{exp} is defined, which is an exposure time scale. Their argument is:

1. If $\tau_{mix} << \tau_{rem}$ and $\tau_{mix} << \tau_{exp}$ then the well mixed assumption is valid
2. If $\tau_{rem} << \tau_{mix}$ or $\tau_{exp} << \tau_{mix}$ then significant errors can arise from treating air as well mixed.

It should be clear that the characteristic mixing time can vary significantly based on the space under consideration. The location of the source, the location of inlets and extracts, any obstacles that may be in the way and the nature of the flow are all factors that can affect this. In their experiments Baughman et al. (1994) found that these characteristic mixing times spanned across a large range of times, from 7-100 minutes, depending on the conditions imposed. Drescher et al. (1995) conducted a very similar experiment, but this time examining forced rather than natural convection. In both cases they concluded that the assumption of instantaneous mixing can lead to significant errors and that it may

not prove valid for certain circumstances, particularly if there is a serious concern about the exposure or detection time such as with the release of a biotoxin such as anthrax. Also Schneider et al. (1999) notes that if dealing with large particles they may sometimes have residence times in the air, which are shorter than the characteristic mixing time. For these larger particles there would not be sufficient time for mixing before the particles deposit on the floor.

Despite these deficiencies, when it is not critical to know the fine details within the room, this assumption can be a very useful one and has been used by many researchers over the years. The assumption leads to a set of coupled ordinary differential equations. Numerical solutions to these equations are significantly easier than those of the full system of partial differential equations that must be solved to find the concentration at specific locations and times. In some cases these ODEs may even be solved analytically.

A form of ventilation traditionally used is mixing ventilation. This is where incoming air is mixed with the air in the room and diluted. This typically results in a relatively uniform interior temperature distribution. Many modern ventilation systems use the concept of displacement ventilation, where cooler air comes from a lower vent and hot air is exhausted from the top of the space. These systems are designed to produce two temperature layers in a space. The bottom layer should be the cooler comfortable layer where occupants are located, while the top layer can be warm and uncomfortable. For the same conditions displacement ventilation is more efficient than mixing ventilation and leads to a more rapid ventilation, because the air being extracted from the top is the hottest air in the space. Therefore, an important feature in many building flows is stratification. This is particularly true for tall spaces where temperature differences can be quite significant. It should be immediately obvious that the instantaneous mixing assumption discussed above will not be valid for stratified spaces. Typically such ventilation methods can be modeled analytically and experimentally by representing heat sources as turbulent buoyant plumes (Linden et al. (1990), Caulfield and

Woods (2002)). The fundamental model for such studies is that of the turbulent plume due to Morton et al. (1956), which addresses the problem of turbulence closure by making the very simple, but powerful 'entrainment' assumption. Baines and Turner (1969) experimentally and analytically studied the interaction of such a plume with a space of finite volume with the so called 'filling box' model. They demonstrated that a buoyant plume will rise to the top of a room, spread out across the ceiling and then drive a descending front into the air surrounding the plume. In 1975 Germeles developed a sophisticated numerical method for determining the evolution of the background density by assuming a separation of timescales between the fast progress plume and the slower evolution of the background. These models have been successfully used to study various forms of ventilation - natural ventilation (Linden et al. (1990)), mechanical ventilation (Caulfield & Woods 2002) and hybrid ventilation (Woods et al. (2003)). Typically these studies have only been interested in looking at the background density evolution and have not included the study of any sort of contaminants. Also most work has been on steady state models, where the sources are time-independent.

CFD can prove a useful tool in the study of contaminant dispersion. Many researchers have successfully used it to model the transport of contaminants within a building. Most of the buildings that have been successfully modeled are not that large and have relatively simple geometries, which is often not the case in industry. Also, even when using simplified models such as a drift flux model (Holmberg and Li 1998), with current computer speeds, it may not always be a viable tool for industry where time lines tend to be short and budgets low. This is not to say that CFD is not used in industry - it is often used as a tool to model specific sections of a building where there may be some concern about which ventilation approach to use. Zhao et al. (2004a) propose using CFD as a stepping stone in multi zone modeling. Using the results from a specific CFD simulation they break the building into zones, which are seen to be well mixed based on an age of air concept. Then using these zones in a multi zone model they run a full year

simulation on the building. While this may well seem to be a useful approach one has to wonder if these zones that are well mixed for one situation will be the zones that are well mixed throughout the whole year. After all Baughman et al. (1994) noted that the same space had a characteristic mixing time that varied from 7-100 minutes depending on the conditions imposed. Another major limitation of CFD for ventilation modeling is that it can often prove to be quite difficult to get the numerical equations to converge when modeling flows that involve stratification (Versteeg and Malalasekra (1996)).

4

Contaminated Ventilated Spaces - Passive Contaminants

4.1 Abstract

Many low energy systems, such as displacement or natural ventilation, rely on temperature stratification within the interior environment, always extracting the warmest air from the top of the room. Understanding buoyancy-driven convection in a confined ventilated space is key to understanding the flow that develops with many of these modern low-energy ventilation schemes. It is widely believed, although not comprehensively studied and validated, that such low energy ventilation systems will be more effective at removing contaminants. In this work we study the transport of an initially uniformly distributed passive contaminant in a displacement-ventilated space. Representing a heat source as an ideal source of buoyancy, analytical and numerical models are developed that allow us to compare the average efficiency of contaminant removal between traditional mixing and modern low energy systems. A set of small scale analogue laboratory experiments was also conducted to further validate our analytical and numerical solutions.

We find that on average traditional and low energy ventilation methods are similar in regards to pollutant flushing efficiency. This is because the concen-

tration being extracted from the system at any given time is approximately the same for both systems. However, very different vertical concentration gradients exist. For the low energy system a peak in contaminant concentration occurs at the temperature interface that is established within the space. This interface is typically designed to sit at some intermediate height in the space. Since this peak does not coincide with the extraction point, displacement ventilation does not offer the same benefits for pollutant flushing as it does for buoyancy removal.

4.2 Introduction

People spend substantial amounts of time indoors, in many cases up to as much as 90 % (Jenkins et al. (1992)) and, therefore, it is important to understand the details of the indoor environment, in particular regarding human comfort, indoor air quality (IAQ) and energy consumption. The U.S. Energy Information Administration states that approximately 10% of the total energy consumption in the US is consumed by heating, cooling and ventilation of buildings. Currently, the US is the largest per capita consumer of energy in the world, but long-term forecasts to 2025 project the strongest growth in energy use will come from developing countries, especially China and India, where buoyant economies will boost demand. Furthermore the US Energy Information Administration states that energy use in developing countries is forecast to soar by 91% over the next two decades, while industrialized nations are expected to increase energy consumption by about one third. Therefore, it is important to try and reduce this growth in consumption and consequent increase in carbon emissions by designing better and more efficient ventilation strategies within buildings.

The adoption of energy-efficient ventilation systems requires that they also provide an acceptable level of IAQ and comfort. In order to reduce energy consumption various low-energy systems such as displacement ventilation, under-floor air distribution, operable windows, night cooling, radiant and evaporative

cooling are under consideration. All these systems have the potential of 'free cooling'. That is, under certain conditions, outside air is used to cool the building and reduce the load on mechanical systems. The introduction of outside air, either through filters or simply by opening a window introduces outside pollutants. Additionally, internal pollutants are generated and need to be extracted from the building.

The many types of airborne contaminants in buildings can be put very broadly into two categories - gaseous and particulate. In this paper we will focus our attention on the gaseous kind, with future work considering particulate contaminants. Gaseous contaminants are usually considered as passive contaminants, that are assumed to follow exactly the air currents in a space. Some of the more common gaseous contaminants that cause concern in buildings are carbon monoxide, carbon dioxide, nitrogen oxides, ozone, sulfur dioxide, moisture, formaldehyde, radon gas and its progeny. Many of these contaminants are combustion byproducts; given the proliferation of transportation and industrial sources, there is increasing concern about the levels of these contaminants in outdoor and, consequently, indoor air. Many gas-phase contaminants have obvious adverse effects on a person's health, comfort and ability to work above threshold concentrations, and teratogenic contaminants are of concern at any concentration level.

Traditional ventilation, such as that provided by a conventional overhead HVAC system, is mixing ventilation, where incoming air is mixed with the air in the room and diluted. This typically results in a relatively uniform interior temperature and contaminant distribution. In contrast, in order to benefit from free cooling, many modern low-energy ventilation schemes require the use of temperature stratification in a space, with a bottom layer of cooler comfortable air where occupants are located, and an upper layer that is comparatively warm and uncomfortable (Linden (1999)). The ability to extract air at elevated temperatures is necessary for energy-efficiency and free cooling. High temperature extraction can be achieved, for example, by displacement ventilation or underfloor air distribution,

where cool air enters the space at floor level and the warm air is extracted at the ceiling. Hence, stratification is an important feature in modern ventilation design. This is particularly true for tall spaces, where vertical temperature differences can be quite significant. It is widely believed (although not comprehensively studied and validated) that such displacement ventilation systems will be more effective at removing passive contaminants than traditional mixing since it is expected that they will be transported to the hot upper layer in rising plumes, where they will be extracted.

Many heat sources within a building (people, electronic equipment etc.) can be regarded as localised and understanding the manner in which they stratify a space is critical to design efficient ventilation schemes. These heat sources can often be modeled as pure sources of buoyancy which give rise to turbulent plumes.

Considerable work has examined the stratification generated by a buoyant plume within a confined space. In an unventilated space the plume produces a continuous stable stratification by the 'filling box' mechanism (Baines and Turner (1969)). Warm air spreads out across the top of the space and then descends into the interior around the plume. At the later times the plume entrains this warm air, thereby continuously increasing the temperature of the air reaching the ceiling. In the absence of heat losses, the temperature everywhere within the space will increase linearly with time.

In a ventilated enclosure a steady-state is eventually reached in which the heat removed by the ventilation equals that input by the plume. When the openings are located at high and low levels, the stratification takes the form of two layers of uniform, but different, temperatures separated by an interface. The values of the temperature and the height of the interface can be calculated for different ventilation strategies (e.g. natural ventilation (Linden et al. (1990), Caulfield and Woods (2002),Woods et al. (2003), Kaye and Hunt (2004)) and displacement or underfloor ventilation(Lin and Linden (2002), Liu and Linden (2006), Coffey and Hunt (2005)).

Few theoretical studies on contaminant transport in low energy ventilated spaces have been conducted. Kaye and Hunt (2006) considered a pollutant flushing problem in a naturally ventilated space containing isolated sources of buoyancy. They modeled the space as two well mixed regions. Additionally, in a follow up paper, Kaye and Hunt (2007), considered the influence of distributed, rather than isolated, heat sources that, for an equal buoyancy input, can result in very different flow rates

In this paper we are concerned with the transport of passive contaminants in 'forced' displacement systems where cool, clean air is introduced into the lower part of a space with an initially uniform concentration of a contaminant. A theoretical model, based on plume theory and an extension of the Baines & Turner (1969) 'filling-box' approach, is given in §4.3. The results of this model are described in §4.4. A set of experiments designed to test the model and a comparison of the results with the theoretical predictions is given in §4.5. The conclusion and applications to IAQ are discussed in §4.6.

4.3 Theoretical Model

Consider a space with a single ideal heat source and inlet and extraction vents at the top and bottom of the room, respectively (figure 4.1). We will consider the rate of removal of a passive contaminant with uniform initial concentration C_0. The flow rates, Q_{in} through the space can be specified as desired either as a fixed ventilation flow supplied by a fan in a mechanical system (Sandberg and Etheridge (1996)) or as determined by the strength of plume and size of openings in a naturally ventilated enclosure (Linden et al. (1990)). The resulting stratification has two layers of uniform temperature with cool air in the lower layer (corresponding to the temperature of the air introduced through the lower vent) and warm buoyant air in the upper layer.

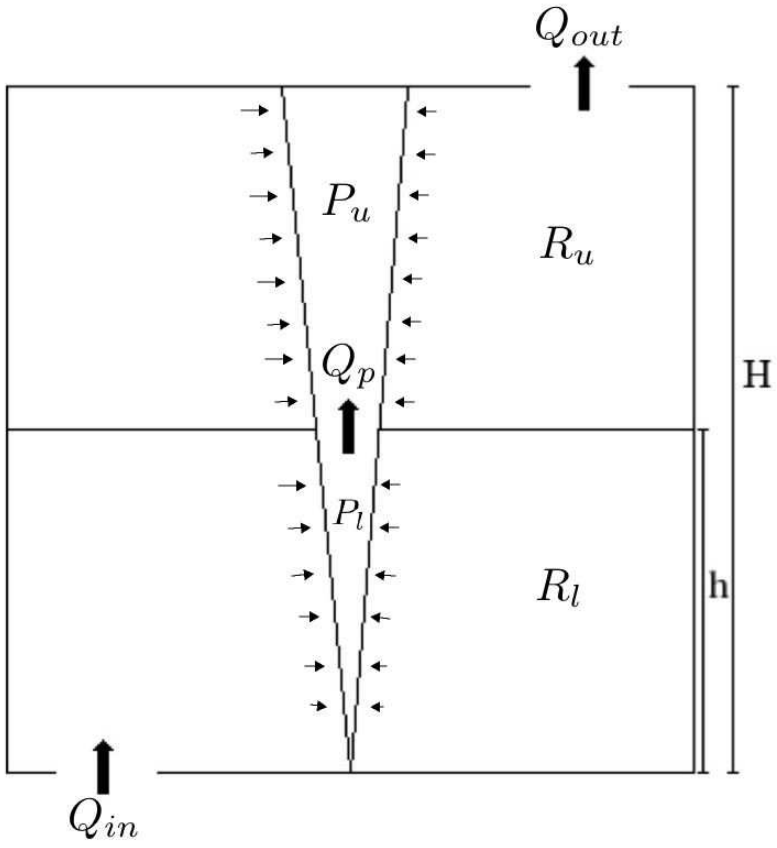

Figure 4.1: Displacement ventilation with a single ideal plume heat source. P(z) is the concentration of contaminant in the plume and R(z) the concentration in the room

4.3.1 Flow in the Space

The flow within the space is determined by coupling the plume flow with the environment outside the plume. For a Boussinesq plume

$$\frac{dQ}{dz} = 2\alpha M^{\frac{1}{2}} \qquad M\frac{dM}{dz} = FQ \qquad \frac{dF}{dz} = \frac{g}{\rho_0}\frac{d\rho_a}{dz}Q, \tag{4.1}$$

where πQ is the volume flux, πM is the specific momentum flux and π F is the specific buoyancy flux (Morton et al. (1956) - hereafter MTT). α is the entrainment coefficient.

The plume is coupled to the ambient flow using the filling box model (see chapter 3 for details). Volume conservation outside the plume is

$$wA = -\pi Q - Q_{out}, \tag{4.2}$$

where $w(z)$ is the vertical velocity outside the plume and Q_{out} is the volume flow rate out of the space through the upper vent. Provided that heat conduction is negligible (i.e. the Péclet number is sufficiently high), the conservation of mass equation is

$$\frac{\partial \rho_a}{\partial t} + w\frac{\partial \rho_a}{\partial z} = 0, \tag{4.3}$$

where ρ_a is the density in the ambient fluid outside the plume. It is necessary to assume that the background density in the room varies on a much slower time-scale than that associated with the evolution of the plume, which requires

$$\left(\frac{5}{6\alpha}\right)^2 \frac{A}{\pi H^2} >> 1, \tag{4.4}$$

(Baines and Turner (1969)). The restriction requires the room to have a small aspect ratio $\frac{A}{H^2}$.

The interface that divides the upper and lower layer corresponds to the height where the plume flowrate is the same as the flowrate through the vents (i.e. when $Q = Q_{in}$ or Q_{out} and where $w(z) = 0$).

4.3.2 Contaminant Transport

Contaminant with concentration $R(z)$ in the room is entrained into the plume, which has contaminant concentration $P(z)$. Conservation of contaminant volume flux in the plume can be expressed as

$$\frac{d}{dz}[PQ] = 2\alpha M^{\frac{1}{2}} R, \tag{4.5}$$

and using (4.1) we obtain

$$\frac{dP}{dz} = \frac{2\alpha M^{\frac{1}{2}}(R-P)}{Q}. \tag{4.6}$$

In addition, neglecting diffusion, the room contaminant conservation equation is

$$\frac{\partial R}{\partial t} + w\frac{\partial R}{\partial z} = 0. \tag{4.7}$$

We now consider the flow in the upper and lower layers separately (see figure 4.1), and solve (4.1), (4.2), (4.5) and (4.6).

The Lower Layer

In the unstratified lower layer ($0 < z < h$) the plume buoyancy flux remains constant ($F(z) = F_0$) and the solutions for Q and M are

$$Q(z) = \frac{6\alpha}{5}\left(\frac{9\alpha F_0}{10}\right)^{\frac{1}{3}} z^{\frac{5}{3}}, \quad M(z) = \left(\frac{9\alpha F_0}{10}\right)^{\frac{2}{3}} z^{\frac{4}{3}}, \qquad 0 < z < h. \tag{4.8}$$

Substituting (4.7) into (4.2) and (4.5), the contaminant transport equations for the lower layer become

$$\frac{dP_l}{dz} = \frac{5}{3z}(R_l - P_l), \tag{4.9}$$

where the subscript l refers to the concentrations in the lower layer and

$$w = \frac{\pi}{A}\left(\frac{6\alpha}{5}\left(\frac{9\alpha F_0}{10}\right)^{\frac{1}{3}}\right)(h^{\frac{5}{3}} - z^{\frac{5}{3}}), \qquad 0 < z < h. \tag{4.10}$$

The Upper Layer

In the upper layer ($h < z < H$) the density outside is the same as the density of the plume at the interface so that the plume is no longer buoyant above the interface ($F = 0$). The momentum flux M is constant and equal to the momentum flux of the plume at the interface.(i.e. $M = M_p$). This implies

$$Q(z) = Q_p + 2\alpha M_p^{\frac{1}{2}}(z-h), \quad M_p = \left(\frac{9\alpha F_0}{10}\right)^{\frac{2}{3}} h^{\frac{4}{3}}, \qquad h < z < H. \tag{4.11}$$

Therefore, the contaminant transport equations become

$$\frac{dP_u}{dz} = \frac{1}{z - \frac{2}{5}h}(R_u - P_u), \qquad w = \frac{\pi}{A}\left(2\alpha\left(\frac{9\alpha}{10}\right)^{\frac{1}{3}} F_0^{\frac{1}{3}} h^{\frac{2}{3}}\right)(h-z), \qquad h < z < H. \tag{4.12}$$

where the subscript u refers to the concentrations in the upper layer.

4.3.3 Non Dimensionalisation

We nondimensionalise the variables as follows:

$$z = \zeta H, \qquad P = C_o p, \qquad R = C_o r, \tag{4.13}$$

$$w = w^* \frac{\pi}{A}\frac{6\alpha}{5}\left(\frac{9\alpha}{10}F_0\right)^{\frac{1}{3}} h^{\frac{5}{3}}, \qquad t = \tau\frac{AH}{Q_{in}} = \tau\frac{AH}{\pi\frac{6\alpha}{5}\left(\frac{9\alpha F_o}{10}\right)^{\frac{1}{3}} h^{\frac{5}{3}}}, \tag{4.14}$$

where C_0 is the initial uniform concentration of contaminant in the space. The replenishing time, which represents the time taken for a volume of fluid equal to the volume of the space to enter that space (i.e. $\frac{V_{room}}{Q_{in}}$) is used to non-dimensionalise time. The characteristic velocity is chosen as the plume flux at the interface divided by the cross sectional area of the room. This is the background ambient velocity that would exist in the absence of ventilation with the exterior (i.e. a pure 'filling box').

Using the above nondimensionalisation the contaminant and velocity equations for the lower and upper layers, respectively, become

$$\frac{dp_l}{d\zeta} = \frac{5}{3\zeta}(r_l - p_l), \qquad w_l^* = (1 - \left(\frac{\zeta}{\zeta_h}\right)^{\frac{5}{3}}) \tag{4.15}$$

and

$$\frac{dp_u}{d\zeta} = \frac{1}{\zeta - \frac{2}{5}\zeta_h}(r_u - p_u), \qquad w_u^* = \frac{5}{3}\left(1 - \frac{\zeta}{\zeta_h}\right). \tag{4.16}$$

4.3.4 Analytical Solutions

In practice it is often difficult to obtain a pure displacement flow in the lower layer and some mixing may occur as a result of inflow through the lower vents. Consequently, we consider two limiting cases for the lower layer: pure displacement ventilation and a well-mixed lower layer (figure 4.2). These cases span the extremes of inflow with no mixing and complete mixing. We do not assume that the upper layer is well mixed, but calculate the development of the flow in the upper layer using a modification of the filling box mechanism. This is in contrast to Kaye and Hunt (2006), who considered the case where both the lower and upper layers are well mixed. While there will be some mixing in the upper layer a well mixed model does not capture some of the interesting dynamics which we observe in the upper layer with both our models and experiments.

Well Mixed Lower Layer

Let the concentration of the lower layer be denoted by c, with the initial condition $c(\tau = 0) = 1$. For the well mixed case (figure 4.2(a)) the concentration in the lower layer to decay exponentially as follows

$$c = e^{-\frac{\tau}{\zeta}} \tag{4.17}$$

Since in this case the lower layer has a uniform concentration c (figure 4.2(a)), the concentration of the fluid being transported by the plume into the

upper layer is also of concentration c (i.e. $p_l = c$ everywhere in the lower layer). This gives us a required boundary condition for (4.14) for p_u in the upper layer.

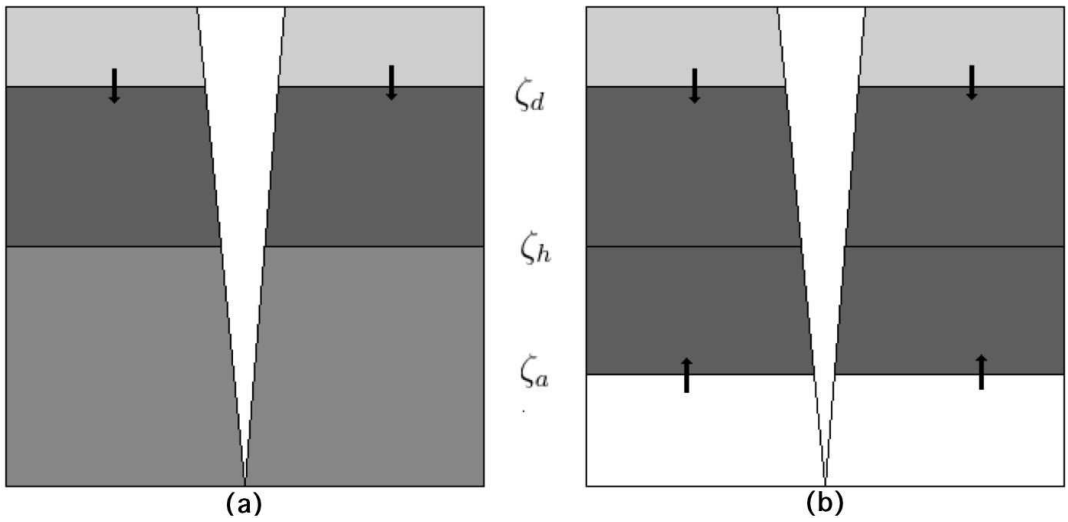

Figure 4.2: Sketch of ascending and descending fronts in the room: (a) corresponds to a well mixed lower layer, while (b) to a displaced lower layer. Darker shades imply higher contaminant concentrations

Displaced Lower Layer

For the case of displacement ventilation in the lower layer there is an ascending front, which we will denote by ζ_a with fresh uncontaminated ambient fluid (c=0) below it and fluid of the initial concentration ($c = 1$) above it. The lower layer is therefore now split into two distinct regions (figure 4.2(b)).

Since from (4.13), the background flow velocity for the lower layer, w_l, is known we can track the position of this ascending front. Its evolution is given by

$$\frac{d\zeta_a}{d\tau} = (1 - \left(\frac{\zeta_a}{\zeta_h}\right)^{\frac{5}{3}}), \tag{4.18}$$

which can be rewritten as

$$\frac{d\zeta_a}{(1-\left(\frac{\zeta_a}{\zeta_h}\right)^{\frac{5}{3}})} = d\tau. \tag{4.19}$$

We write the left hand side as its Laurent/Frobenius series expanded about $\zeta = 0$

$$\frac{d\zeta_a}{(1-\left(\frac{\zeta_a}{\zeta_h}\right)^{\frac{5}{3}})} = d\zeta_a \sum_{n=0}^{\infty} \left(\frac{\zeta_a}{\zeta_h}\right)^{\frac{5n}{3}}. \tag{4.20}$$

Equation (4.18) be integrated and the solution to (4.17), with the initial condition at $\tau = 0$, $\zeta_a = 0$ (i.e. we are tracking the first ascending front), is

$$\sum_{n=0}^{\infty} \left(\frac{(\frac{3}{5n+3})\zeta_a^{\frac{5n+3}{3}}}{\zeta_h^{\frac{5(n)}{3}}}\right) = \tau. \tag{4.21}$$

The long time limit (as $t \to t_\infty$ and $h_a \to h$) gives:

$$\tau_\infty = 3\zeta_h \sum_{n=0}^{\infty} (\frac{1}{5n+3}). \tag{4.22}$$

This series does not converge, which suggests that it takes an infinite amount of time for all the contaminant to be removed from the lower layer (in practice of course this contaminant layer becomes so thin as to not be important). While (4.19) is a solution for the ascending front it is difficult to determine the height of the interface at a given time due to the nonlinearity of the equation. [1]

Given ζ_a we can solve for the contaminant concentration in the plume using (4.13). Below ζ_a, $p_l = 0$ since the ambient concentration is zero. Above ζ_a, the room concentration is 1, which results in

$$\frac{dp_l}{(r_l - p_l)} = \frac{5}{3}\frac{d\zeta}{\zeta}, \quad p_l(z = \zeta_a) = 0. \tag{4.23}$$

[1] *Note: The sum in the equation for h_a can be expressed as the following tabulated function, which might make it easier to find the solution with in a numerical iterative scheme:* $\sum_{n=0}^{\infty} \left(\frac{(\frac{3}{5n+3})h_a^{\frac{5n+3}{3}}}{h^{\frac{5(n+1)}{3}}}\right) = \frac{3h_a}{5h^{\frac{5}{3}}} LerchPhi\left(\frac{h_a^{\frac{5}{3}}}{h^{\frac{5}{3}}}, 1, \frac{3}{5}\right)$

This means that the plume and background concentrations in the lower layer are

$$r_l = 0, \quad p_l = 0, \quad 0 < \zeta < \zeta_a \tag{4.24}$$

and

$$r_l = 1, \quad p_l = 1 - \left(\frac{\zeta_a}{\zeta}\right)^{\frac{5}{3}}, \quad \zeta_a < \zeta < \zeta_h. \tag{4.25}$$

The Upper Layer

Using w_u^* (4.14) the interface equation for the upper layer is

$$\frac{d\zeta}{d\tau} = w_u^* = \frac{5}{3}\left(1 - \frac{\zeta}{\zeta_h}\right). \tag{4.26}$$

Integrating and using the boundary condition that at time $\tau = \tau'$, $\zeta = 1$ (this is how τ' is defined) we get

$$\zeta = \zeta_h + (1 - \zeta_h)e^{\frac{-5(\tau - \tau')}{3\zeta_h}}. \tag{4.27}$$

Define $\tau' = 0$ as the starting time, which marks the 'first descending front', ζ_d. In the same manner as for the displaced lower layer there will be a region, which will remain at the initial concentration, below this first front. The front will migrate downwards as follows

$$\zeta_d = \zeta_h + (1 - \zeta_h)e^{-\frac{5}{3}\frac{\tau}{\zeta_h}}. \tag{4.28}$$

We, therefore, have two regions in the upper layer of the space, a lower part, below the descending front ($\zeta_h < \zeta < \zeta_d$), where the concentration is 1, and an uppermost layer ($\zeta_d < \zeta < 1$), where the concentration is changing over time.

Below the descending front

Below the descending front $r = 1$, so the concentration in the plume, subject to the boundary condition that p is continuous across the interface (i.e. $p_l(\zeta = \zeta_h)$ in the upper layer is $p_u(\zeta = \zeta_h)$ from our lower layer equations) is

$$r = 1, \quad p = 1 - \frac{3(1 - p(\zeta_h))\zeta_h}{5\zeta - 2\zeta_h}, \quad \zeta_h < \zeta < \zeta_d. \tag{4.29}$$

Above the descending front

This region is more difficult to model, because the background concentration r changes over time and is not constant with height. From (4.24) for the upper layer we know that r is constant along the position defined by

$$\zeta = \zeta_h + (1 - \zeta_h)e^{\frac{5(\tau - \tau')}{3\zeta_h}}, \tag{4.30}$$

where τ' is the time when this concentration front is at the top of the chamber,

$$\tau' = \tau - \frac{3\zeta_h}{5} ln\left(\frac{\zeta - \zeta_h}{1 - \zeta_h}\right). \tag{4.31}$$

Therefore, at some height ζ and time τ, the background concentration $r(\zeta, \tau)$ is the same as the background concentration $r(1, \tau')$ at the top of the room, which, in turn, is the concentration in the plume at the top of the room at time τ', i.e.

$$r(\zeta, \tau) = r(1, \tau') = p(1, \tau'). \tag{4.32}$$

Hence the plume concentration equation can be written as

$$\frac{dp}{d\zeta} = \frac{p\left(\zeta = 1, \tau = \tau - \frac{3\zeta_h}{5} ln\left(\frac{\zeta - \zeta_h}{1 - \zeta_h}\right)\right) - p(\zeta, \tau)}{\zeta - \frac{2}{5}\zeta_h}, \tag{4.33}$$

which has the general solution

$$p(\zeta) = \frac{5\int_{\zeta_d}^{\zeta} r(\zeta')d\zeta' + p(\zeta_d)(5\zeta_d - 2\zeta_h)}{5\zeta - 2\zeta_h}, \qquad r(\zeta, \tau) = p(1, \tau'). \tag{4.34}$$

Consider the integral form of conservation equation for the contaminant in the region above the descending front

$$\frac{d}{dt}\left(\int_{\zeta_d}^{1} r d\zeta\right) = q(\zeta=\zeta_d)p(\zeta=\zeta_d) - q_{out}r(\zeta=1). \tag{4.35}$$

Noting that $r(1,\tau) = p(1,\tau)$ and defining $r^* = \int_{\zeta_d}^{1} r d\zeta$ (4.33) can be written as

$$\frac{dr^*}{d\tau} = f(\tau) - c_1 r^*, \tag{4.36}$$

where

$$f(\tau) = p(\zeta_d)\left(\frac{5(1-\zeta_d)}{5-2\zeta} + \frac{5(\zeta_d-\zeta)}{3\zeta}\right), \qquad c_1 = \frac{5}{5-2\zeta}. \tag{4.37}$$

The general solution to (4.34) and (4.35) is

$$r^* = \frac{\int (e^{c_1\tau} f(\tau)) d\tau + D}{e^{c_1\tau}}. \tag{4.38}$$

For the well mixed lower layer case the solution is:

$$r^* = C_1 e^{(\frac{5\tau}{2\zeta-5})} - \frac{\zeta-1}{7\zeta-5}\left(5\zeta e^{(\frac{-\tau(7\zeta-5)}{\zeta(2\zeta-5)})} - 7\zeta e^{(\frac{-25\tau(\zeta-1)}{3\zeta(2\zeta-5)})} + 5e^{(\frac{-25\tau(\zeta-1)}{3\zeta(2\zeta-5)})}\right)e^{(\frac{5\tau}{2\zeta-5})}, \tag{4.39}$$

where for the initial condition $r^*(\tau=0) = 0$

$$C_1 = \frac{(\zeta-1)(5-2\zeta)}{7\zeta-5}. \tag{4.40}$$

Unfortunately, due to the difficulty in solving equation(4.18) we cannot find an analytic solution for the displaced lower layer case. Instead we integrate (4.16) and (4.33) numerically and present the results of this semi-analytical result.

Figure 4.3 shows the average concentration within the space for the three cases: (a) an entirely well mixed room, (b) a well mixed lower layer, (c) a displaced lower layer, for three values for the interface height $\zeta_h = 0.2, 0.5$ and 0.8.

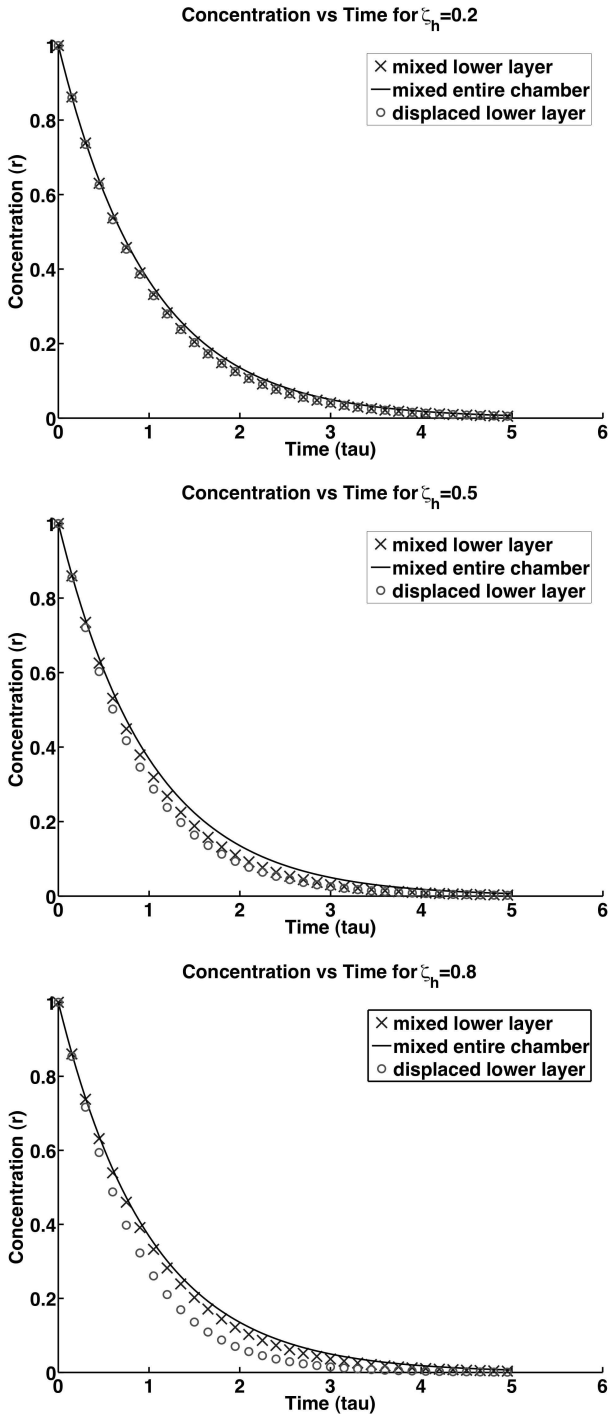

Figure 4.3: Comparison of Concentrations averaged over the whole height of the box. Well-Mixed Entire(–), Well-Mixed Lower Layer(×), Displaced Lower Layer(∘) vs Time for $\zeta_h = 0.2, 0.5, 0.8$

We present the entirely well mixed room case because first, it allows us to compare the efficiency of contaminant removal of a displacement ventilation system to that of a traditional mixing system. Second, it allows us to discuss the validity of the 'well-mixed' assumption. This assumption is typically used in building simulations, which treat each room as a well mixed space that communicates with its neighboring spaces via integral conservation laws. It is widely believed that this assumption is probably not a good one for displacement ventilated spaces due to the vertical non uniformity.

The first and probably most surprising thing to note from figure 4.3 is that the well mixed assumption matches the other models in accounting for the global amount of contaminant within the room. The differences become larger between ideal displacement and the fully mixed model as the interface height increases. Therefore, this suggests that displacement ventilation only offers a small benefit in removing a contaminant over mixing ventilation, in terms of the total amount of contaminant in the room.

4.3.5 Comparison with Kaye and Hunt (2006)

In this section we compare the results of this paper with those of Kaye and Hunt (2006), who assumed perfect mixing in both the upper and lower layers. Since the average concentrations are approximately the same (figure(4.3)), we only compare the model where we assume a well mixed lower layer. The concentration in the lower layer is given by (4.17). We, therefore, define the decay rate of the lower layer as $\phi_{low} = \frac{1}{\zeta}$, which is identical to the decay rate of the lower layer in Kaye and Hunt (2006) (when rewritten with the current nondimensionalisation). This should be obvious since the mechanism for pollutant removal from the lower layer is identical for our well mixed model and that of Kaye and Hunt (2006). Therefore, any differences between the models can only occur in the upper layer. The average concentration of the upper layer is given by

$$\bar{c}_u = \frac{1}{1-\zeta}\bigg((\zeta_d - \zeta_h) + r^*\bigg), \tag{4.41}$$

which can be written as

$$\bar{c}_u = \frac{1}{7\zeta - 5}\bigg((2\zeta - 5))e^{\frac{-5}{5-2\zeta}\tau} + 5\zeta e^{\frac{-\tau}{\zeta}}\bigg). \tag{4.42}$$

Following Kaye and Hunt (2006) we define the upper layer decay rate as $\phi_{up} = \frac{5}{5-2\zeta}$. This is different from that of Kaye and Hunt (2006), which is $\phi_{ip}^{HK} = \frac{1}{1-\zeta}$ (again converted to the current nondimensionalisation). It can readily be seen that $\phi_{up} < \phi_{up}^{HK}$ for all values of ζ, which suggests that the upper layer flushes pollutant out more quickly in the Hunt & Kaye model than the present one. Therefore, we expect the Kaye and Hunt (2006) model to remove contaminant more quickly, which is precisely what is observed and discussed below.

Combining the lower and upper layer concentrations, the average concentration in the entire box is given by

$$\bar{c} = \frac{(-2\zeta^2 + 7\zeta - 5)e^{-\frac{5}{5-2\zeta}\tau} + 2\zeta^2 e^{-\frac{\tau}{\zeta}}}{7\zeta - 5}. \tag{4.43}$$

Figure 4.4 depicts isocontours of concentration across a wide range of interface heights ($0.1 < \zeta < 0.9$) against time for (a) the well mixed lower layer model (b) the model of Kaye and Hunt (2006) and (c) the difference between these two. The plots displayed in figure 4.3 are cross sectional cuts of these isocontours for $\zeta = 0.2, 0.5, 0.8$. Qualitatively the models behave similarly with the most rapid decay corresponding to values of $\zeta = 0.5$ in both cases. This value of ζ also acts as a line of up/down quasi-symmetry (i.e. the average concentration for $\zeta = 0.5 + x'$ is approximately the same as that for $\zeta = 0.5 - x'$). It is a line of exact symmetry for Hunt & Kaye's model. However, it is only approximately true for our model. Quantitatively, there is some disagreement. The average concentrations predicted by Hunt & Kaye's model are always smaller than those of our model as illustrated in figure 4.4 (c). The peak differences occur just after $\tau = 1$ for

interfaces close to the middle of the room and then become smaller at later times. This quantitative disagreement may not appear too significant with the maximum values corresponding to 6% of the initial concentration. However these differences can be as large as 33% when compared to each other.

Since the concentration in the lower layer is identical for our model and that of Kaye and Hunt (2006) any differences that are observed can only be attributed to the concentration in the upper layer. Figure 4.5 displays equivalent isocontours to those of figure 4.4, but only for the upper layer average concentration. Unlike the plots of figure 4.4, the results predicted by the two models differ both qualitatively and quantitatively. There is still an up down symmetry for Hunt & Kaye's model, but this symmetry is broken in the present model, with the concentrations in the upper layer increasing monotonically with interface height. The quantitative differences between the models is also large and increases with higher values of ζ, peaking close to $\tau = 1$ at a value of 0.25. Recall though, that such large differences were not observed when considering the average quantity of contaminant in the whole box. This is because, while the largest differences in upper layer concentration occur for higher values of ζ, this also implies that the weighted effect (i.e. $\bar{c}_{up}(1-\zeta)$) on the total average contaminant is smaller.

In order to understand why these differences in the average concentration of the upper layer occur it is essential to understand the vertical distribution of contaminant within the upper layer. This is discussed in detail in §4.4.

4.4 Numerical Method

The analytical solution provides sufficient information to calculate the total amount of contaminant and provides an approximate description of the contaminant distribution within the space. However, the detailed structure of the upper layer above the descending front is not resolved and in order to determine the vertical concentration profile we solve the system of equations using a modifica-

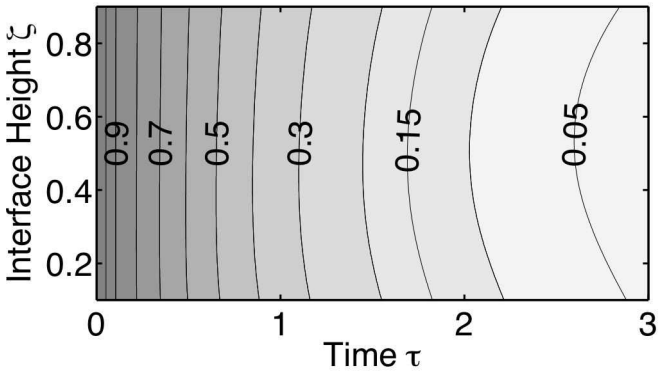

(a)

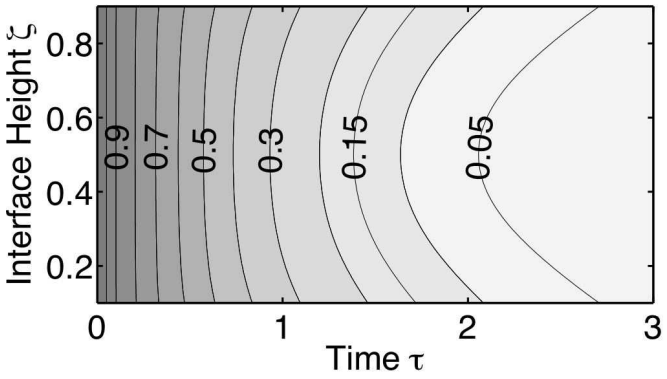

(b)

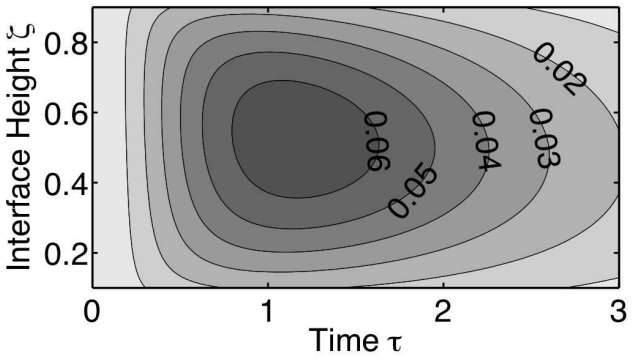

(c)

Figure 4.4: Isocontour plot of the average concentration across the entire box for time against interface height. (a) Our Solution (b) Kaye and Hunt (2006) (c) The Difference between (a) and (b)

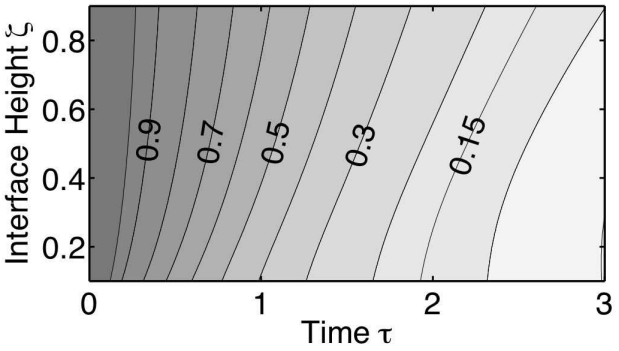

(a)

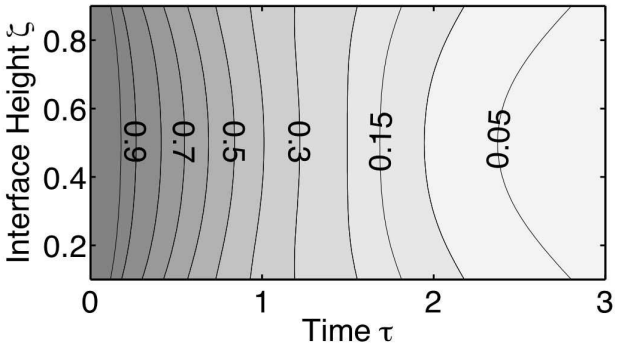

(b)

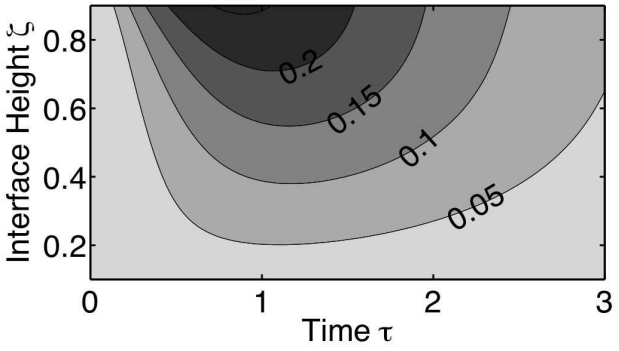

(c)

Figure 4.5: Isocontour plot of the average concentration in the upper layer against time for a full range of interface heights. (a) Present solution (well-mixed lower layer) ((b) Kaye and Hunt (2006) (c) The difference between (a) and (b)

tion of a numerical scheme originally developed by Germeles (1975). This scheme is described in detail in Chapter 3.

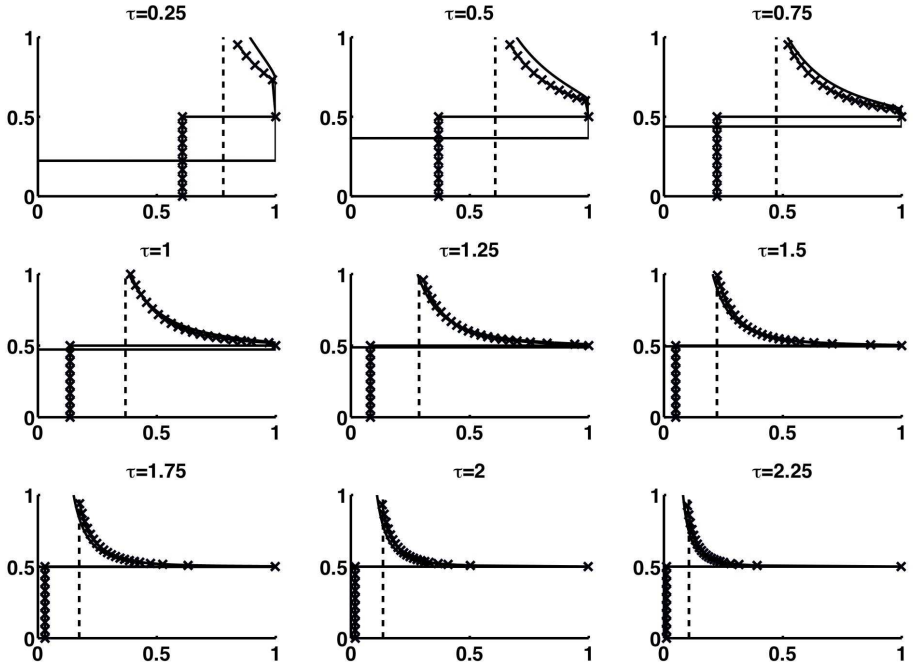

Figure 4.6: Comparison of concentration profiles at intervals of 0.25 τ for $\zeta_h = 0.5$ for an entirely well mixed space (– –), a well mixed lower layer (–) and a displaced lower layer (x-). The x-axis represents concentration and the y-axis height in the room

Figure 4.6 displays the vertical concentration profiles computed with the Germeles algorithm for an interface height corresponding to half the height of the room. Both displaced and well-mixed lower layer cases are considered. For the sake of comparison the case of an entirely well mixed room (vertical dashed line) is also shown. In the previous section we showed that the average reduction of contaminant is approximately the same for all three cases. Here, however, we see that the vertical distribution of contaminant is very different for displacement and mixing ventilation.

The concentration at the top of the room for all three models is approx-

imately the same at all times. Therefore, the concentration of contaminant being extracted is about the same in all cases, which is why the reduction in average concentration does not vary significantly between the three systems. On the other hand, the 'occupied' lower layer concentration is always less in both two-layer models than in the entirely well mixed case, which is clearly desirable. However, the concentration of contaminant in the upper layer is always higher. Further, the peak in contaminant concentration is always located at and just above the height of the interface. This stems from the background velocity field - see figure 4.7. In the upper layer the flow is all downward, while in the lower layer it is upwards. The interface dividing the upper and lower layers corresponds to the height where the background velocity is zero. Therefore, the high initial concentration in the upper layer is continuously being pushed down towards the interface, causing the peak level to occur there.

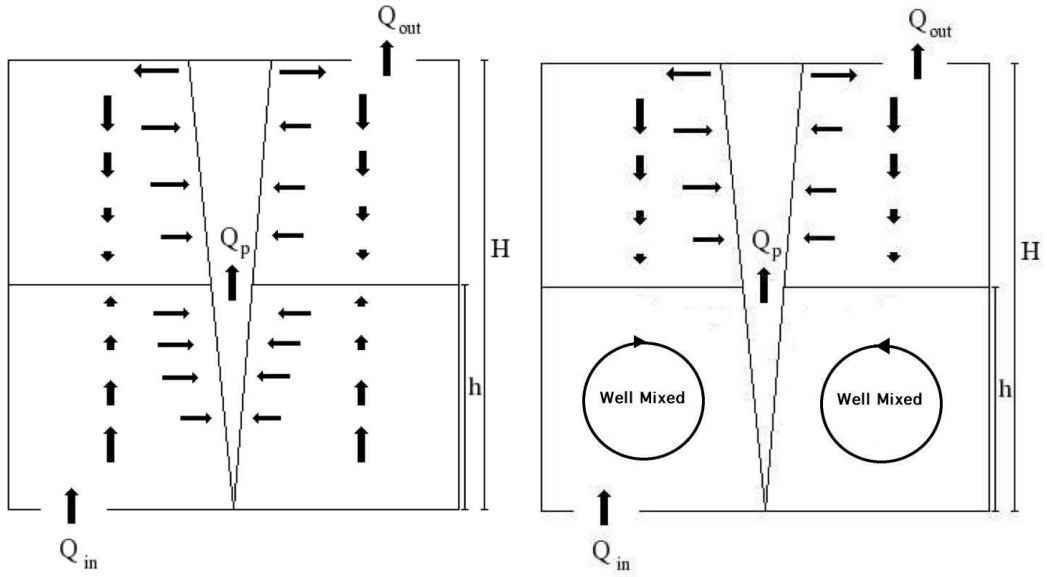

Figure 4.7: Background velocity fields for the displaced and well mixed lower layer cases

4.5 Experiments

A series of analogue laboratory experiments, based on the salt bath technique (Linden (1999)) was conducted to compare to the results of the theoretical models. The space is represented by a plexiglass tank (30x30x40 cm) within which there is a low momentum plume source (Hunt et al. (2000)). There are openings on the lower and upper surfaces through which we pump and extract water. The plume source is located at the top centre of the tank and injects negatively buoyant (heavier) salt water. The geometry is inverted compared to the model described in the previous sections. Due to the Boussinesq behaviour of the system this inversion has no effect on the dynamics. Freshwater is pumped in through the upper openings using an aquarium pump connected to a reservoir of freshwater. The saltier (equivalent to the warmer in our model) water is extracted from the lower vents. By adjusting the flow rate into the tank we can adjust the interface height for a given value of source buoyancy flux.

In order to achieve ideal displacement it is desirable to have fluid with the least possible momentum entering the space in order to minimise mixing in the upper (lower in model) layer. However, due to space restrictions, which also occur in real buildings, there is a limit to how much area can be dedicated to inlet vents. In our experiments there are twelve 2.5 cm diameter holes spread across the top of the plexiglass tank, which act as inlet vents. Further, in order to reduce the momentum of the incoming fluid, horizontal struts, 5 cm wide, are placed 2.5 cm above the inlet holes. These reduce the momentum and deflect the incoming flow horizontally.

Two reservoirs of freshwater supply the tank. One is 'contaminated' with food dye, while the other is uncontaminated. Initially the system is fed with contaminated fluid and the plume is turned on until the system reaches steady state and is uniformly contaminated. Then the source of ambient fluid is switched to the uncontaminated reservoir. Concentration measurements were obtained by dye

concentration. The plexiglass tank was backlit with a fluorescent light source and the experiments were recorded and analysed with the image processing package DigImage. The light intensity at each point in the tank is recorded and correlated to the concentration of contaminant present. Using pre-determined calibration curves of light intensity against concentration the local concentration of contaminant within the box can be inferred. The vertical concentration profiles are then horizontally averaged across the entire width of the tank, excluding the zone with the plume in order to reduce noise. The standard deviation associated with this averaging process is small (typically less than 5 % of the average value), suggesting good accuracy.

4.6 Experimental Results

Figure 4.8 displays the results from a series of experiments for an interface at $0.25H$, $0.5H$ and $0.75H$. The measured levels of contaminant over time are compared to those predicted by the theoretical models. As can be seen the qualitative comparison is good. The lower layer seems to be better described by the well mixed model for the two lower interfaces, although some displacement behaviour is definitely visible, particularly at early times. The quantitative disagreement can probably be attributed to the fact that it is virtually impossible to create an ideal displacement ventilation. The finite area and momentum of the fluid entering through the vents inevitably causes some level of mixing, which, as mentioned above, we attempted to minimise by placing the deflecting plates above the inlets. The location of the inlets also plays an important role, because certain parts of the lower layer will become contaminated faster than others and so the plume will not necessarily be exposed to average amount of contaminant instantly. This is very much an issue for real displacement ventilation systems where such considerations are important. However, despite these shortcomings of the experiments we get good quantitative agreement.

One of the most important features present is the peak in concentration of contaminant at the interface level. Quantitatively the agreement is not all that good here and this is probably due to the finite thickness of the interface, which can exchange fluid with the surrounding space, thus loosing high concentration contaminant by entrainment into the plume and replenishing it with lower concentration fluid from the lower and upper layers. However, this concentration peak is clearly observed to be a robust feature of the experiments and marks a significant difference from well-mixed ventilation.

4.7 Discussion

The present study looks at the transport of a contaminant in a displacement ventilation system with a single source of buoyancy. In order to study this problem the 'step down' method is used, where the space is initially filled uniformly with contaminant. Then fresh uncontaminated air is introduced into the space through the vent. For a passive contaminant the results are equivalent and exactly opposite to the 'step up' method, where contaminant enters an initially uncontaminated space.

The analytical solutions indicate that this problem displays some interesting and perhaps unexpected behaviour. It is widely believed that along with its efficiency at removing buoyancy from a space, displacement ventilation is also better at removing a contaminant. However, the present study suggests that this may not be true. Displacement ventilation takes advantage of the natural stratification that will arise in a space, extracting air of the warmest temperature, that naturally rises, from the top of the room. Nevertheless this air that is being extracted may not be the most contaminated since the velocity field for these low energy systems advects contaminants towards the interface between the lower and upper layers. Thus the contaminant extraction process does not utilize the mechanism that offers displacement ventilation its improved energy efficiency. Instead, the

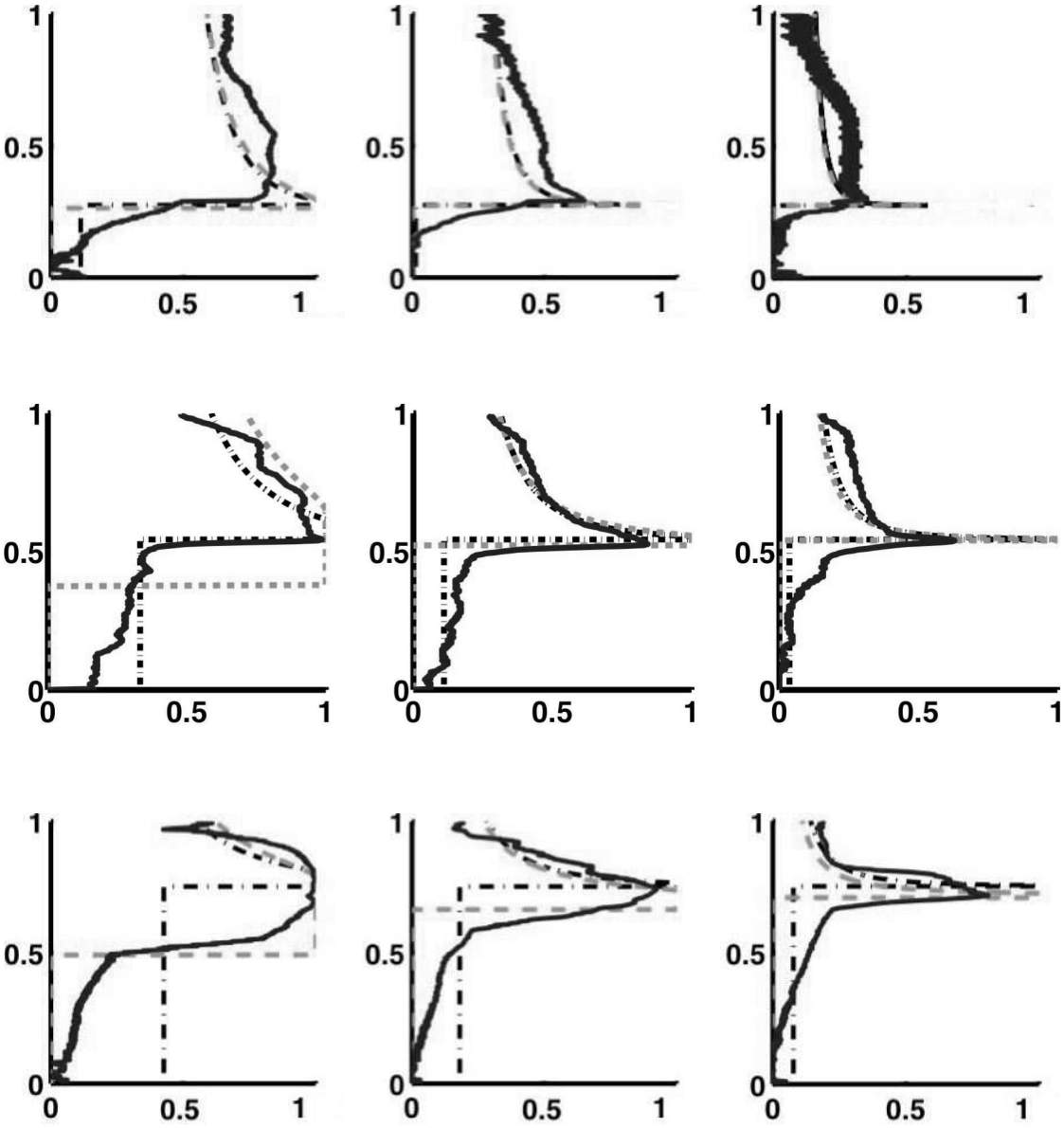

Figure 4.8: Vertical concentration profiles for $\zeta_h = 0.25$ (top row), $\zeta_h = 0.5$ (middle row) and $\zeta_h = 0.75$ (bottom row) at time intervals of 0.6 τ, 1.2 τ and 1.8 τ. Experiments (–), Well Mixed Lower Layer (-.), Displaced Lower Layer (- -)

concentration at the outlet vent is relatively insensitive to the ventilation scheme, giving similar overall flushing rates.

In §4.4 and §4.5 it is observed that the peak level of contaminant for this 'step down' analysis occurs at the interface between the upper and lower layers. Therefore, depending on the location of this interface, while people sitting down may be in the clean lower layer, someone who stands up may have their head at the peak concentration height. As such the height of the interface is not only important from a comfort perspective, but also becomes a critical parameter in the design for IAQ. Another issue to consider is the following. In this experiment we have filled the room with contaminant initially and then introduced fresh air through the lower vents. What if the source of contaminant is the ventilation system? This corresponds to the 'step-up' case discussed above. Now the exact opposite system to that we just described exists, which means that the highest concentration of contaminant will exist in the 'occupied' lower layer.

There is a simple explanation as to why displacement ventilation does not exhibit the same benefits for removal of contaminants and it does for heat. The efficiency of displacement ventilation at removing heat stems from the fact that warmest air is always extracted from the top of the room. In terms of a passive contaminant this high efficiency mechanism does not take place since the location of maximum contaminant and temperature does not coincide.

Finally, we have compared displacement and mixing systems for the same volume flow rate. In practice displacement ventilation offers two methods of energy savings. Either the incoming air is introduced at a warmer temperature than with a mixing system, thus saving energy on the cooling system, or the incoming flow rate could be reduced, thus saving on fan power. This study suggests that the first option is the more sensible one in terms of IAQ since a lower flow rate will yield an even lower contaminant removal efficiency. It is often also the most sensible from an energy approach since cooling is typically more expensive than fan power.

It is important to point out that the flow modeled in this paper is forced

displacement flow. However, there is no reason to expect the behaviour to be any different for the buoyancy driven flow such as displacement natural ventilation. The only difference is that in one case the flow is forced through the space and the plume only provides the resulting stratification, while for natural ventilation the buoyancy provided by the plume leads to a stratification that in turn causes the flow through the system. Once both systems reach steady state they behave in a similar manner and therefore all the analysis and observations made should hold for both systems.

For the other common case if an isolated release at a specific location within a space this model may not be applicable. While it is widely believed that studying the 'step up', 'step down' and isolated release cases are equivalent (Coffee & Hunt 2005), we believe that displacement ventilation does not dilute the space as effectively as mixing ventilation. Therefore, local concentrations of contaminant should be higher and the efficiency of removal will depend on the location of the source.

The text in chapter 4, in part, has been accepted for publication in the *Journal of Fluid Mechanics*, ('Contaminants in Ventilated Filling Boxes') 2007 (D Bolster & PF Linden). I was the primary researcher on this project.

5

Contaminated Ventilated Spaces - Particulate Contaminants

5.1 Abstract

In this work we study the transport of particulate contaminants in a displacement-ventilated space. Representing heat sources as ideal sources of buoyancy, analytical models are developed that allow us to compare the average efficiency of contaminant removal between traditional and modern low energy systems. We considered three types of contamination scenarios - removal of an initially uniform contaminant (step-down), contaminant entering a room via the ventilation system (step-up) and a point source contaminant within the room. We find that only considering average concentrations can be deceptive in evaluating an occupant's exposure to contaminants, because significant vertical gradients in the contaminant field can exist within the displacement ventilated space. While the main focus of this work is on particles where the dominant mode of deposition is by gravitational settling, we also include a section with additional deposition mechanisms and show that the qualitative observations we make for gravitationally dominated particles carry over to cases where additional mechanisms must be included.

5.2 Introduction

In the previous chapter we studied the transport of a passive contaminant in a displacement ventilated space and while this is important in understanding ventilation system efficiency, there is another type of contaminant that must also be considered - particulates. The concentration and composition of indoor particles are major determinants of environmental quality, since inhalation exposure poses potentially adverse effects on people's health. Such particles can penetrate into buildings from the outdoors or can be emitted from indoor sources such as smoking, cooking, occupants, building materials or even during a deliberate malicious release. The study of particulate matter is more complicated than that of passive contaminants. With particles there are various other phenomena that can occur - deposition, resuspension, coagulation and filtration, which are all difficult to model and quantify. In particular, gravitational settling raises the concern that particles may not be removed as efficiently from a system that is extracting air from the top of a room, which is typical of low-energy ventilation systems.

Much previous work has been done in the field of contaminant modelling in buildings. Most of it is based on reduced order zonal models (Feustel (1999), Schneider et al. (1999) and Zhao et al. (2004b)). In zonal models, buildings are typically broken into several zones, which interact with one another. Each of the zones is assumed to be well mixed at all times.

This approximation of uniform and instantaneous mixing is very convenient and can often be justified for cases with strong internal air motion. However, this assumption may not always be appropriate, particularly in low energy ventilation systems where there is a deliberate creation of nonuniformity in temperature. In such cases exposure to the contaminants may depend significantly on a person's location within a space. Ozkaynak et al. (1982) found that pollutant levels in a kitchen with the oven on depended heavily on the sampling location. Rodes et al. (1991b) discovered that personal sampling almost always reveals a higher exposure

to contaminants that would be predicted from indoor air monitoring that assumes perfect mixing. Lambert et al. (1993) showed that the levels of suspended particles in a non-smoking section of a restaurant were 40-65 % less than that in the smoking section.

Various CFD studies have also been conducted (e.g. Holmberg and Li (1998), Zhang and Chen (2006) and Zhao et al. (2004b)) on the transport of contaminants in specific building geometries. However, even with current computer speeds, full scale simulations can be prohibitively expensive. Additionally, while useful in specific cases, these studies do not always provide practical information about the general behaviour of contaminants in low-energy ventilation systems.

In general, an efficient manner of air quality control is to remove the contaminant before it has time to mix throughout the space, which means extracting it from near the source, where the concentration will be highest. Therefore, it is important to understand how the contaminant will disperse in the room. In most indoor environments the transport of the pollutant is advective, since the diffusion rate is relatively small. An approximate diffusion timescale is 5 days for a typical space, yet from experience we know that the actual dispersion rate is more on the order of minutes or hours.

5.3 Mathematical Models

In order to understand the fate of particles in a ventilated space it is necessary to understand the flow within the space. As mentioned previously, many modern low-energy ventilation schemes, such as displacement or natural ventilation, exploit vertical temperature stratification in a space. So it is critical to understand how heat sources within a ventilated enclosure stratify that space. Many heat sources within a building can be regarded as localised and can often be modeled as pure sources of buoyancy. Using the plume equations developed by Morton et al. (1956) along with the 'filling' (Baines and Turner (1969)) and

'emptying-filling' box models (Linden et al. (1990)) we can model the flow in such low energy buildings, and calculate the transport of particulate contaminants within the interior space.

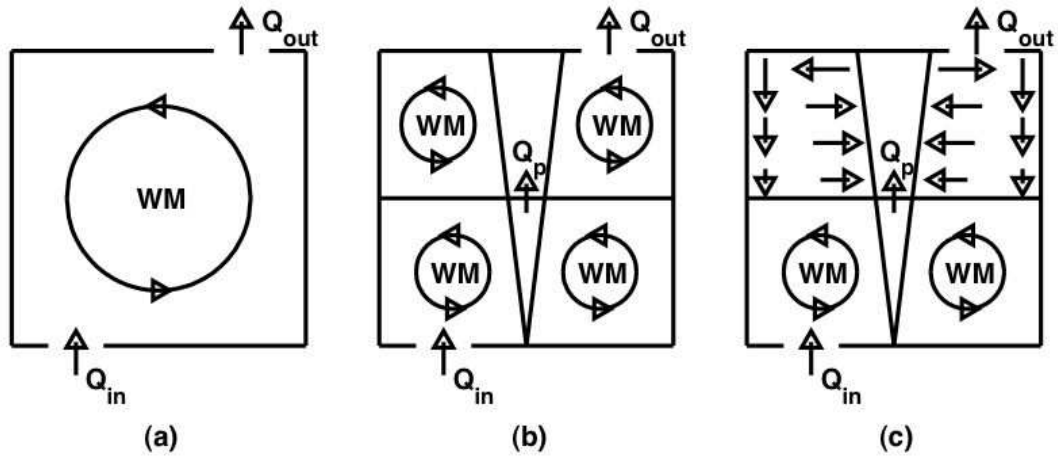

Figure 5.1: Three models of ventilation. (a) Traditional Mixing System, (b) and (c) Low Energy Displacement Ventilation. WM means well mixed. The arrows in (c) depict the general direction of flow

Figure 5.1 shows a schematic of the three models that we consider. We analyse two low-energy ventilation models ((b) and (c)) and one traditional mixing model (a). In the low-energy models we consider the space either mechanically or naturally ventilated with fresh air entering through a low level vent and hot buoyant air leaving via a vent at high level. Heat sources in the space are represented by ideal plumes.

5.3.1 Contamination Scenarios Considered

For each of the models depicted in figure 5.1 , we consider three types of contamination situations:

1. Step Down (Natural Attenuation) : This is the situation where a space is initially uniformly filled with a contaminant and fresh, uncontaminated air is introduced into the space.

2. Step Up (External Contaminant) : Here we consider a space that is initially uncontaminated. Then a contaminant is introduced in through the ventilation system

3. Isolated Source in Plume : Here we consider a space that is initially uncontaminated. Then a contaminant is introduced as a point source located within the plume. We choose this location because people are often the source of heat as well as the source of contaminants in buildings. Additionally, it is also the only type of point source that we can currently adequately describe with our model.

5.3.2 Model (a) - Entirely Well Mixed Space

In this model we treat the entire room as well mixed (figure 5.1(a)). The reason for this is twofold. First, it allows us to compare low-energy ventilation systems to traditional mixing systems, which minimize stratification by mixing the space. Second, many building software packages treat buildings as networks of spaces that are each assumed to be well mixed. As many researchers have previously pointed out (e.g. Baughman et al. (1994), Klepeis (1999)), this assumption is questionable and so we test it here. The concentration in a well mixed space, K_{wm}, satisfies the conservation equation

$$\frac{dK_{wm}}{dt} = -\frac{Q_{in} + Q_f}{SH} K_{wm} + \frac{Q_{in}}{SH} K_{in} + \frac{Q_{in} K_s}{SH}, \tag{5.1}$$

where Q_{in} is the flow rate into the space, $Q_{fall} = v_{fall} S$ is defined as the settling flow rate, v_{fall} is the settling velocity, assumed here to be the Stokes settling velocity, K_{in} is the concentration of contaminant in the incoming air, K_s is the concentration associated with a point source (defined in greater detail in appendix A), S is the room cross sectional area and H is the height of the room. Q_{fall} quantifies the amount of deposition that will take place. We neglect deposition of particles to the ceiling and sidewalls and assume that particles settle out of the

lower and upper layers at this settling velocity. This is a reasonable assumption for larger particles ($> 0.1\mu m$), where the predominant mechanism of deposition is gravitational settling and Brownian effects are negligible (Lai and Nazaroff (2000)). For ultrafine particles ($< 0.1\mu m$) deposition will also be driven by Brownian effects. However, for such particles gravitational effects are small and the dominant mode of transport through the ventilated space will be advection and similar to that of a passive contaminant (Bolster and Linden (2007), Zhang and Chen (2006)).

5.3.3 Model (b) - Well Mixed Two Layer Model

In this section we consider model (b) from figure 5.1. We take an approach similar to that of Kaye & Hunt (2005) and assume that the upper and lower layers are always well mixed. The justification for this assumption is that the plume will cause some mixing in the upper layer. However, in a previous study on passive contaminants (Bolster and Linden (2007)) we found that this assumption does not describe the complete dynamics of the system. None the less, at least for passive contaminants, it has been shown to be an adequate model (Kaye and Hunt (2006)) and is very appealing due to its simplicity. We also assume that the lower layer is well mixed. Since the incoming flow will have a finite amount of momentum, a certain amount of mixing will be inevitable and in our previous work on passive contaminants we showed that this is a reasonable assumption. Thus the governing equations for conservation of contaminant in each of the layers are

$$\frac{dK_l}{dt} = -\left(\frac{Q_p + Q_{fall}}{Sh}\right)K_l + \frac{Q_{fall}}{Sh}K_u + \frac{Q_{in}}{Sh}K_{in}$$

$$\frac{dK_u}{dt} = \frac{Q_p}{S(H-h)}K_l - \left(\frac{Q_{fall} + Q_p}{S(H-h)}\right)K_u + \frac{Q_p K_s}{S(H-h)} \tag{5.2}$$

where K_l and K_u are the concentrations of contaminant in the lower and upper layers respectively. h is the height of the lower layer and Q_p is the plume flow rate across the interface and at steady state $Q_p = Q_{in}$.

5.3.4 Model (c) - Mixed Lower Layer, Unmixed Upper Layer

Here we consider model (c) from figure 5.1 For a well-mixed lower layer and unmixed upper layer the conservation equations for the upper and lower layer are slightly modified from the previous section. Instead of removing fluid of the average concentration of contaminant, we must now account for the fact that the upper layer can have concentration gradients in it, thus leading to the following conservation equations

$$\frac{dK_l}{dt} = -\left(\frac{Q_p + Q_{fall}}{Sh}\right)K_l + \frac{Q_{fall}}{Sh}K_u(z=h) + \frac{Q_{in}}{Sh}K_{in},$$

$$\frac{d\bar{K}_u}{dt} = \frac{Q_p}{S(H-h)}\Big(K_l - K_u(z=H)\Big) - \left(\frac{Q_{fall}}{S(H-h)}\right)K_u(z=h) + \frac{Q_p K_s}{S(H-h)}. \tag{5.3}$$

In order to understand the dynamics of the upper layer it is important to understand the flow within the space, which is determined by coupling the plume flow with the environment outside the plume. Exact details of this are given in Bolster and Linden (2007).

Contaminant with concentration $K(z)$ in the room is entrained into the plume, which has contaminant concentration $P(z)$. Since the vertical velocities in the plume are typically much larger than those in the background, we neglect the effect of gravitational settling within the plume and only consider it in the ambient. Conservation of contaminant volume flux in the plume can be expressed as

$$\frac{dP}{dz} = \frac{2\epsilon M^{\frac{1}{2}}(K-P)}{Q}, \tag{5.4}$$

which in the lower and upper layers can be written as

$$\frac{dP}{dz} = \frac{5}{3z}(K-P) \quad 0 < z < h,$$

$$\frac{dP}{dz} = \frac{1}{z - \frac{2}{5}h}(K - P) \quad h < z < H. \tag{5.5}$$

In addition, neglecting diffusion, the room contaminant conservation equation is

$$\frac{\partial K}{\partial t} + w_c \frac{\partial K}{\partial z} = 0, \tag{5.6}$$

where w_c is the velocity of the contaminant field, which includes the effect of gravitational settling. In the upper layer this can be shown to be

$$w_c = \frac{\pi}{A}\left(2\epsilon\left(\frac{9\epsilon}{10}\right)^{\frac{1}{3}} F_0^{\frac{1}{3}} h^{\frac{2}{3}}\right)(h - z) - v_{fall}, \tag{5.7}$$

where v_{fall} is the settling velocity, assumed to be the Stokes settling velocity of a spherical particle.

5.4 Nondimensionalisation

We nondimensionalise as follows:

$$t = \tau \frac{SH}{Q_p}, \qquad K = K_{ref}\kappa, \qquad h = H\zeta, \tag{5.8}$$

where K_{ref} is a reference concentration, which will be different for each of the three situations considered. For the step-down method, it is the initial concentration of contaminant in the space($K_{ref} = K_0$). For the step-up system it is the concentration of contaminant entering the spaces ($K_{ref} = K_{in}$) and for the point source case it is the concentration of the source($K_{ref} = K_{point}$). This results in the following dimensionless equations:

(a)

$$\frac{d\kappa}{d\tau} = -(1 + \alpha)\kappa + \kappa_{in} + \kappa_s, \tag{5.9}$$

(b)

$$\frac{d\kappa_l}{d\tau} = \frac{-(1 + \alpha)\kappa_l + \alpha\kappa_u + \kappa_{in}}{\zeta},$$

$$\frac{d\kappa_u}{d\tau} = \frac{\kappa_l - (1+\alpha)\kappa_u + \kappa_s}{1-\zeta}, \tag{5.10}$$

(c)

$$\frac{d\bar{\kappa}_l}{d\tau} = \frac{\alpha}{\zeta}\Big(\kappa_u(\zeta=\zeta_h) - \bar{\kappa}_l\Big) + \frac{1}{\zeta}\Big(\kappa_{in} - \bar{\kappa}_l\Big),$$

$$\frac{d\bar{\kappa}_u}{d\tau} = \frac{-\alpha}{1-\zeta}\Big(\kappa_u(\zeta=\zeta_h)\Big) + \frac{1}{1-\zeta}\Big(\bar{\kappa}_l - \kappa_u(\zeta=1) + \kappa_s\Big). \tag{5.11}$$

where $\alpha = \frac{Q_{fall}}{Q_p}$, which is a dimensionless representation of the particle settling velocity.

5.5 Results

All of the above equations are linear and can be solved analtyically. In this section we present the general solutions to the governing equations without considering the specific contamination conditions. The contamination scenarios mentioned previously will be discussed later in this section.

5.5.1 General Results of Model Equations

Model (a)

The governing equation, (5.9), can be integrated to give the average concentration throughout the room. It is described by a simple exponential equation

$$\kappa^{(a)} = \kappa_o e^{-(1+\alpha)t} + \frac{\kappa_{in} + \kappa_s}{1+\alpha}\Big(1 - e^{-(1+\alpha)t}\Big), \tag{5.12}$$

where κ_o is the initial contaminant concentration in the room and κ_{in} is the concentration of contaminant entering the room.

Model (b)

The system of equations, (5.10), can be solved by Laplace transforms or as an eigenvalue problem. The solution is

$$\kappa_l^{(b)} = \frac{(1+\alpha)\kappa_{in} + \alpha\kappa_s}{\alpha^2+\alpha+1} + e^{-\frac{-(1+\alpha)}{2\zeta(1-\zeta)}\tau}\Bigg(\Bigg(\kappa_o - \frac{(1+\alpha)\kappa_{in} + \alpha\kappa_s}{\alpha^2+\alpha+1}\Bigg)\cosh\left(\frac{A_1\tau}{2\zeta(1-\zeta)}\right)$$

$$+\frac{\kappa_o(\alpha-1+2\zeta)(\alpha^2+\alpha+1) + \kappa_{in}(\alpha^2+1-2\zeta(\alpha^2+\alpha+1)) - \kappa_s(\alpha^2+\alpha)}{A(\alpha^2+\alpha+1)}$$

$$\sinh\left(\frac{A_1\tau}{2\zeta(1-\zeta)}\right)\Bigg), \tag{5.13}$$

$$\kappa_u^{(b)} = \frac{\kappa_{in} + (1+\alpha)\kappa_s}{\alpha^2+\alpha+1} + e^{-\frac{-(1+\alpha)}{2\zeta(1-\zeta)}\tau}\Bigg(\Bigg(\kappa_o - \frac{\kappa_{in} + (1+\alpha)\kappa_s}{\alpha^2+\alpha+1}\Bigg)\cosh\left(\frac{A_1\tau}{2\zeta(1-\zeta)}\right)$$

$$+\frac{\kappa_o(\alpha+1-2\zeta\alpha)(\alpha^2+\alpha+1) + \kappa_{in}(-1-\alpha) - \kappa_s(\alpha^2+2\alpha+1-2\zeta(\alpha^2+\alpha+1))}{A(\alpha^2+\alpha+1)}$$

$$\sinh\left(\frac{A_1\tau}{2\zeta(1-\zeta)}\right)\Bigg), \tag{5.14}$$

where

$$A_1 := \sqrt{1+2\alpha+\alpha^2+4\zeta^2+4\zeta^2\alpha+4\zeta^2\alpha^2-4\alpha\zeta-4\zeta-4\zeta\alpha^2}. \tag{5.15}$$

In the limit of $\alpha \to 0$, $\kappa_{in} = 0$, and in the current nondimensionalisation this solution collapses to that of Kaye and Hunt (2006).

Model (c)

In order to close this system of equations, (5.11) we must find analytical expressions for $\kappa_u^{(c)}(\zeta = \zeta_h, t)$ and $\kappa_u^{(c)}(\zeta = 1, t)$. It is necessary to examine the full temporal evolution of the contaminant transport to determine these quantities.

Because diffusion is being neglected due to high Peclet numbers, the method of characteristics can be used to determine the concentration of contaminant in the upper layer at the interface height. This concentration will be that at the top of the room a period τ_d earlier, where τ_d is the time taken for a front of descending particles to travel from the top of the room to the interface. It can be shown from (5.7) that

$$\tau_d = \frac{3}{5}\zeta_h \ln\left(\frac{1-(1-\frac{3}{5}\alpha)\zeta_h}{\zeta-(1-\frac{3}{5}\alpha)\zeta_h}\right). \tag{5.16}$$

Therefore, in order to close this system of equations, the only quantity required is an estimate of the contaminant concentration at the top of the room. Assuming that the plume spreads instantaneously across the entire plan area of the ceiling, and that a perfectly mixed layer forms, we can equate the background concentration to that of the plume at the top of the room (see appendix B)

$$\kappa_u^{(c)}(\zeta = 1, t) = \frac{5(1-\zeta_h)\bar{\kappa}_u(\tau = t) + 3(\bar{\kappa}_l(t = \tau) + \kappa_s)\zeta_h}{5 - 2\zeta_h}\left(\frac{1}{1+\frac{3\alpha\zeta}{5-2\zeta}})\right)$$

$$\kappa_u^{(c)}(\zeta_h, t) = \kappa_u^{(c)}(\zeta = 1, t - \tau_d). \tag{5.17}$$

An analytical solution to this system of equations has been found and can be computed. However, it is very laborious and involves many summations which must be computed and gives very little insight into the physical behaviour of the system. Instead, the equations are solved numerically using a Runge-Kutta scheme, which is more efficient. The solutions of the numerical and analytical systems are identical. [1]

[1] For the interested reader, the analytical solution method is presented in an appendix

5.5.2 Step Down

Here we consider the removal of a uniformly distributed contaminant from the space by introdcuing uncontaminated air in through the ventilation system. In this case $\kappa_{in} = 0$, $\kappa_o = 1$ and $\kappa_s = 0$ which can be substituted into the results presented in the previous section 5.5.1. Figure 5.3 displays a sample of solutions for the average contaminant concentration for each of the three models at three values of interface height, $\zeta = 0.25, 0.5$ and 0.75, and three values of $\alpha = 0.1, 1$ and 10. Except for the case of $\alpha = 10$ and $\zeta = 0.25$ the average amounts of contaminant are similar for the three cases, suggesting that each system exhibits comparable efficiency vis-a-vis overall contaminant removal. This conclusion applies over a wide range of parameter space corresponding to typical physical situations. Although the average concentrations are approximately the same, this does not imply that the vertical concentration profiles are also the same, merely that the concentration being extracted is similar. In the next section of the paper we study these vertical concentration profiles.

Quantity of Particulates Deposited

A quantity that may be useful to know is the percentage of particulate contaminants that escape the room through the upper vent and the percentage that is deposited on the floor. The percentage of contaminant deposited, Γ_{dep}, can be found as the integral of the product concentration and settling flowrate over time

$$\Gamma_{dep} = \int_0^{\tau \to \infty} \kappa_l(\tau')\alpha\zeta d\tau'. \tag{5.18}$$

The quantity Γ_{dep} is a measure of the percentage of contaminant that a person occupying the lower layer will be exposed to, since all deposition occurs in the lower layer.

Figure 5.3 displays Γ_{dep} for all three models over a wide range of parameter

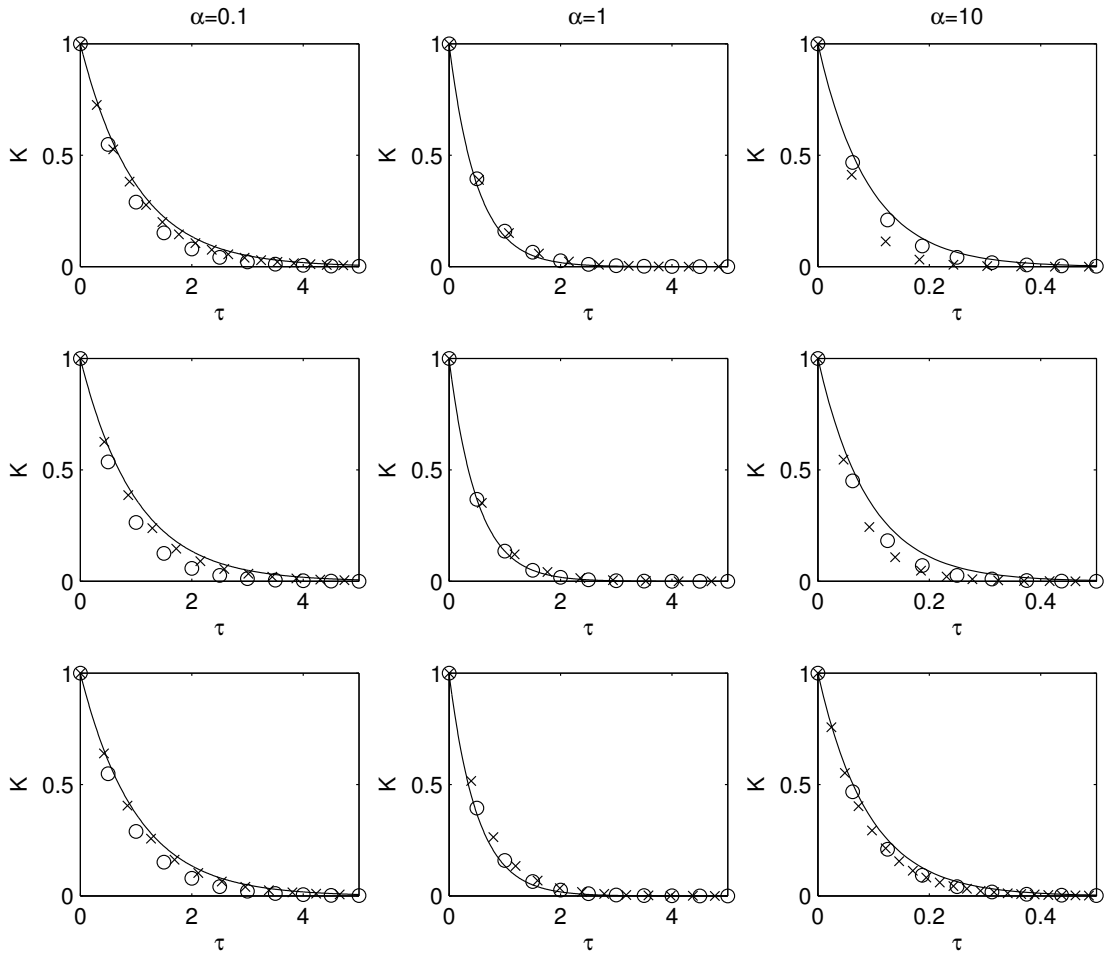

Figure 5.2: Step-Down case - Average Concentration for Three model with various α and ζ. One layer well mixed (–), Two Layer well mixed (o), Two Layer Unmixed (x). The top row corresponds to $\zeta = 0.25$, the middle row to $\zeta = 0.5$ and the bottom row to $\zeta = 0.75$

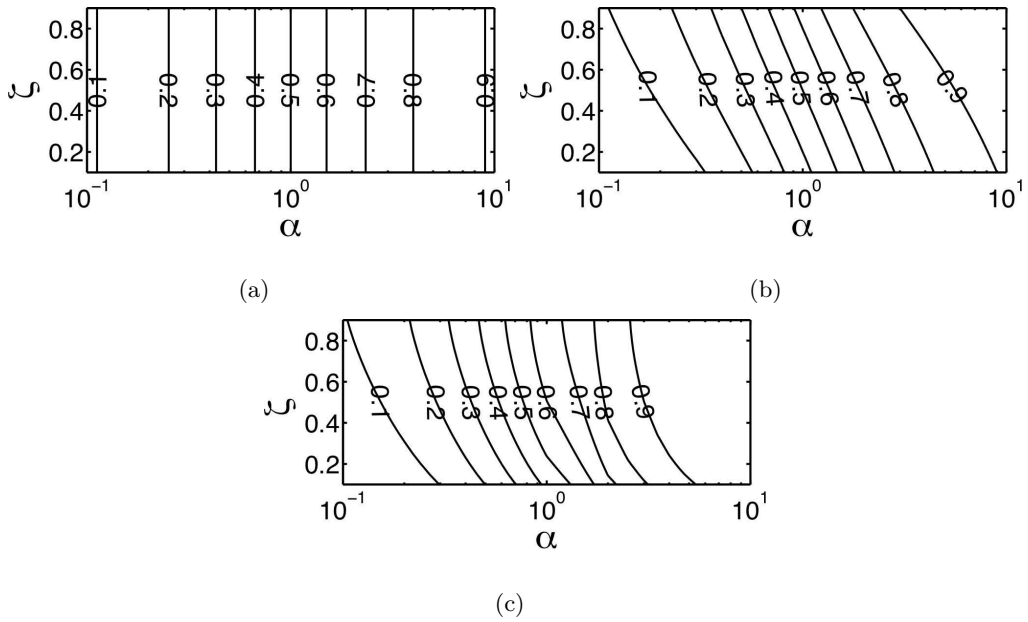

Figure 5.3: Isocontours of fraction of total initial particles deposited on the floor

space. The quantitative values of Γ_{dep} are roughly similar for the three cases, although there are interesting qualitative differences. For the two-layer models, (b) and (c), there is a monotonic increase in Γ_{dep} as ζ increases. For the unmixed upper layer, the quantity of deposited contaminant is always smaller than for the well-mixed two-layer system. As shown in Bolster and Linden (2007), where we compare the effective draining rates of the upper and lower layers of both these systems, it can be shown that the unmixed upper layer case is less effective at removing contaminant from the upper layer. The mechanism of contaminant removal is the same here and, additionally, there is transport back down to the lower layer from the upper layer due to settling. This leads to the larger quantities of deposition observed in model (c). The largest differences in Γ_{dep} between models (b) and (c), equal to 0.11, occur for $\zeta = 0.35$ and $\alpha = 2$. A contour plot of these differences in shown in figure 5.4.

Figure 5.5 compares Γ_{dep} for the single-layer well-mixed space to the two-layer models. The line where the predicted amount of deposition is equal for both models is shown on each plot. For smaller particles (i.e. α small) and lower

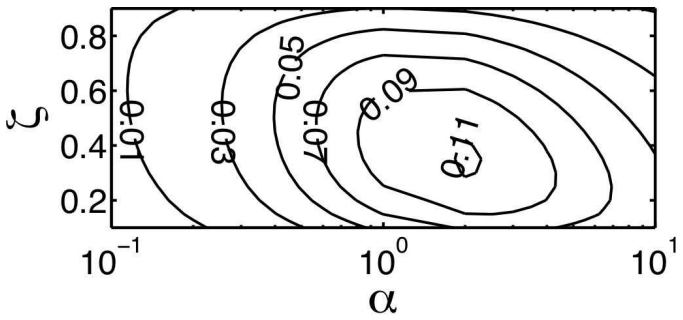

Figure 5.4: Isocontours of the difference in fraction of deposited particles between models (c) and (b) $\Gamma^c_{dep} - \Gamma^b_{dep}$

interfaces (i.e. ζ small), the two-layer systems predict lower values of Γ_{dep}, while for larger values of these parameters the single well-mixed space predicts lower values. Since Γ_{dep} is effectively a measure of the quantity of contaminant that occupants in the lower layer have been exposed to, this plot shows that for certain locations of interface and particle sizes, the low energy systems reduce exposure. However, for larger particles and higher interfaces, the traditional mixing ventilation system outperforms the low energy systems.

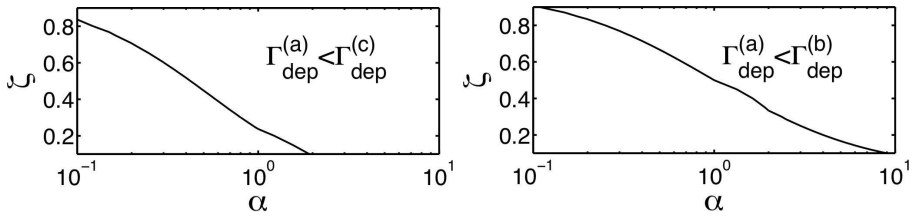

(a) (b)

Figure 5.5: Comparison of Γ_{dep} for the single-layer well-mixed space to the two-layer models. (a) To the right of the line $\Gamma^a_{dep} < \Gamma^c_{dep}$ (b)To the right of the line $\Gamma^a_{dep} < \Gamma^b_{dep}$

5.5.3 Step Up

Now we consider the opposite situation, where a room is initially completely uncontaminated and a contaminant is introduced via the ventilation system. This can correspond to a number of scenarios, such as a leak in a ventilation system, a malicious release, or an external contaminant entering the building through natural ventilation. Here $\kappa_o = 0$, $\kappa_{in} = 1$ and $\kappa_s = 0$, which should be substituted into the results presented in section 5.5.1. Unlike the step-down scenario considered previously, the step-up case has some interesting steady state characteristics. For passive contaminants this steady state corresponds to a uniformly distributed concentration of contaminant equal to that of the source. However, the influence of gravitational settling leads to nontrivial steady state distributions. Therefore, we will first consider these and then the transient approach to these steady states.

Steady State

From (5.12) we predict that the well mixed space in model (a) tends to a uniform contaminant concentration of

$$\kappa^{(a)} = \frac{1}{1+\alpha}. \tag{5.19}$$

This is lower than the concentration of fluid entering the space, because there is an additional sink in the deposition term that does not extract fluid, but does extract contaminant.

For the two-layer cases both systems tend to the same steady state since ultimately both layers will be well mixed. It can be shown from (5.13) and (5.14) that for these systems at steady state

$$\kappa_u^{(b,c)} = \frac{1}{(\alpha+1)^2 - \alpha}, \qquad \kappa_l^{(b,c)} = \frac{(1+\alpha)}{(\alpha+1)^2 - \alpha}. \tag{5.20}$$

Therefore, at steady state, the concentration in the lower layer is always greater than that in the upper layer and occupants are exposed to the highest concentra-

tions in the space. Interestingly, this steady state is also independent of ζ, the interface height.

We can compare the steady state value of the concentration of lower layer for models (b) and (c) to the well mixed case, which results in

$$\frac{\kappa_l^{(b,c)}}{\kappa^{(a)}} = \frac{(1+\alpha)^2}{(1+\alpha)^2 - \alpha} > 1. \tag{5.21}$$

Interestingly this ratio is independent of ζ the interface height. It is plotted in figure 5.6(b). Additionally, regardless of the value of α the lower layer always has a higher level of contaminant than the well mixed case. Thus people are always exposed to a higher concentration in the low energy ventilation system, regardless of whether mechanism (b) or (c) captures the true behaviour of the system. It is worth noting that there is maximum a value for the ratio $\frac{\kappa_l^{(b,c)}}{\kappa^{(a)}} = 1.33$ at $\alpha = 1$, which means that this corresponds to the worst case scenario regarding a comparison between traditional and low energy ventilation systems.

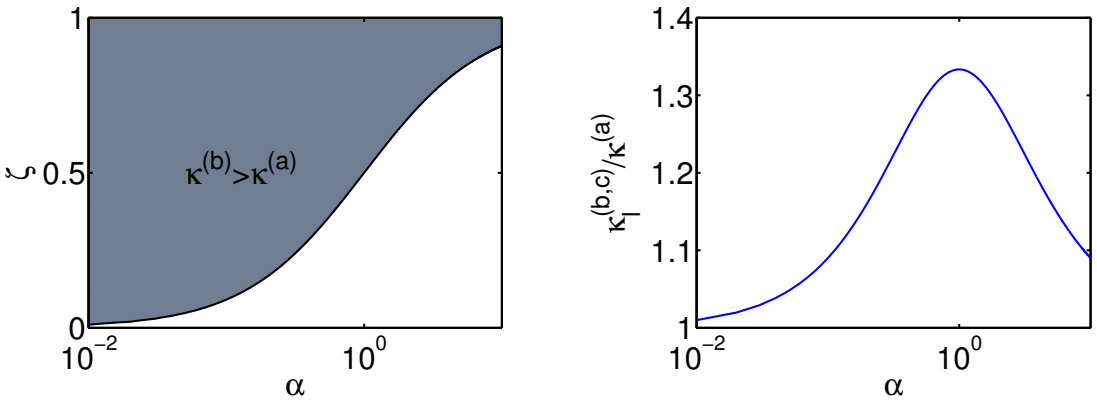

Figure 5.6: (a) Comparison of the steady state average concentration across the entire height of the space for the single layer vs two layer models (b) Ratio of the steady state concentrations of the lower layer in the two layer models to the single layer concentration ($\frac{\kappa^{(b,c)}}{\kappa^{(a)}} > 1$).

However, if we only consider the overall average concentration at steady

state of model (a) vs. models (b) and (c) we find

$$\frac{\bar{\kappa}^{(b,c)}}{\bar{\kappa}^{(a)}} = \frac{\zeta\kappa_l + (1-\zeta)\kappa_u}{\frac{1}{1+\alpha}} = \frac{(1+\zeta\alpha)(1+\alpha)}{\alpha^2+\alpha+1} \tag{5.22}$$

Figure 5.6 (a) depicts the ranges of α and ζ where the average concentration for the traditional mixing system is higher than the low-energy two-layer systems.

Transient Routes to Steady State

We present the transient evolution of average concentration for the step-up case for the same values of α and ζ as we did for the step-down case. The results are plotted in Figure 5.7. In this case, as we predicted in the discussion on steady states, the evolution of concentrations can be very different. Notice particularly, that for larger particles, $\alpha = 10$, the difference can be quite significant, although the time scales to reach steady state are comparable. This figure is slightly deceptive in that it makes the low energy systems appear more efficient at removing large particles, which they are provided only average concentrations are considered. However, recall that the lower layer concentration is always higher than the well mixed case, thus exposing occupants to higher levels of contaminant.

5.5.4 Point Source

Steady State

As for the step-up case, the ultimate steady state that the system reaches will differ for the traditional and low energy systems. Systems (b) and (c) will reach the same steady state by different mechanisms, while (a)tends to a different state. Here $\kappa_o = 0$, $\kappa_{in} = 0$ and $\kappa_s = 1$, which should be substituted in to the results presented in section 5.5.1.

The well mixed space in model (a) tends to a uniform contaminant concentration of (this is calculated by assuming a source of κ_s in the space as is

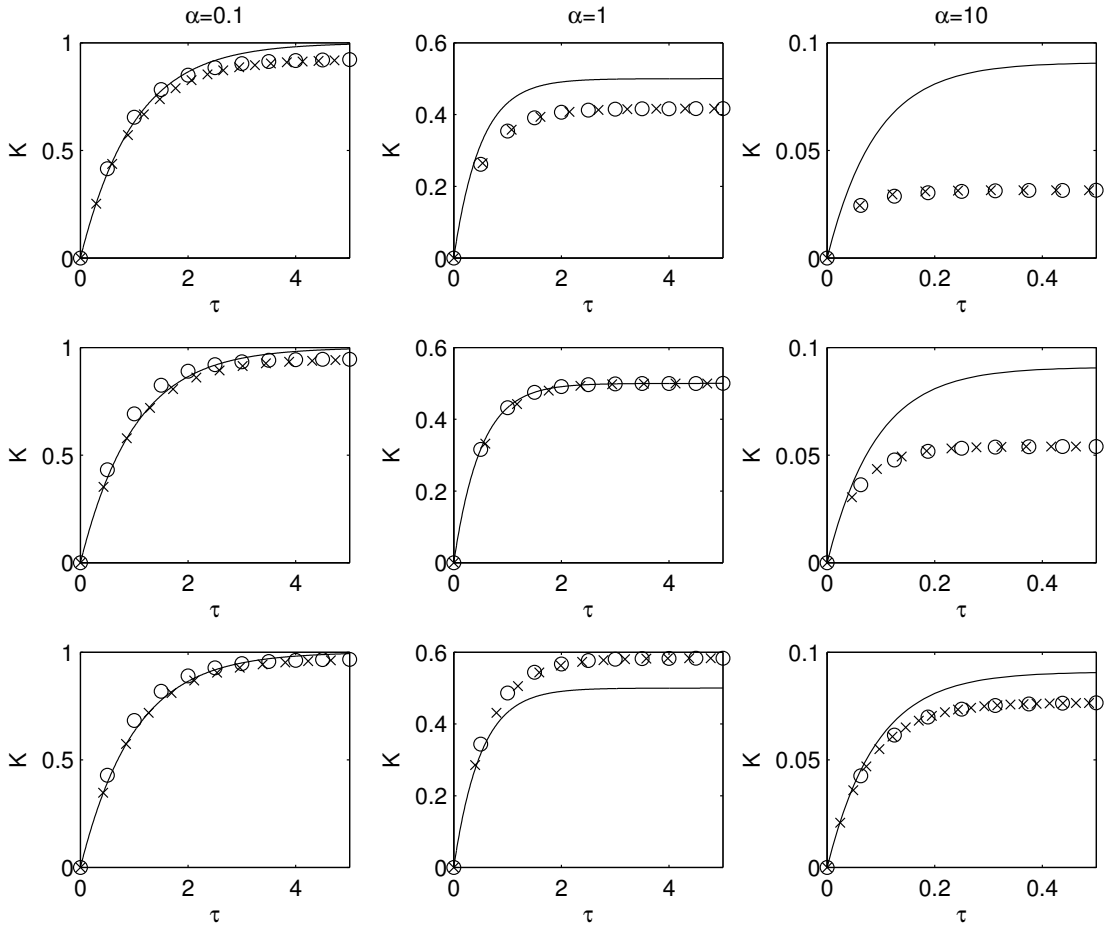

Figure 5.7: Step-Up Case - Average Concentration for Three model with various α and ζ. One layer well mixed (–), Two Layer well mixed (o), Two Layer Unmixed (x). The top row corresponds to $\zeta = 0.25$, the middle row to $\zeta = 0.5$ and the bottom row to $\zeta = 0.75$

perceived in the upper layer equation above - see appendix A for details)

$$\kappa^{(a)} = \frac{1}{1+\alpha}. \tag{5.23}$$

This is lower than the concentration of fluid entering the space, because of the sink effect of deposition that does not extract fluid, but does extract contaminant.

For the two-layer cases both systems tend to the same steady state where both layers are well mixed. For this situation the upper and lower layer concentration fields are

$$\kappa_u^{(b,c)} = \frac{1+\alpha}{(\alpha+1)^2-\alpha}, \qquad \kappa_l^{(b,c)} = \frac{\alpha}{(\alpha+1)^2-\alpha} \tag{5.24}$$

respectively. At steady state, the concentration in the upper layer is always greater than that in the lower layer and people, who only occupy the lower layer, are only exposed to the lowest concentrations in the space. Again, these steady state values are independent of ζ.

Comparing the concentration of the lower layer for models (b) and (a) we obtain

$$\frac{\kappa_l^{(b),(c)}}{\kappa^{(a)}} = \frac{\alpha^2+\alpha}{\alpha^2+\alpha+1} < 1, \tag{5.25}$$

which indicates that for this type of point source the low-energy system always does a better job removing contaminants than the traditional system, regardless of the interface location or particle size. This ratio is zero for $\alpha = 0$, which corresponds to a passive contaminant, and approaches 1 as $\alpha \to \infty$. This is reasonable because the source is effectively in the upper layer and for, $\alpha = 0$, no contaminant can fall back into the lower layer. However, as α increases, more contaminant can fall through, thus increasing the concentration of the lower layer.

On the other hand, if we only consider the average contaminant removal, we can see from figure 5.8 that there are regions, particularly as the particle size increases, where the two layer system is worse (grey region) at removing contaminants than the one-layer well-mixed system. However, since from a practical

perspective we only care about concentrations in the lower layer, this is not really the point of interest and is merely shown here to illustrate that an average contaminant concentration value is deceptive in predicting an individual's exposure as illustrated in the experiments by Ozkaynak et al. (1982).

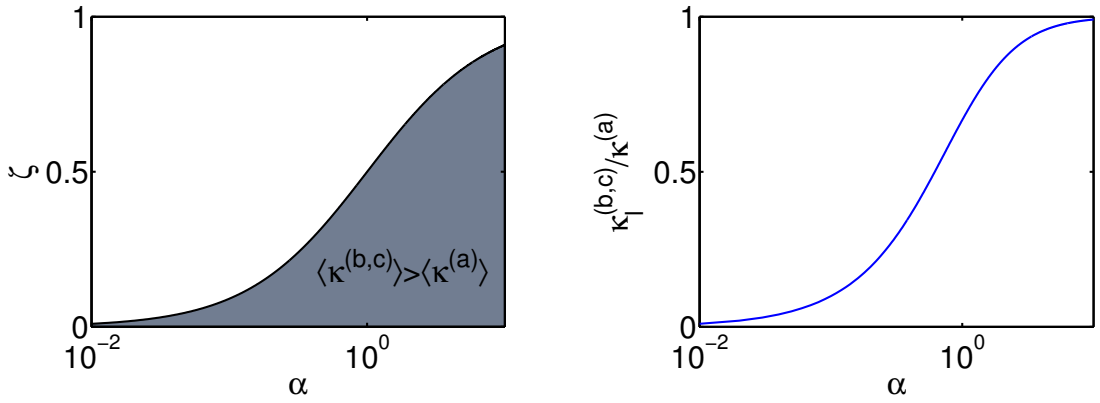

Figure 5.8: (a)Comparison of the steady state average concentration across the entire height of the space for the single layer vs two layer models (b) Ratio of the steady state concentrations of the lower layer in the two layer models to the single layer concentration ($\frac{\kappa^{(b,c)}}{\kappa^{(a)}} < 1$).

Transients

Once again we track the average concentrations predicted by the three models for various values of settling velocity and interface height. As with the step up case we see that both the two-layer models predict similar values. However, these values can differ significantly from those predicted by the well-mixed model (a). For small α as the interface height, ζ, increases the average concentration for the two layer systems decreases, while the one layer system remains unchanged, since the average concentration for the two layer case is $\kappa_{avg} = \zeta\kappa_l + (1-\zeta)\kappa_u$. Now, recall from the previous section, that for a point source with small α, the vast majority of the contaminant remains in the upper layer and that the steady state concentration for the upper layer is independent of ζ. Therefore, as the interface

height rises, there is less contaminant in the space. As α increases the difference between the upper and lower layer concentrations decreases, because now more particles can fall through to the lower layer. Therefore, the average concentration of the system is closer to that of a well mixed space. Again, it is worth pointing out that the lower layer concentration is always less than this average and also lower than the well-mixed value.

5.6 Numerical Method - Germeles Algorithm

While the solutions to model (c) above are interesting for comparison purposes, it provides only sufficient information to calculate the average amount of contaminant and provides no description of the contaminant distribution within the upper layer. This model displays stratification of contaminant in the upper layer in a manner that models (a) and (b) do not. The detailed structure of the upper layer is not resolved and, therefore, in order to determine the vertical concentration profile we can employ a modification of the numerical scheme originally developed by Germeles (1975), which is described in Chapter 3.

5.6.1 Case 1 - Step Down

A sample set of solutions for three values of α at various times at an interface of $\zeta = 0.5$ are shown in figure 5.10. As expected, when using the Germeles algorithm, the upper layer is concentration stratified and the well-mixed assumption is questionable. As with passive contaminants (see Bolster and Linden (2007)) the interface location plays an important role, always corresponding to the maximum concentration in the upper layer. The biggest difference between this case and passive contaminants is that the concentration at the interface decreases with time. In the passive case there is a front that falls from the ceiling towards the interface, below which the concentration remains that which is initially in the room. For the passive case the descent time of this front to the interface can be

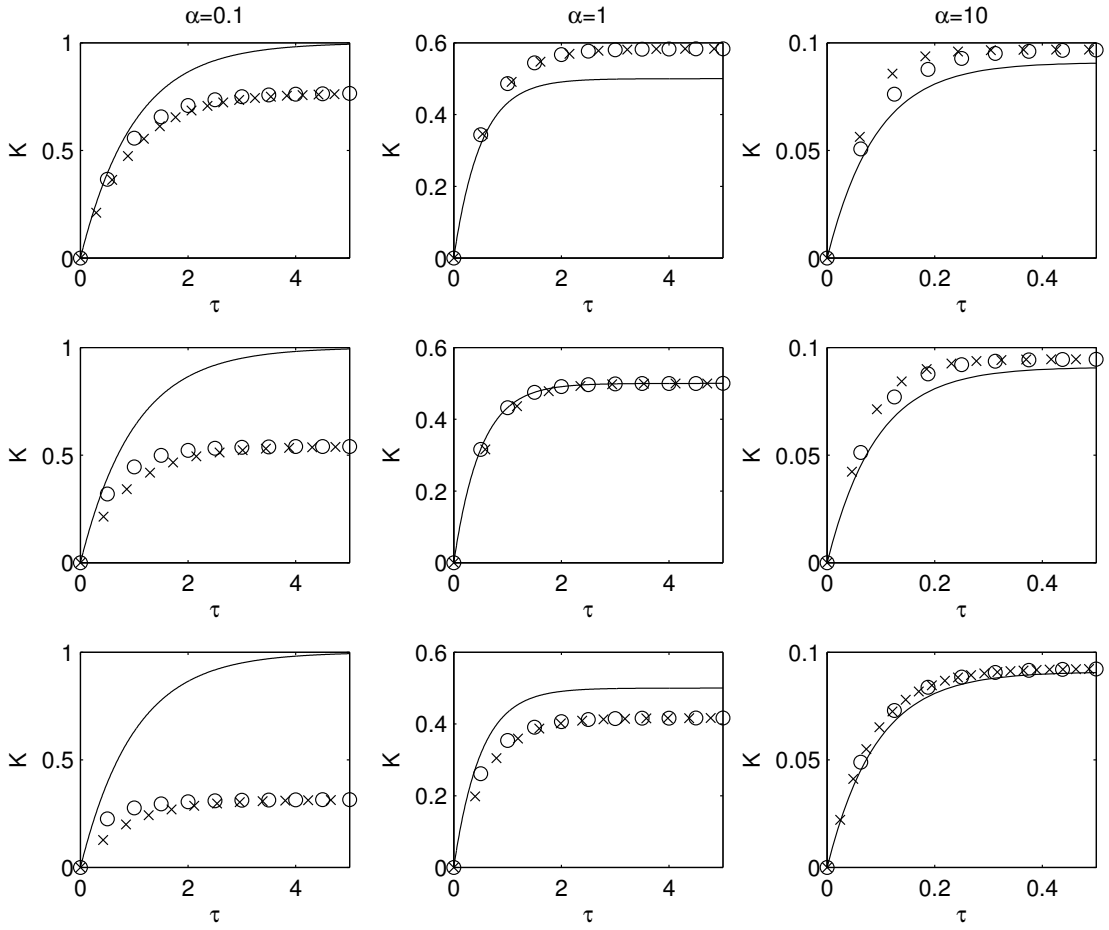

Figure 5.9: Point Source - Average Concentration for Three model with various α and ζ. One layer well mixed (–), Two Layer well mixed (o), Two Layer Unmixed (x). The top row corresponds to $\zeta = 0.25$, the middle row to $\zeta = 0.5$ and the bottom row to $\zeta = 0.75$

shown to be infinity. However, for particulate contaminants, this front will fall more quickly due to gravitational settling and actually reach the interface in finite time. Physically, this can be interpreted as the fact that particles can fall through the interface, whereas passive contaminants can not. The descent time of this first front, τ_d can be calculated from (5.16) and decreases with increasing particle size. It approaches infinity as $\alpha \rightarrow 0$.

Additionally, the interface always corresponds to the region of maximum concentration, because, if the concentrations in the upper layer fall below those of the lower layer (which does not happen for passive contaminants), the lower layer has the highest concentration levels and thus so does the lower side of the interface. From an occupant's perspective this increased exposure in the lower layer and interfacial region is worrying.

Once again, as with passive contaminants, the reason this low-energy ventilation system is not more efficient at contaminant removal than a traditional system can be explained from the plots in figure (5.10). Low energy systems are efficient from a heat removal perspective because the warmest fluid is being extracted from the top of the room. However, the location of the warmest fluid does not coincide with the region of maximum contamination. Therefore, this energy efficient mechanism does not translate across to contaminant removal efficiency.

5.6.2 Case 2 - Step Up

A sample set of solutions for the step-up case is shown in figure 5.11. Again, it is worth noticing that during the initial transient stage there can be significant gradients in the concentration field in the upper layer. This time though, the concentration in the upper layer increases with height, because through re-entrainment of contaminant from the background into the plume, the concentration at the top of the room is increasing.

It is also worth noting that the upper layer concentration is always less than that of the lower layer, as found at steady state from (5.24). The steady state

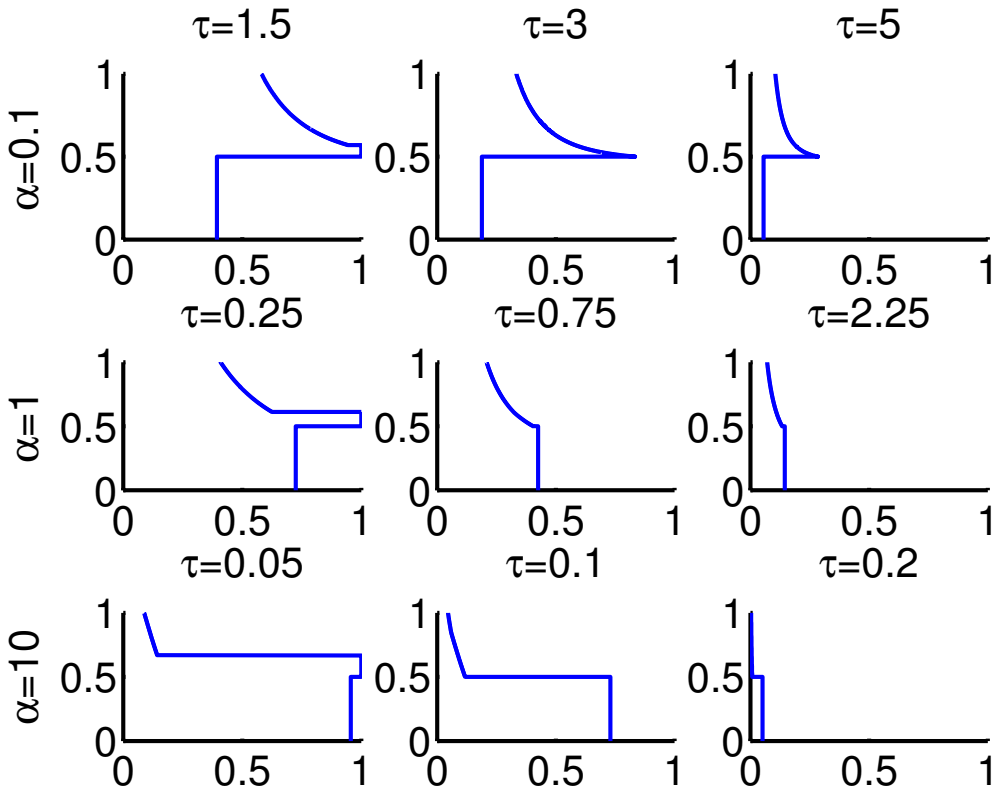

Figure 5.10: Step Down Germeles vertical concentrations for $\zeta = 0.5$ over several α at different times. The x-axis represents concentration and the y-axis height in the room

values shown in figure 5.11 correspond to the predicted values of (5.24). Therefore, if the source of contamination is the inlet of the ventilation system occupants in the lower layer will be exposed to the highest levels of contaminant in the room.

Once again, for this case these low-energy ventilation systems do not exploit the same mechanism as they do with heat removal, thus reducing their potential contaminant removal efficiency.

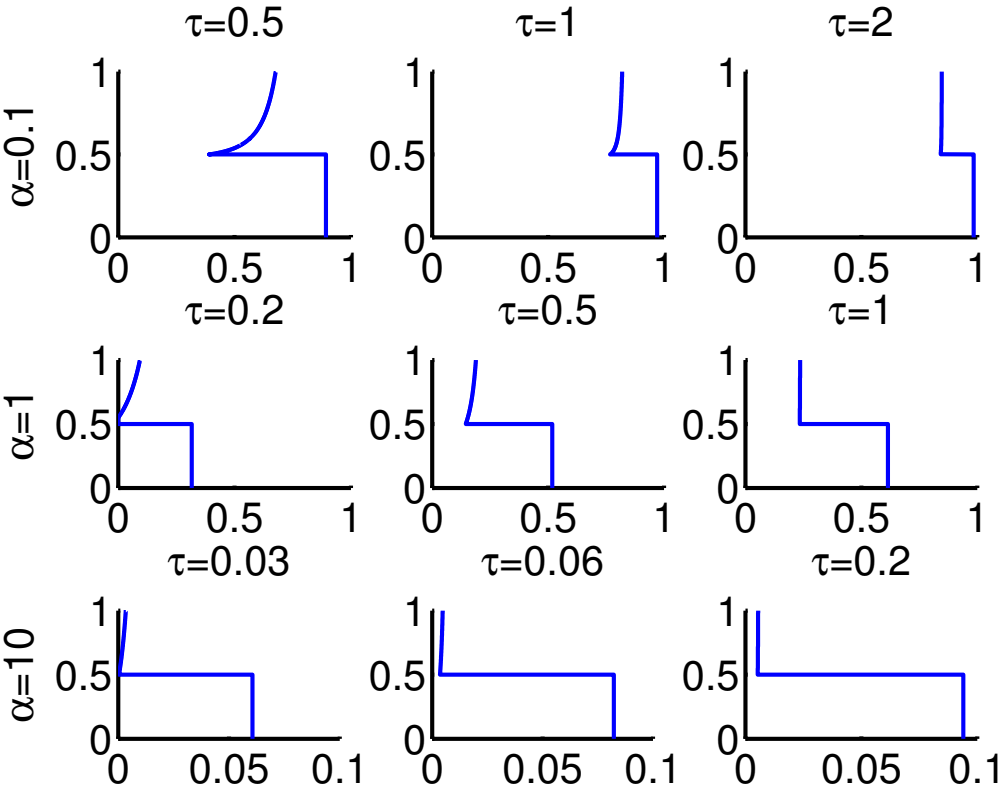

Figure 5.11: Step Up Germeles vertical concentrations for $\zeta = 0.5$ over several α at different times. The x-axis represents concentration and the y-axis height in the room

5.6.3 Case 3 - Point Source

Figure 5.12 shows the vertical concentration profiles, as calculated with the Germeles algorithm for a point source located in a plume, for various values of α and an interface at half the height of the room. Once again, there are significant gradients in the concentration field in the upper layer, particularly at early times. As with the step-up case the concentration in the upper layer increases with height, because via re-entrainment of contaminant from the background into the plume, the concentration at the top of the room is increasing. Therefore the concentration at the top of the room is the maximum concentration in the upper layer.

The concentration in the upper layer is also always greater than the concentration in the lower layer. This makes this scenario very different from either of the previous two. Now, the concentration being extracted from the top of the space is always the maximum concentration in the space. Therefore, the concentration extraction process is exploiting the same mechanism as the temperature extraction mechanism that makes these low energy systems so appealing. This translates into optimum efficiency of contaminant removal, which can clearly be seen in the previous discussion on averages and transients in this scenario.

Another feature shown in figure 5.12 is that ratio of the concentration of upper to lower layers approached unity as α decreases, thus approaching an entirely well mixed space.

5.7 Experiments

In order to validate the models presented here and gain some further insight into the dynamics of particles in low energy ventilation systems, a series of full scale laboratory experiments were conducted. A chamber of cross sectional area 1.3 $\times$ 2.6 m and height 1.8 m was ventilated by a displacement system. A heat source of $65W$ is placed in the center of the room. The heat source consisted of a light bulb, which is encased in a specially constructed wooden enclosure to

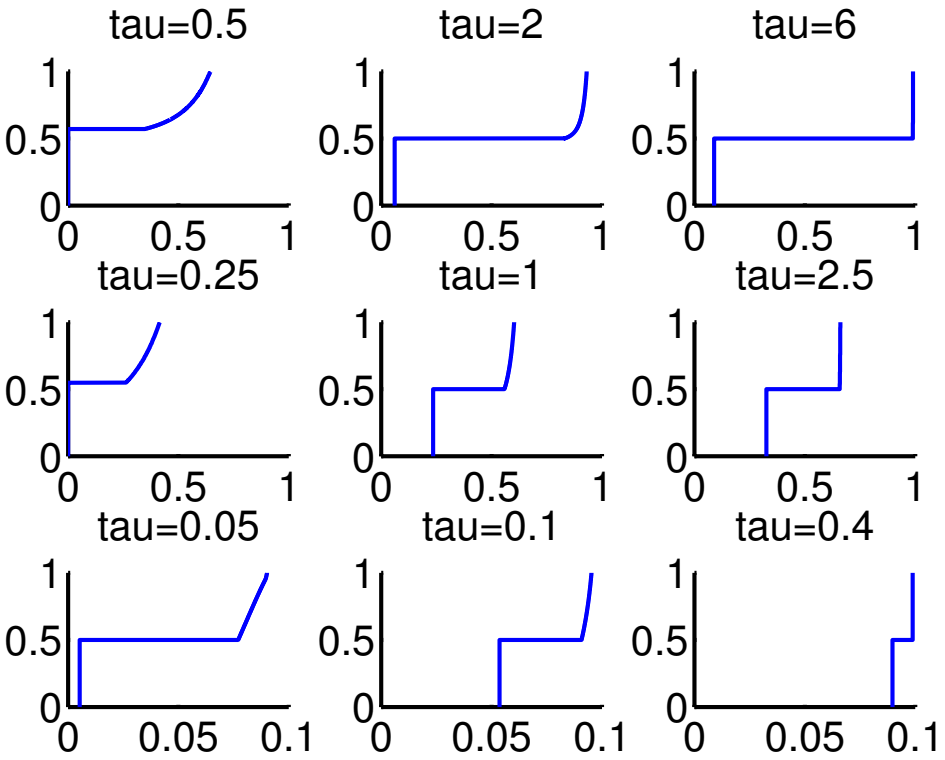

Figure 5.12: Point Source Germeles vertical concentrations for $\zeta = 0.5$ over several α at different times. The x-axis represents concentration and the y-axis height in the room

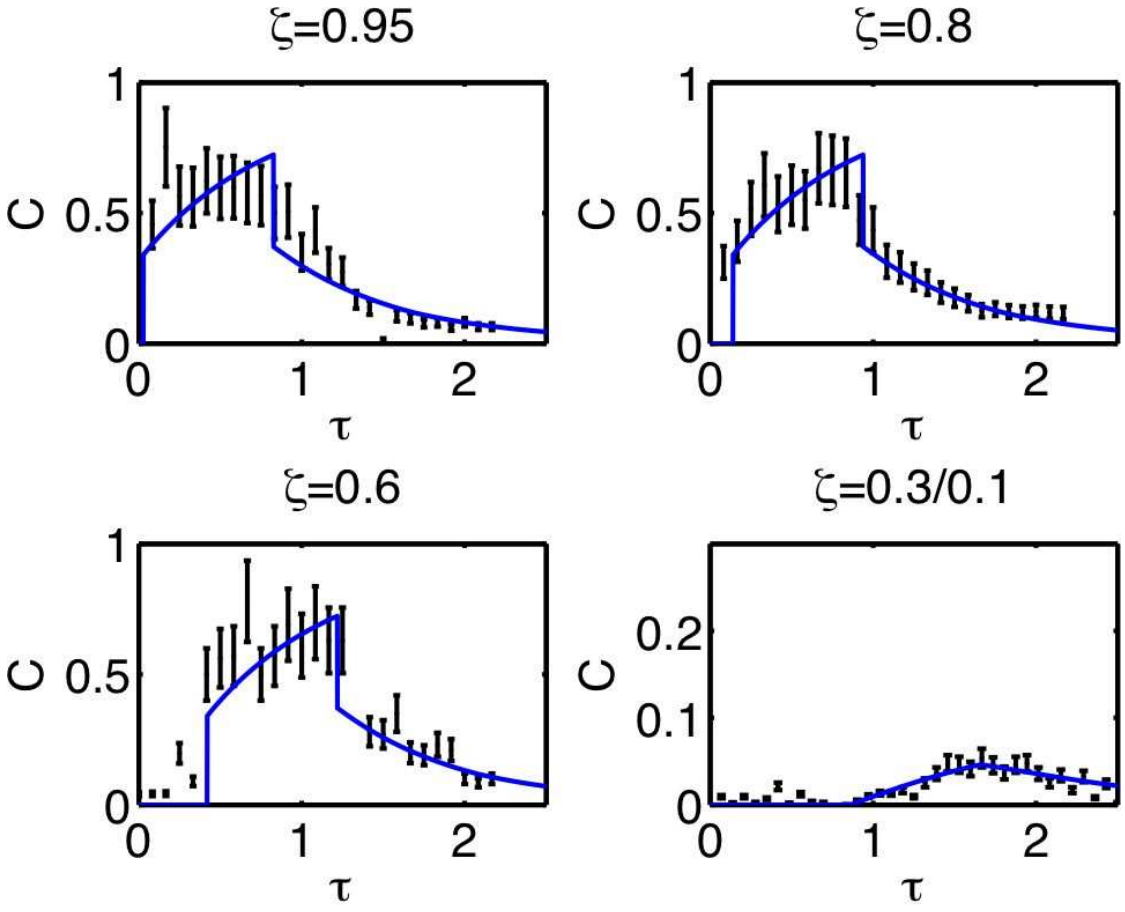

Figure 5.13: Experimental Results for $\alpha = 0.1$

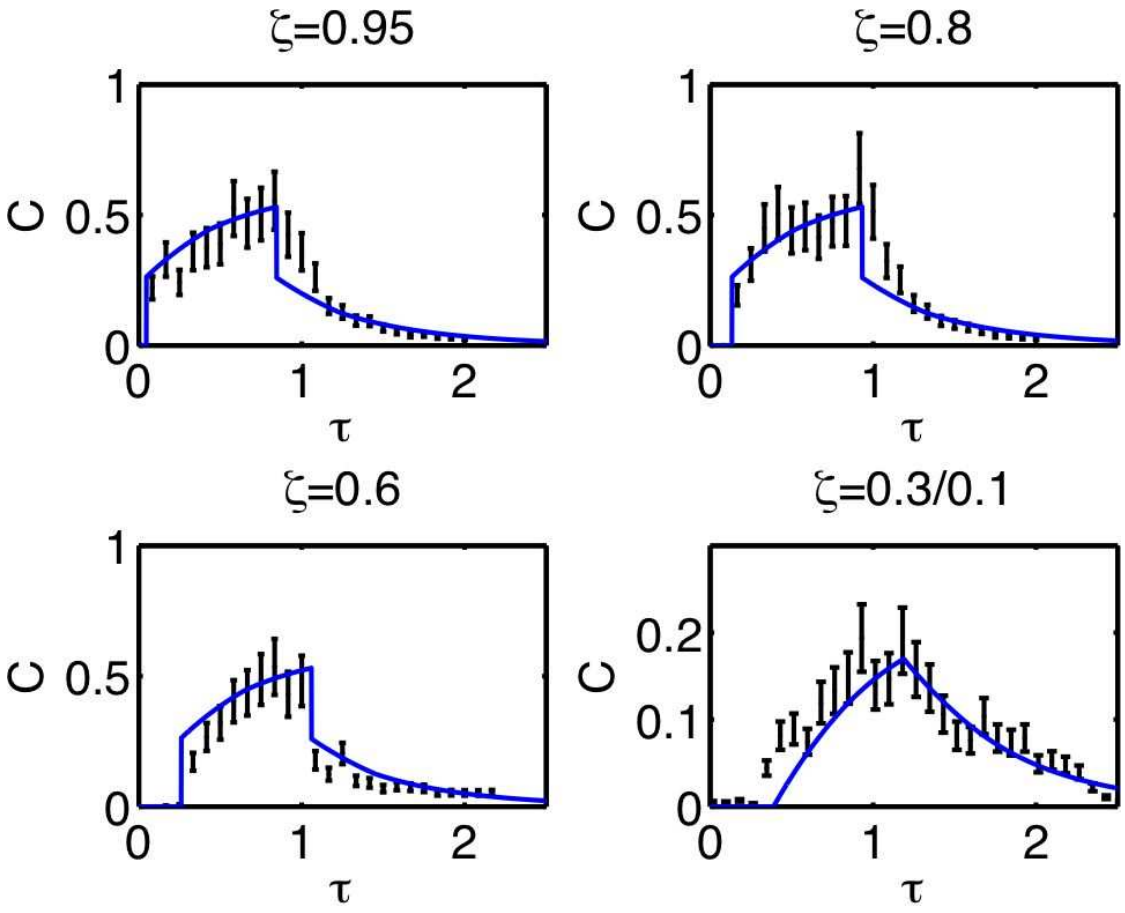

Figure 5.14: Experimental Results for $\alpha = 0.625$

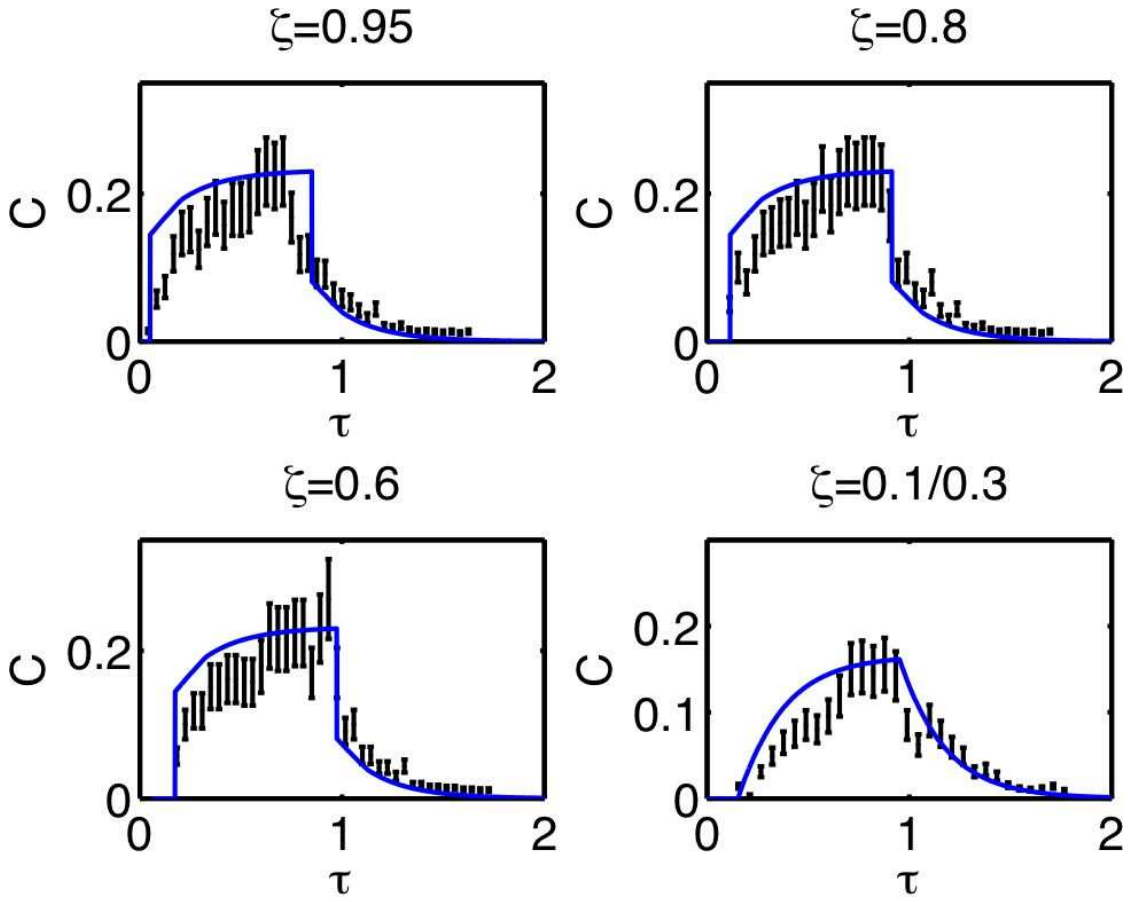

Figure 5.15: Experimental Results for $\alpha = 2.5$

minimise radiative losses.

Because of the difficulties involved in generating a step-up or step-down situation with particles, the only situation which we consider here is the point source in the plume, which still demonstrates the interesting dynamics associated with this flow.

The interface dividing the upper and lower layers is designed to sit at a height corresponding to half the height of the room (i.e. $\zeta = 0.5$). Three values of $\alpha = 0.1$, 0.625 and 2.5 are considered. Unfortunately values of $\alpha > 2.5$ were inaccessible with our current equipment. Once the temperature in the room has reached steady state, monodisperse particles of known size are injected vertically in coflow into the plume with a medical nebulizer. The particles used are polystyrene 'Microbead NIST Traceable Particle Size Standard' manufactured by Polysciences Inc. and are manufactured to within a $\pm 2.5\%$ size standard. The flow rate of injection is very small compared to the flow rate in the plume and so its effect is considered to be negligible. Running the nebulizer does not affect the temperature field and so this seems a reasonable conclusion.

The contaminant source was turned on for a certain amount of time $\tau_{on} = \frac{5}{6}\tau$, where τ is the flushing time (i.e. $\frac{Volume}{Q_{in}}$ and then switched off. A Model 237A/B Met One Particle Counter was used to detect and count particles. It is placed at various heights within the room and particle concentrations were measured periodically every 30 seconds. The particle concentrations are tracked until they return to the background noise levels, so that both the increase and drop in concentrations were captured.

The results of these experiments are shown in figures 5.13 to 5.15. The error bars on the experimental data are associated with the uncertainty in the measurement of particle concentration and the rate of release by the nebulizer, which corresponds to roughly $\pm 20\%$. In all three cases the qualitative agreement between experiment and models is good. The quantitative agreement is also pretty good with the model within the $\pm 20\%$ error bars. However, there are some regions

of larger disagreement and occasional measurements that are quite far off the predicted value. These can stem from external infiltration or some other contaminant source that we could not control in our experiment.

An important feature to note in the experimental data, which is particularly obvious in figures 5.13 and 5.14, is that the upper layer is clearly not well mixed as there is a measurable time delay in the concentration field at $\zeta = 0.6$ compared to $\zeta = 0.95$ associated with the advection of particles from the top of the room to that height. Experimentally, this time delay is not so obvious for the larger particles (i.e. $\alpha = 2.5$) because, due to faster settling, the time for particles to descend becomes comparable to the measurement time and so the concentration fields for the three upper values of ζ become indistinguishable.

Additionally, for the largest particles, there seems to be a delay in the experimental data for the initial rise of concentration in the upper layer compared to the theoretical prediction. The peak predicted value is comparable, but the time taken to get there is longer. This is probably because we neglect the effect of settling within the plume. The present models predict an instant increase in concentration once the source is turned on. This comes from the assumption that the plume time scale is much faster than that of the background, which is true. However, there may be a lag in this due to settling effects. This theoretical over-prediction of the upper layer concentration also leads to an over-prediction of the lower layer concentration.

5.8 Additional Mechanisms of Deposition

While gravitational effects dominate the deposition mechanisms for large particles (typically $> 1\mu m$, although this is dependent on the friction velocity at a boundary, which for a displacement system should be less than for traditional mixing system), the deposition of particles smaller than this can be strongly driven by Brownian diffusion (Lai and Nazaroff (2000)). Therefore, for such particles the

governing equations (5.9)-(5.11) must be modified to account for this. Since the ultimate steady state for both two layer models is the same we focus on model (b) here. Accounting for additional settling to all surfaces the governing equations become

(a)

$$\frac{dK_{wm}}{dt} = -\frac{Q_{in} + Q_{dw}}{SH} K_{wm} + \frac{Q_{in}}{SH} K_{in} + \frac{Q_{in} K_s}{SH}, \tag{5.26}$$

(b)

$$\frac{dK_l}{dt} = -\left(\frac{Q_p + Q_{dl}}{Sh}\right) K_l + \frac{Q_{df}}{Sh} K_u + \frac{Q_{in}}{Sh} K_{in}$$

$$\frac{dK_u}{dt} = \frac{Q_p + Q_{dr}}{S(H-h)} K_l - \left(\frac{Q_{du} + Q_p}{S(H-h)}\right) K_u + \frac{Q_p K_s}{S(H-h)} \tag{5.27}$$

where Q_{dw} is the flow rate at which particles settle out of the well mixed space, Q_{dl} is the flow rate at which particles settle out of the lower layer, Q_{df} is the flow rate of particles that flow from the upper to lower layer across the interface, Q_{du} is the flow rate at which particles settle out the upper layer and Q_{dr} is the flow rate at which particles cross the interface from the lower to upper layers. These quantities are evaluated as follows:

$$Q_{dw} = v_v A_v + v_d A_d + v_u A_u \quad Q_{dl} = v_v A_v^l + v_d A_d + v_u A_u \quad Q_{df} = v_u A_u$$

$$Q_{du} = v_v A_v^u + v_d A_d + v_u A_u \quad Q_{dr} = v_d A_d \tag{5.28}$$

where v_v is the deposition velocity of a particle depositing on to a vertical surface, v_d is the deposition velocity of a particle depositing on to a downward facing horizontal surface, v_u is the deposition velocity of a particle depositing on to an upward facing horizontal surface, A_v is the total area of vertical boundaries in the space, A_v^l is the area of vertical boundaries in the lower layer, A_v^u is the area of vertical boundaries in the upper layer, A_u is the area of an upward facing boundary and A_l is the area of downward facing boundaries. The deposition velocities can

be evaluated using equations presented in Table 2 in Lai and Nazaroff (2000). We treat the interface in the two layer model as a 'ficticious' rigid boundary through which fluxes can occur.

In dimensionless terms (5.26) and (5.27) become:

(a)

$$\frac{d\kappa_{wm}}{d\tau} = -(1+\alpha_{dw})\kappa + \kappa_{in} + \kappa_s, \tag{5.29}$$

(b)

$$\frac{d\kappa_l}{d\tau} = \frac{-(1+\alpha_{dl})\kappa_l + \alpha_{df}\kappa_u + \kappa_{in}}{\zeta},$$

$$\frac{d\kappa_u}{d\tau} = \frac{(1+\alpha_{dr})\kappa_l - (1+\alpha_{du})\kappa_u + \kappa_s}{1-\zeta}, \tag{5.30}$$

where $\alpha_{di} = \frac{Q_{di}}{Q_{in}}$ represents the dimensionless forms of the various deposition flow rates defined in 5.28. The subscript i can represent the subscripts w, l, f, u or r. By accounting for these additional mechanisms we introduce several new dimensionless parameters. In the limit of large particles, the deposition velocities to upward facing surfaces reduces to the settling velocity, while the deposition to downward facing and vertical surfaces reduces to zero and we recover the equation presented in sections 5.3-5.5.

Rather than consider the transient evolution to steady state, based on the discussion and observations we made earlier, we will focus on the ultimate steady states, which is shown to be

$$\kappa^{(a)} = \frac{\kappa_{in} + \kappa_s}{1+\alpha_{dw}} \tag{5.31}$$

$$\kappa_l^{(b,c)} = \frac{(1+\alpha_{du})\kappa_{in} + \alpha_{df}\kappa_s}{1+\alpha_{dl}+\alpha_{du}(1+\alpha_{dl}) - \alpha_{df}(1+\alpha_{dr})} \tag{5.32}$$

$$\kappa_u^{(b,c)} = \frac{(1+\alpha_{dr})\kappa_{in} + (1+\alpha_{dl})\kappa_s}{1+\alpha_{dl}+\alpha_{du}(1+\alpha_{dl}) - \alpha_{df}(1+\alpha_{dr})} \tag{5.33}$$

Step Up Case

For the step up situation we considered previously (i.e. $\kappa_{in} = 1$ and $\kappa_s = 0$) we again compare the upper to lower layer concentrations in the two layer system. We also compare the lower layer concentration in the two layer system to the concentration in the traditional well mixed space.

$$\frac{\kappa_l^{(b,c)}}{\kappa_u^{(b,c)}} = \frac{1 + \alpha_{du}}{1 + \alpha_{dr}} \tag{5.34}$$

Because α_{du} includes deposition to vertical and horizontal surfaces, while α_{dr} only involves deposition to a downward facing horizontal surface, it is readily seen that $\alpha_{du} > \alpha_{dr}$ and therefore $\kappa_l^{(b,c)} > \kappa_u^{(b,c)}$. Once again for the step-up case the concentration in the lower layer is always greater than it is in the upper layer, even with the additional settling mechanisms for fine and ultrafine particles. Now we compare the lower layer concentration in the two layer system to the concentration in the traditional mixing space

$$\frac{\kappa_l^{(b,c)}}{\kappa^{(a)}} = \frac{(1 + \alpha_{du})(1 + \alpha_{dw})}{1 + \alpha_{dl} + \alpha_{du}(1 + \alpha_{dl}) - \alpha_{df}(1 + \alpha_{dr})} \tag{5.35}$$

It is relatively straightforward using (5.28) to show that the denominator is greater than the numerator in (5.35). Therefore, as we observed previously, occupants are exposed to higher levels of contaminants in the low energy system when a step-up case is considered.

Point Source Case

In the same manner we can consider the point source situation ($\kappa_{in} = 0$ and $\kappa_s = 1$), where

$$\frac{\kappa_l^{(b,c)}}{\kappa_u^{(b,c)}} = \frac{\alpha_{df}}{1 + \alpha_{dl}} \tag{5.36}$$

Now, from (5.28) we know that$\alpha_{df} < \alpha_{dl}$. Therefore, the lower layer concentration is always less than that in the upper layer. Similarly

$$\frac{\kappa_l^{(b,c)}}{\kappa^{(a)}} = \frac{\alpha_{df}(1+\alpha_{dw})}{1+\alpha_{dl}+\alpha_{du}(1+\alpha_{dl})-\alpha_{df}(1+\alpha_{dr})} \tag{5.37}$$

Once again using (5.28), we can show that the denominator is less than the numerator in (5.37). Therefore, as we observed previously, occupants are exposed to lower levels of contaminants in the low energy system when a point source is considered.

5.9 Conclusions

In this paper we have considered the transport of particulate contaminants in a displacement ventilated space. We compared three models, one representing a traditional ventilation system and the other two representing the displacement-ventilated space. We considered three types of contamination scenarios, namely a step-down, a step-up and a point-source contaminant. Several important differences between the traditional and low-energy systems were noted.

While for passive contaminants it is often argued that studying one of the step-up, step-down and point-source contamination scenarios is equivalent to studying them all, this is not the case for particulate contaminants and the low energy displacement system described here. The influence of gravitational settling is to introduce an 'irreversibility' or 'preferential direction' to the flow, which destroys the symmetry of the step-up, step-down and point source methods. Therefore, it is important to understand the differences between these three scenarios as each one gives important information about real contamination scenarios. The governing equations presented in this paper are all linear, and therefore each scenario can be studied separately, and superposition of solutions can be used to study more complex situations.

It is widely believed that low-energy displacement ventilation systems are better than traditional mixing systems at removing contaminants from a space. This is because there is a belief that these systems will use the same mechanism

for contaminant removal as they do for heat removal, where they are are clearly more efficient. The heat extraction problem exploits the natural stratification that develops, extracting the warmest air that naturally sits at the top of the room. However, there is no physical justification as to why this location should correspond to the location of maximum contaminant concentration too. In fact many times it does not (Bolster and Linden (2007)).

For the step-down case we considered the quantity of particles deposited to the floor as an indicator of the fraction of contaminant that an occupant has been exposed to. For smaller particles and low interfaces (i.e. small α and ζ) the low-energy displacement system performs better than the traditional mixing system. However, for larger particles this index indicates that the low energy systems cause higher levels of exposure. Allowing for gradients in the upper layer (i.e. model (c)) leads to higher exposure than the well-mixed upper layer, because the concentration at the interface is higher than at the top of the room (like the passive contaminant case in Bolster and Linden (2007)), thus allowing higher concentrations to settle back down to the lower layer.

Similarly for the step-up case, we showed that, at steady state, the concentration in the lower layer is greater than that of the upper layer. Further, this lower layer concentration is larger than that for an equivalent traditional ventilation system. The largest difference occurs for particles with $\alpha = 1$, where the lower layer concentration in the displacement system is 33% higher than that in the traditional system.

On the other hand, when considering the point-source scenario, we predict a higher steady-state concentration in the upper layer compared to the lower layer. The lower layer concentration will always be less than that in an equivalent traditional system, thus reducing occupants' exposure to contaminants. This is because, unlike the step-up and step-down cases, this situation exploits the same mechanism as the heat removal problem, always extracting the most contaminated air from the top of the room.

It is clearly important to consider the types of sources that are likely to be encountered in a real building. For example, in a well designed surgical operating theater, the ventilation system typically filters out most contaminant before introducing air into the room. Therefore, it is unlikely that the step-up scenario is relevant. In an operating theater the most common sources of contaminants are the surgeons, nurses and patients (Smith (1975)), which would correspond to the point source problem described herein. As such, a displacement system may provide better air quality than a traditional mixing ventilation system. On the other hand, if we consider a naturally ventilated space, where external sources can play an important part in contamination, the step-up scenario may be relevant.

Another important point to note is that it is not always sufficient to estimate the average amount of contaminant within a space. As shown for all three contamination scenarios, computing the average concentrations only can lead to an overly optimistic picture since local concentrations can often be significantly higher. In many cases one ventilation system can outperform another based on average concentrations. However, when considering individual exposure this may no longer hold true. Apart from the obvious reason of minimising occupant exposure to contaminants, it is also important to emphasise this point, because most multi-zone network models used in building simulations only compute average concentrations within each space, which can lead to naive predictions of contaminant concentration.

The text in chapter 5, in part, will be submitted for publication in *Atmospheric Environment* (D Bolster & PF Linden). I was the primary researcher on this project.

6

Transients in Natural Ventilation 1 - Sudden Changes in Buoyancy

6.1 Abstract

We examine transients caused by sudden changes in heat load in a naturally ventilated chamber. The space we consider has an isolated heat source, modeled as an ideal plume, and is connected to the exterior via openings at the top and bottom. Pressure differences between the exterior and interior that arise due to the buoyancy in the space drive a natural ventilation flow through the space that generates a two-layer system with buoyant (warm) fluid in the upper layer and ambient fluid in the lower layer. We assume that these two layers are well mixed and develop a mathematical model to study transients associated with sudden changes in the source buoyancy. We track the location of the interface dividing the cool lower and hot upper layers, since from a comfort perspective it is important to ensure that this interface does not descend for an extended period of time to a height where occupants are located. We extend this model to allow stratification to evolve in the upper layer in order to study the limitations of the well-mixed assumption. We compare both models to small scale laboratory experiments and find that neither model is significantly better than the other, and that

both models give good agreement with the experiments.

Using these models we identify many appealing features of natural ventilation, beyond energy savings. These include the fact that a well designed natural ventilation system is self controlling. Furthermore, the manner in which it controls itself is very robust, because the larger the change in heat load the faster the system will readjust. Also there is a resistance against the interface penetrating deeply into the occupied zone, even for very large changes in heat load.

6.2 Introduction

In order to understand natural displacement ventilation, it is imperative to understand how the thermal stratification in a room develops due to a localized source of heat. Many heat sources, such as people, machinery and computers, can be regarded as localized and understanding the manner in which they stratify a space is critical to design adequate ventilation schemes. These heat sources are often modeled as an ideal plume, if it is a pure source of buoyancy (e.g. a radiator, a person, a computer).

Additionally many real heat sources in buildings provide a time-varying heat load. However, most theoretical studies of natural ventilation only deal with steady state situations. It is therefore important to extend previous work to capture the effects of time changing heat sources.

Killworth and Turner (1982) studied the filling box model in an enclosed space (no ventilation) for a pure plume with a time varying buoyancy flux. They noted that as long as the plume buoyancy flux at every height is larger than the buoyancy in the background of the room the plume can penetrate the whole way through the space and spread at the top. However, if the source buoyancy flux is not sufficiently large, the plume becomes a fountain above the level of zero relative buoyancy, which stops rising at the level of zero momentum. It will then fall back and spread horizontally at some height between these two levels.

Killworth & Turner found that modeling the spread of the plume at the level of zero buoyancy better matched their experimental data than at the level of zero momentum. Similar observations were made by Kumagai (1984) and Cardoso and Woods (1993), who studied the 'filling box' model for a room which has some ititial background stratification.

Kaye and Hunt (2004) studied the initial transient that evolves in the 'emptying filling box' when the heat source is initially turned on. As in Linden et al. (1990), they showed that the steady-state flow is characterized entirely by a dimensionless vent area. They identified that for certain values of this vent area the depth of the buoyant upper layer may overshoot the steady layer depth during the initial transient. They also determined the critical value of the dimensionless area for this overshoot to occur.

Other than Kaye and Hunt (2004) most natural ventilation models ('emptying filling boxes') only consider the steady states associated with the flow. The work presented here extends these models by considering a heat source whose buoyancy flux changes at some time. Specifically, we consider the situation where there is a sudden change in source buoyancy flux, which could correspond a piece of equipment being turned on/off or people entering/exiting a room.

In §6.3 of this paper we describe the mathematical model applicable to the above case. We consider a case starting from some initial steady state, then change the source buoyancy flux and observe the transition to the next steady state. In §6.4 we present and discuss the results from the model described in §6.3. §6.5 considers the limitations of the well-mixed assumption in our model, by considering a model that does account for stratification and comparing the results of these two models and in §6.6 we present the results of laboratory experiments.

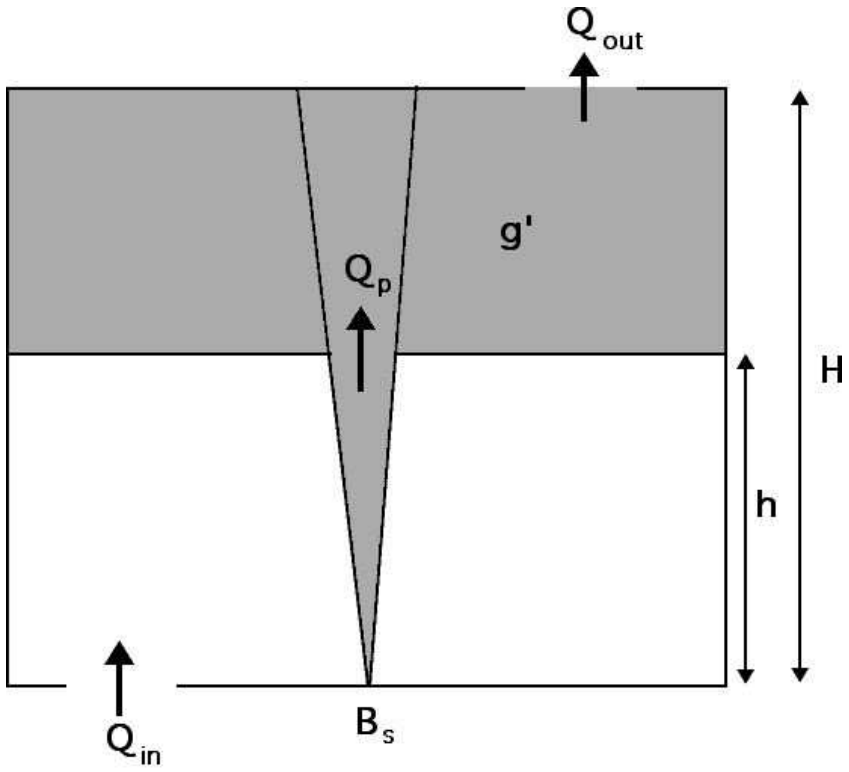

Figure 6.1: Natural Ventilation with a single ideal plume heat source

6.3 Well Mixed Model

Figure 6.1 is a schematic depicting a two-layer well-mixed model for natural ventilation. A heat source is represented by a single ideal plume (i.e. no source volume and momentum flux) located on the floor. Linden et al. (1990) showed that at steady state the stratification has two uniform layers separated by an interface. The height h of this interface depends only on the area of the inlet and outlet vents and not on the source buoyancy flux of the plume. This is one of the features of natural ventilation that is so appealing. It is a self-controlling system that will provide the same temperature in the lower layer regardless of the strength of the heat source. Since typically, the lower layer is the only one that is occupied and the temperature of the upper layer is relatively unimportant from a comfort perspective, this property makes natural displacement ventilation very robust.

As mentioned, all of the above assumes steady state. However, most realistic sources are not steady. If the buoyancy flux of the source is varying over time this will in turn cause the interface height h to change. As the new steady state is attained the interface will settle back to its original height. We are interested in determining the temporal variation of this interface between these two steady states where the initial and final interface heights are the same.

A key assumption of the model depicted in figure 6.1 is that the buoyant upper layer is well mixed at all times. While the layers are uniform at steady state, a change in buoyancy flux is expected to produce a temporary stratification in the upper layer. For the moment we will ignore this stratification and assume that both layers remain uniform in temperature as they evolve. From our experimental observations it is evident that this assumption is not strictly valid and that during the transitions from one steady state to the next some stratification will evolve in the upper layer. Kaye and Hunt (2004) suggest that the only source of error of this assumption should be to underpredict the buoyancy of the fluid leaving the box,

which in turn will lead to an underprediction for the time taken for the buoyancy of the layer to reach a steady state. They also argue that there will be some level of mixing in the upper layer due to the finite thickness outflow from the top of the plume.

By assuming that the upper and lower layer are well mixed at all times the system can be fully described by two conservation equations that are coupled, nonlinear ODEs. The conserved quantities we consider are the volume and buoyancy of the upper layer.

6.3.1 Conservation of Volume

The volume flow rates in and out of the room (figure 6.1) are always equal

$$Q_{in} = Q_{out}, \tag{6.1}$$

Therefore, applying conservation of volume to the upper layer ($y > h$) in the chamber leads to

$$\frac{dV}{dt} = Q_p - Q_{out}, \tag{6.2}$$

where V is the volume of the upper layer and Q_p is the volume flux of the plume at the interface height.

Using Bernoulli's equation it can be shown that the flow rate in and out of the room is

$$Q_{out} = A^* \sqrt{g'(H-h)}. \tag{6.3}$$

where A^* is the weighted area of the upper and lower openings as described in Linden et al. (1990) . The reduced gravity of the upper layer is defined as

$$g' = g\frac{\rho - \rho_a}{\rho_a}. \tag{6.4}$$

Since the lower layer is uniform, Q_p can be calculated using the solution for an ideal plume in an unstratified environment developed by Morton et al. (1956)

$$Q_p = cB^{\frac{1}{3}} z^{\frac{5}{3}}, \tag{6.5}$$

where B is the source buoyancy flux and c is a constant based on the plume entrainment constant. Substituting (6.5) and (6.3) into (6.2) results in an equation for the evolution of the interface height

$$\frac{dh}{dt} = \frac{A\sqrt{g'(H-h)}}{S} - \frac{cB^{\frac{1}{3}} z^{\frac{5}{3}}}{S}, \tag{6.6}$$

where S is the cross sectional area of the room.

6.3.2 Conservation of Buoyancy

The conservation of buoyancy of the upper layer can be written as

$$\frac{dg'V}{dt} = B_p - Q_{out} g', \tag{6.7}$$

where B_p is the buoyancy flux of the plume at the interface. Because the lower layer is unstratified B_p and B, the source buoyancy flux, are equal. Using this fact and substituting (6.3) into (6.7), conservation of buoyancy can be reduced to

$$\frac{dg'}{dt} = \frac{1}{S(H-h)}[B - cg'B^{\frac{1}{3}} h^{\frac{5}{3}}]. \tag{6.8}$$

6.3.3 Sudden change in buoyancy

We consider a sudden discontinuous change in the source buoyancy flux from some initial steady value B_0 to a different value $B_0 + \Delta B$, where ΔB can be positive or negative, corresponding to an increase or a decrease in buoyancy from the heat source.

We nondimensionalise the conservation equations (6.6) and (6.8) as follows

$$z = \zeta H, \qquad g' = \frac{\delta B_u^{\frac{2}{3}}}{cH^{\frac{5}{3}}}. \tag{6.9}$$

For natural ventilation, two important time scales are typically considered. These are the draining, T_d, and filling, T_f, time scales, defined in (6.10) below. In this present situation there are four time scales since there will be two draining and two filling times, corresponding to the initial and final source buoyancy fluxes.

For the initial buoyancy flux B_0

$$T_{d1} = \frac{c^{\frac{1}{2}} S H^{\frac{4}{3}}}{A B_0^{\frac{1}{3}}} \qquad T_{f1} = \frac{S}{c B_0^{\frac{1}{3}} H^{\frac{2}{3}}}. \tag{6.10}$$

Similarly, for the final buoyancy flux $B_0 + \Delta B$

$$T_{d2} = \frac{c^{\frac{1}{2}} S H^{\frac{4}{3}}}{A(B_0 + \Delta B)^{\frac{1}{3}}} \qquad T_{f2} = \frac{S}{c(B_0 + \Delta B)^{\frac{1}{3}} H^{\frac{2}{3}}} \tag{6.11}$$

When $B = B_0$, (6.6) and (6.8) reduce the relations presented by Kaye and Hunt (2004), namely

$$\frac{d\zeta}{dt} = \frac{1}{T_{d1}} \sqrt{\delta(1-\zeta)} - \frac{1}{T_{f1}} \zeta^{\frac{5}{3}}, \qquad \frac{d\delta}{dt} = \frac{1}{T_{f1}} \left(\frac{1 - \zeta^{\frac{5}{3}} \delta}{1 - \zeta} \right). \tag{6.12}$$

When $B = B_0 + \Delta B$

$$\frac{d\zeta}{dt} = \frac{1}{T_{d1}} \sqrt{\delta(1-\zeta)} - \frac{1}{T_{f2}} \zeta^{\frac{5}{3}}, \qquad \frac{d\delta}{dt} = \frac{1}{T_{f2}} \left(\frac{\left(\frac{B_0 + \Delta B}{B_0} \right)^{\frac{2}{3}} - \zeta^{\frac{5}{3}} \delta}{1 - \zeta} \right). \tag{6.13}$$

We nondimensionalise time with the geometric mean of the filling and draining timescales associated with the initial source buoyancy flux. This allows any ΔB to be compared easily to another since the nondimensional time depends only on the initial B, i.e.

$$t = \tau \sqrt{T_{d1} T_{f1}} = \frac{S H^{\frac{1}{3}}}{C^{\frac{1}{4}} A^{\frac{1}{2}}} \left(\frac{1}{B_0^{\frac{1}{3}}} \right). \tag{6.14}$$

When $B = B_0$ (6.12) becomes

$$\frac{d\zeta}{d\tau} = \sqrt{\frac{1}{\mu}}\sqrt{\delta(1-\zeta)} - \sqrt{\mu}\zeta^{\frac{5}{3}}, \qquad \frac{d\delta}{d\tau} = \sqrt{\mu}\left(\frac{1-\zeta^{\frac{5}{3}}\delta}{1-\zeta}\right) \tag{6.15}$$

and when $B = B_0 + \Delta B$ (6.12) becomes

$$\frac{d\zeta}{d\tau} = \sqrt{\frac{1}{\mu}}\sqrt{\delta(1-\zeta)} - \sqrt{\mu}\chi\zeta^{\frac{5}{3}}, \qquad \frac{d\delta}{d\tau} = \sqrt{\mu}\chi\left(\frac{\chi^2-\zeta^{\frac{5}{3}}\delta}{1-\zeta}\right), \tag{6.16}$$

where

$$\mu = \frac{T_{du}}{T_{fu}} = \frac{C^{\frac{3}{2}}H^2}{A} \qquad \chi = \left(1 + \frac{\Delta B}{B_0}\right)^{\frac{1}{3}}. \tag{6.17}$$

Equation (6.17) defines the system's two governing dimensionless parameters. The ratio μ of the draining and filling time scales is the same as that presented by Kaye and Hunt (2004). It is a nondimensional vent area and solely determines the steady state interface height. The second dimensionless parameter, χ represents the ratio of initial and final source buoyancy fluxes. When $\chi > 1$, B increases and conversely when $\chi < 1$ there is a decrease in B.

The above model is consistent with Kaye and Hunt (2004), because as $B_u \to B_l$, $\chi \to 1$ and Kaye & Hunt's equations are recovered. Figure 6.2 reproduces the initial overshoot that they observed when the source of buoyancy is initially switched on. This initial overshoot will be discussed in more detail in the following two sections.

6.4 Results

In this section we examine the deviations of interface height from the steady state value during transitions from one steady state to the next. Figures 3 and 4 demonstrate several examples of this deviation.

Figure 6.3 illustrates the effect of changing χ for a fixed value of $\mu = 5$. Figure 6.3 (a) corresponds to a drop in buoyancy (i.e. $\chi < 1$), which causes the

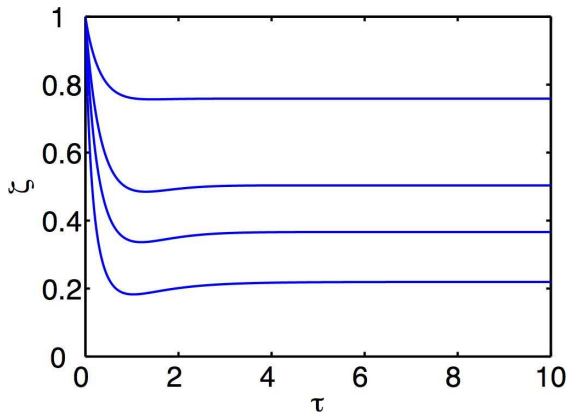

Figure 6.2: Initial overshoot beyond steady state predicted by Kaye and Hunt (2004) when the source of buoyancy is first turned on for various values of μ. From top to bottom $\mu = 0.75$, 4, 7.5 and 50

interface height to rise initially and then fall back down. Figure 6.3 (b) shows that for an increase in source buoyancy (i.e. $\chi > 1$) the opposite happens. As χ shifts further from $\chi = 1$, the jump becomes larger. Also, increasing values of χ result in a quicker return to the steady state interface height. A physical explanation for these behaviours is given below.

Figure 6.4 illustrates the influence of μ by holding $\chi = 0.5$ fixed and plotting the interface height for various values of μ. The magintude of these jumps is largest for intermediate values of μ corresponding to a steady state interface close to half the height of the room. This behaviour is further illustrated in figure 6.5, which plots the maximum deviation from steady state against μ for various values of χ. Figure 6.5 (a) corresponds to $\chi < 1$ and (b) to $\chi > 1$.

Figures 6.3–6.4 illustrate that as χ deviates further from 1 the size of the jump increases. It should also be noted that a smaller deviation occurs for an increase than an equivalent reduction in B (i.e. $\chi = \chi' > 1$ produces a smaller deviation than $\chi = \frac{1}{\chi'}$). This is illustrated particularly well in figure 6.5 where the magnitudes in figure 6.5(a) are much larger than those in figure 6.5(b). In particular, it becomes increasingly difficult to push the interface down with increasing

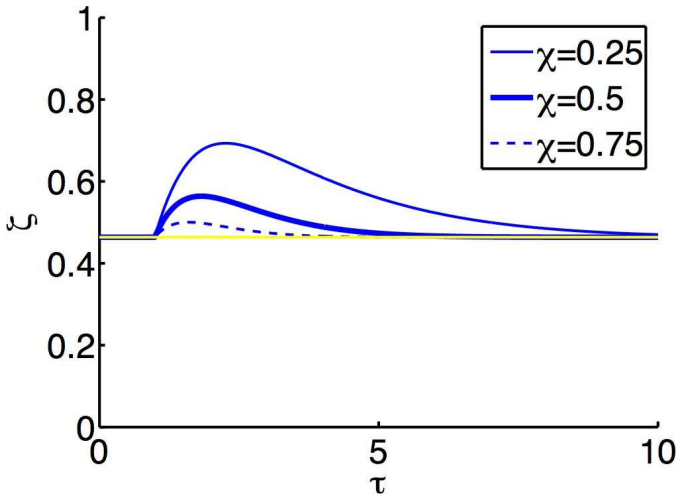

(a)

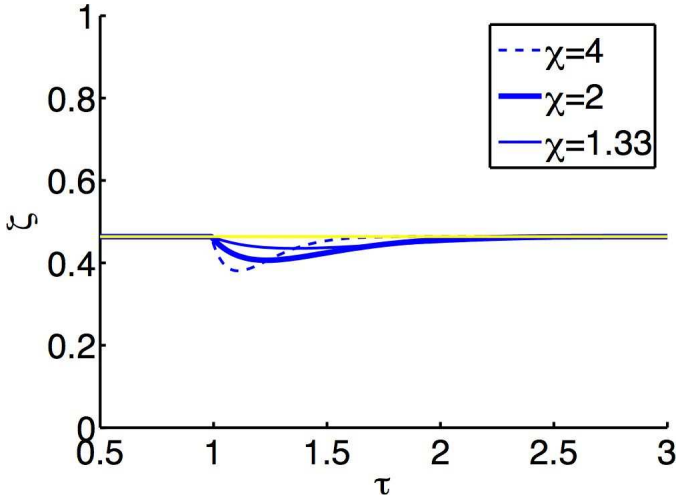

(b)

Figure 6.3: Interface height for various values of χ and $\mu = 5$: (a) decrease in source buoyancy ($\chi < 1$) (b) increase in source buoyancy ($\chi > 1$)

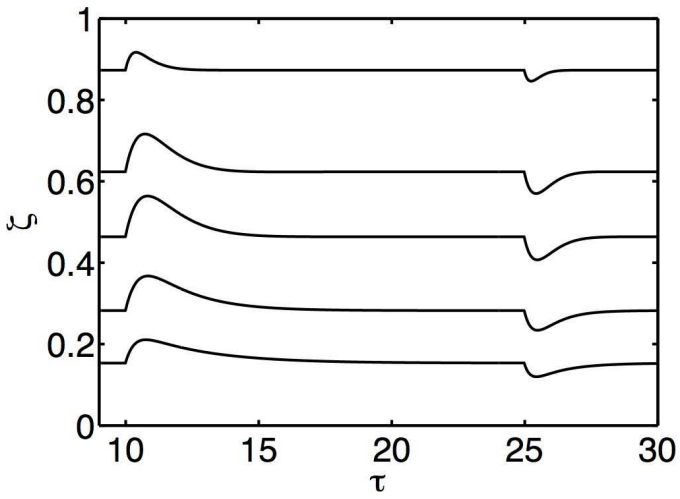

Figure 6.4: Interface height for various values of $\mu = 0.5$, 2, 5, 20 and 50 and $\chi = 0.5$

χ. For example $\chi = 10$, which corresponds roughly to a 1000 times increase in source buoyancy flux only produces a minor change in the amplitude of deviation compared with $\chi = 4$, which corresponds only to a 64 fold increase in source buoyancy.

Now we give some physical insight into the above observations. The adjustment between two steady state interface heights can be explained by referring to Morton et al. (1956) and their solution for the volume flux Q of an ideal plume in an unstratified environment given in (6.5)

We first consider the situation where the source buoyancy flux is increased. From equation (6.5) it is evident that once B is increased the volume flux at the interface will also increase. This causes an imbalance between the flow rate into the upper layer and out of the room, forcing the upper layer to 'fill' and thus the interface to fall. This drop in interface height in turn causes the plume volume flux into the upper layer to decrease. From (6.8) we can see that the volume flux out of the space depends on two things, the buoyancy and depth of the upper layer. Since both these are increasing the volume flux exiting the top of the room will also increase. This, in turn, causes the interface to rise again to its

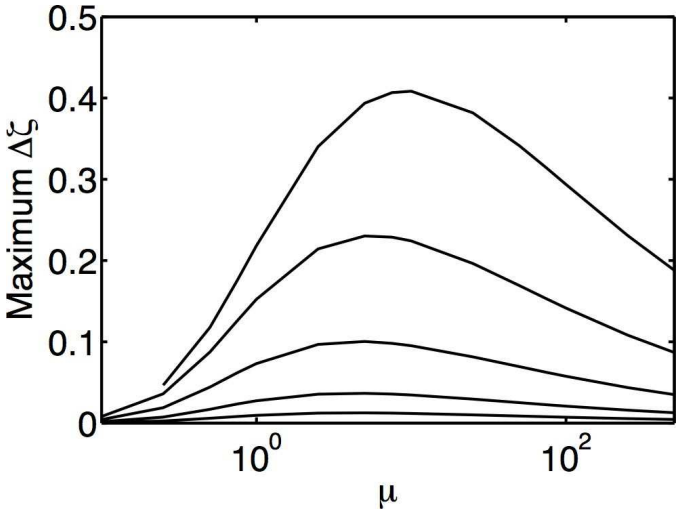

(a)

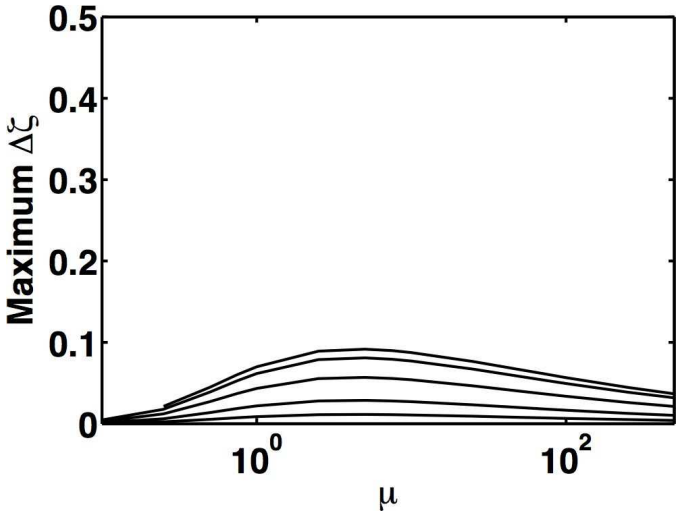

(b)

Figure 6.5: Maximum deviation of interface from steady state value : (a) $\chi < 1$ (from top to bottom χ=0.1, 0.25, 0.5, 0.75 and 0.9) and (b) $\chi > 1$ (from top to bottom χ=10, 4, 2, 1.5 and 1.1) for a range of μ.

steady state value. It is important to note that the final flow rate through the room is larger than its initial value, now that the source buoyancy flux is higher. The opposite occurs when there is a decrease in B, causing the interface to rise and subsequently fall.

From a mathematical perspective, the second term on the right hand side of (6.6) changes when the source buoyancy flux changes. If the source buoyancy flux increases then the left hand side becomes negative, causing the interface to drop and vice versa for a decrease in B.

A typical plot of dimensionless flow rates through the room, q_{out} and q_p, against time in figure 6.6 helps illustrate this phenomenon. When the buoyancy changes there is a sharp change in q_p, while there is some delay in q_{out} reaching its new steady state values. The points where q_p and q_{out} intersect correspond to the turning points (i.e. maximum and minimum overshoot). It is worth noting that the change in q_p is non monotonic while that in q_{out} is monotonic. This is because q_p depends on the interface height, which changes non monotonically during the transition between steady states (i.e. for an increase in source buoyancy the interface descends and then rises and vice versa for a decrease), while q_{out} depends on the total buoyancy in the upper layer, which varies monotonically from its initial to its next steady state value. Another way to think of this is that while the steady state interface height is always the same, regardless of the source buoyancy flux, the steady state value of the upper layer buoyancy depends on the strength of the source and is proportional to $B^{\frac{2}{3}}$.

Another important question is why, for an equivalent change in B, the jump from steady state is always larger when the source buoyancy is decreased compared to when it is increased? This behaviour results from the fact that Q_p increases nonlinearly with height ($\propto z^{\frac{5}{3}}$) (see (6.5)). Therefore, the imbalance in Q_p and Q_{out} is larger when the interface rises than when it falls, leading to a larger deviation from the steady state value.

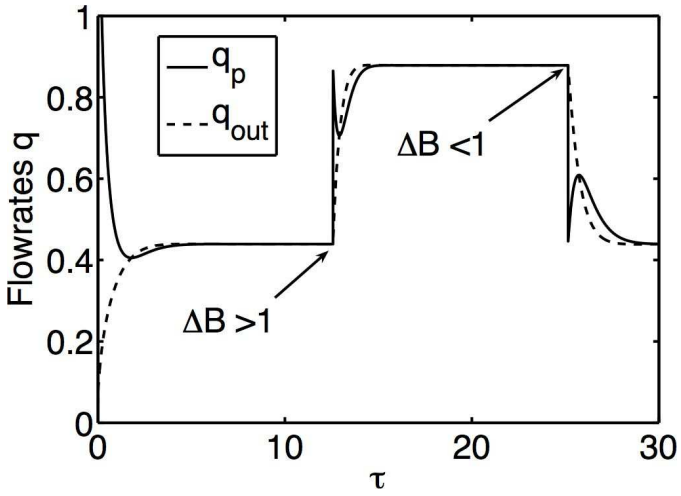

Figure 6.6: Flowrates out of the box, q_{out} and flowrate of the plume,q_p across interface against time. The plume is turned on at $\tau = 0$, the initial steady state is indicated by the constant and equal values of q_p and q_{out}, attained around $\tau = 4$. The buoyancy flux is increased at $\tau = 12$ and the new steady state is achievd at $\tau \approx 15$. Finally, the buoyancy flux is decreased at $\tau = 24$ with the original steady state attained at $\tau = 30$

6.4.1 No overshoot on the return

As shown in figure 2 and first noted by Kaye and Hunt (2004), when the source is first turned on the interface descends from the ceiling and 'overshoots' to a point below its ultimate steady state height. When the interface height deviates from its steady state value due to a sudden change in B as studied in this paper, we note that there is no overshoot beyond the steady value when the interface returns. In this section we illustrate mathematically why this happens and subsequently interpret this phenomenon physically. We also discuss the initial overshoot.

When a deviation from the steady state height, ζ_{ss} occurs there must be a maximum/minimum after which it returns to ζ_{ss}. Thus there exists a point, ζ_m where $\frac{d\zeta}{d\tau} = 0$ which, from (6.16) is given by

$$\frac{\zeta_m^{\frac{10}{3}}}{1-\zeta_m} = \frac{\delta}{\mu^2\chi^2}. \tag{6.18}$$

Based on observations of many simulations we assume that δ, the dimensionless buoyancy, is bounded between its initial and final value (i.e. it changes monotonically from its initial to final value with no overshoot beyond its final state). This behaviour is to be expected since the upper layer has a larger steady state buoyancy when B increases and vice versa. From (6.15) and (6.16) we note that the initial and final steady state nondimensional buoyancies of the upper layer are

$$\delta_{initial} = \zeta^{\frac{-5}{3}}, \qquad \delta_{final} = \chi^2\zeta^{\frac{-5}{3}}, \tag{6.19}$$

where χ is greater or less than one depending on whether there is a jump or drop in buoyancy, respectively - i.e.

$$\Delta B > 0 \Rightarrow \zeta^{\frac{-5}{3}} < \delta < \chi^2\zeta^{\frac{-5}{3}}, \qquad \Delta B < 0 \Rightarrow \chi^2\zeta^{\frac{-5}{3}} < \delta < \zeta^{\frac{-5}{3}}. \tag{6.20}$$

During the transient, $\frac{\delta}{\mu^2\chi^2}$ the right hand side of (6.18), varies from

$\frac{1}{\mu^2\chi^2\zeta^{\frac{5}{3}}} \rightarrow \frac{1}{\mu^2\zeta^{\frac{5}{3}}}$. At the turning point $\frac{d\zeta}{d\tau} = 0$, but $\frac{d\delta}{d\tau} \neq 0$. Otherwise some other steady state could exist.

For $\Delta B > 0$, $\frac{d\delta}{d\tau} > 0$, which from (6.16) implies

$$\frac{\delta}{\chi^2} < \zeta^{\frac{-5}{3}}. \tag{6.21}$$

and vice versa for $\Delta B < 0$.

Combining (6.21) and (6.18) we obtain

$$\Delta B > 0 \Rightarrow \frac{\zeta^{\frac{15}{3}}}{1-\zeta} < \frac{1}{\mu^2}, \tag{6.22}$$

$$\Delta B < 0 \Rightarrow \frac{\zeta^{\frac{15}{3}}}{1-\zeta} > \frac{1}{\mu^2}. \tag{6.23}$$

The left hand side, $\frac{\zeta^{\frac{15}{3}}}{1-\zeta}$, of the inequalities (6.22) and (6.23) is a monotonically increasing function in ζ. This explains why a turning point below ζ_{ss} is observed for an increase in buoyancy and vice versa for a drop in buoyancy.

The maximum/minimum value of interface height ζ_m that can be reached during a change in buoyancy can be bounded. For $\Delta B > 0$, combining (6.20) and (6.18) it can be shown that

$$\frac{1}{\mu^2\chi^2} < \frac{\zeta_m^{\frac{15}{3}}}{1-\zeta_m} < \frac{1}{\mu^2}. \tag{6.24}$$

A similar inequality exists for $\Delta B < 0$

$$\frac{1}{\mu^2\chi^2} > \frac{\zeta^{\frac{15}{3}}}{1-\zeta} > \frac{1}{\mu^2}. \tag{6.25}$$

So, for an increase in buoyancy, (6.24), shows that ζ is always greater than some steady interface height associated with an equivalent $\hat{\mu} = \mu^2\chi^2$, and always less than the steady state value associated with μ, thus explaining why the steady height is never overshot. Similarly, (6.25) bounds ζ to remain above the steady height for a drop in buoyancy.

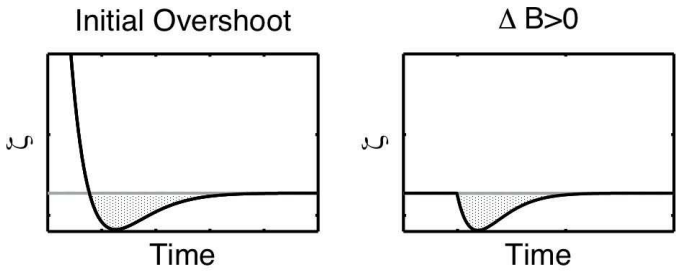

Figure 6.7: The initial overshoot is physically similar to the situation where there is a sudden increase in source buoyancy flux

Now that we have answered why no overshoot is observed when settling back to the steady state interface height as a result of a sudden change in buoyancy, it is also important to understand why an overshoot can take place during the establishment of the initial steady state. First, we should note that physically the transition between steady states and the initial overshoot are quite different. The initial 'overshoot' occurs when a source of buoyancy is initially turned on. This corresponds to $\Delta B > 0$. Consequently, from the discussion above, if a turning point does exist, it must exist at a height below the steady state interface height. Therefore, the initial overshoot is similar to the deviation from the steady state height during a sudden increase in source buoyancy as shown in figure 6.7. The main difference is that the initial condition for the interface height is not the steady state value, but rather $\zeta = 1$. In a similar fashion to above we assume δ varies only between its initial and final value

$$1 < \delta < \zeta^{-\frac{5}{3}}. \tag{6.26}$$

Combining (6.26) and (6.18) the following inequality is obtained

$$\frac{1}{\mu^2} < \frac{\zeta^{\frac{10}{3}}}{1-\zeta} < \frac{\zeta^{\frac{-5}{3}}}{\mu^2}. \tag{6.27}$$

Note that $\frac{\zeta^{\frac{10}{3}}}{1-\zeta}$ is also a monotonically increasing function, which is always greater than $\frac{\zeta^{\frac{15}{3}}}{1-\zeta}$. Therefore the solution to $\frac{1}{\mu^2} = \frac{\zeta^{\frac{10}{3}}}{1-\zeta}$ lies below ζ_{ss}, allowing ζ to fall below

its steady height.

6.5 Comparison with Stratified Model

A key assumption of the model presented in §6.3 and §6.4 is that the upper layer is considered to be well mixed. In practice, this is not true as the plume will generate a 'filling box' stratification when its buoyancy at the interface is different from the upper layer buoyancy. In this section we develop a Germeles-type model to account for the upper layer stratification and compare the results with those of the well-mixed model.

6.5.1 Theory

The conservation equations (6.6) and (6.8) can be modified to account for the fact that the upper layer is not well mixed. The corresponding conservation equations are

$$\frac{dh}{dt} = \frac{A\sqrt{I}}{S} - \frac{CB^{\frac{1}{3}}h^{\frac{5}{3}}}{S}, \tag{6.28}$$

$$\frac{dI}{dt} = \frac{B}{S} - \frac{I\sqrt{I}g'(z=H,t)}{S}, \tag{6.29}$$

where $I = \int_h^H g'dz$ is the integrated buoyancy in the upper layer.

Defining the average buoyancy of the upper layer $\bar{g'} = \frac{I}{(H-h)}$ and non dimensionalizing as before leads to

$$\frac{d\zeta}{d\tau} = \frac{1}{\sqrt{\mu}}\sqrt{\bar{\delta}(1-\zeta)} - \sqrt{\mu}\zeta^{\frac{5}{3}}, \tag{6.30}$$

$$\frac{d\bar{\delta}}{d\tau} = \sqrt{\mu}\left(\frac{1-\bar{\delta}\zeta^{\frac{5}{3}}}{1-\zeta}\right) + \frac{1}{\sqrt{\mu}}\sqrt{\frac{\bar{\delta}}{1-\zeta}}(\bar{\delta} - \delta(\zeta=1)). \tag{6.31}$$

The only significant difference for the stratified system is the second term in the buoyancy equation (6.31) $\left(\frac{1}{\sqrt{\mu}}\sqrt{\frac{\bar{\delta}}{1-\zeta}}(\bar{\delta}-\delta(\zeta=1))\right)$. We now ask when this term will be important and when it may be neglected?

Assuming that all other terms are the same order for the well mixed and stratified cases, which does not seem unreasonable, the most important parameter in the above equations is μ. The ratio of the first to second terms in the buoyancy equation (6.31) is proportional to μ. As such, for larger values of μ the first term should dominate and the second term becomes negligible, which is indeed what we observe in our simulations below. Large values of μ correspond to small dimensionless vent areas (6.17), in which case the upper layer is large. For deep upper layers the contribution of buoyancy from the plume at any given time is small compared to the total amount of buoyancy in the upper layer, whereas for shallow layers this contribution can be significant. As such the effect of stratification becomes less important for large μ.

In terms of the time taken to return to steady state, the mixed and stratified systems will also behave differently. For the stratified case the buoyancy extracted from the top of the room will always be the highest. Therefore, if B is increased we expect the system to adjust more slowly for a stratified system than for the mixed case. Conversely, a stratified system should respond more quickly to a decrease in buoyancy. Mathematically, this is represented by the additional term in (6.31), which is always negative or zero thus increasing the adjustment time for an increase in buoyancy and decreasing it for a drop.

6.5.2 Numerical Model

In order to determine the impact of this additional term in the buoyancy conservation equation we solve the problem using a Germeles algorithm, which allows a stratification to evolve in the upper layer. The algorithm is described in chapter 3.

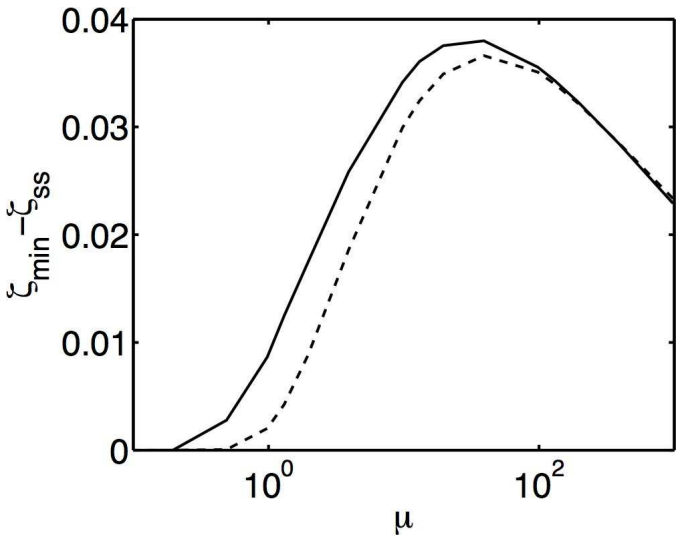

Figure 6.8: The size of the initial overshoot beyond steady over a range of μ predicted by the well-mixed model (– –) and the Germeles model (–)

6.5.3 Initial Overshoot

In this section we examine the initial overshoot when a source of buoyancy is turned on in an initially unstratified box as considered by Kaye & Hunt (2004). Figure 6.8 shows the magnitude of the overshoot beyond steady state against μ for both the well-mixed and Germeles models. For all values of μ the overshoot is larger for the stratified case. At large values of μ there is little difference in the size of overshoot since the upper layer is deep as we predicted from the discussion on (6.31). For very small values of μ there is almost no overshoot at all. Kaye and Hunt (2004) showed that for the well-mixed case no overshoot will occur for $\mu < 0.25$, which we also observe. However for the stratified case an overshoot will exist for even smaller values of μ. Finally, at intermediate values of μ the biggest difference in overshoot occurs. Even so, the largest difference is less than 1% of the height of the room.

6.5.4 Jump in Buoyancy

In this section we consider an increase in source buoyancy flux. The system is allowed to evolve to steady state for some initial buoyancy flux. There is a sudden increase in the buoyancy to a value χ^3 times larger than the initial one. The interface height is compared for the well-mixed and Germeles models.

Figure 6.9 shows the magnitude of the overshoot beyond the steady state value for both models over a range of μ and for various values of χ. As with the initial overshoot we observe that the difference in predicted overshoot by the well-mixed and Germeles model are insignificant for $\mu > 100$. A difference for values of μ smaller than this does exist. Once again these differences are very small. The maximum overshoot occurs for values of $\mu \sim O(1)^1$, which corresponds to a steady interface height near the middle of the room. Note also that the magnitude of the overshoot does not appear to change siginificantly for values of χ greater than 5. No matter how much harder the system is forced the interface will not descend further.

6.5.5 Reduction in Buoyancy

Here we examine a reduction in source buoyancy flux in the same manner as the last section. Figure 6.10 shows the maximum amplitude in the deviation from the steady state interface height for the well-mixed and Germeles model over a range of μ and for various values of χ. Once again we observe a negligible difference in overshoot between the two models for values of $\mu > 100$. Any differences that are observed for smaller values of μ are small, with the largest again occurring around $\mu = 5$. In contrast to the increase in buoyancy flux, the amplitudes do vary significantly with χ.

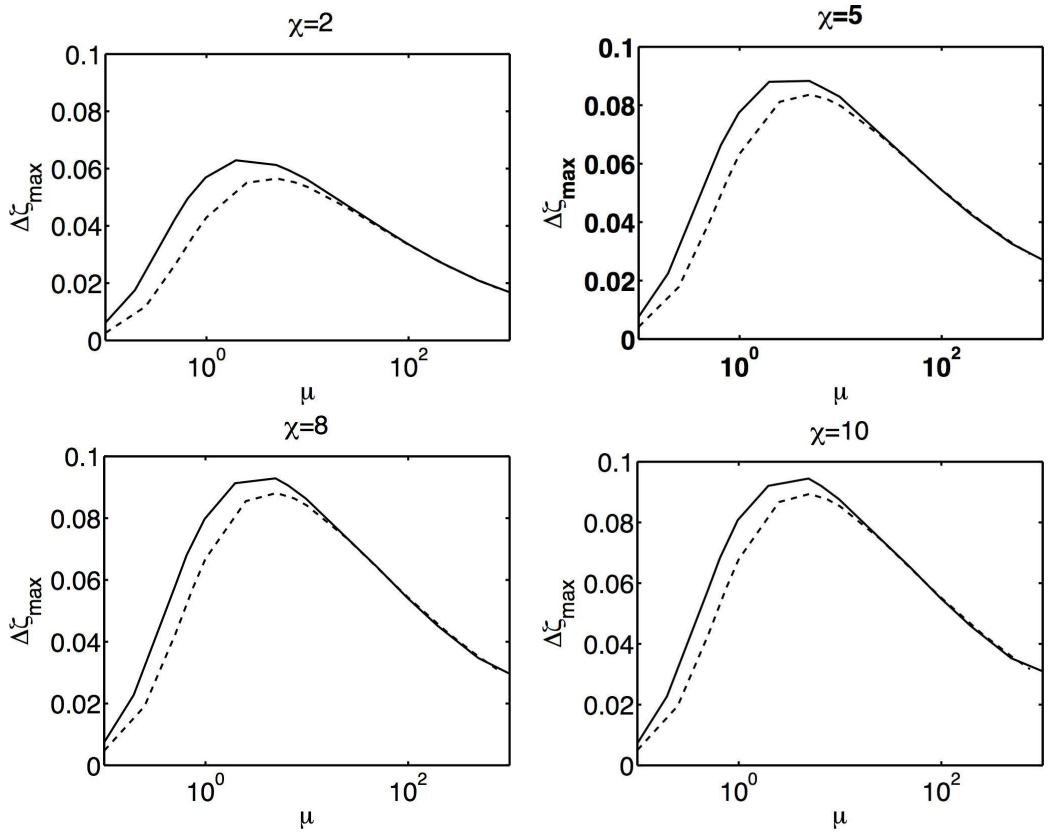

Figure 6.9: The maximum deviation from steady state for a rise in B for the well-mixed (– –) vs stratified (–) models for various values of $\chi > 1$

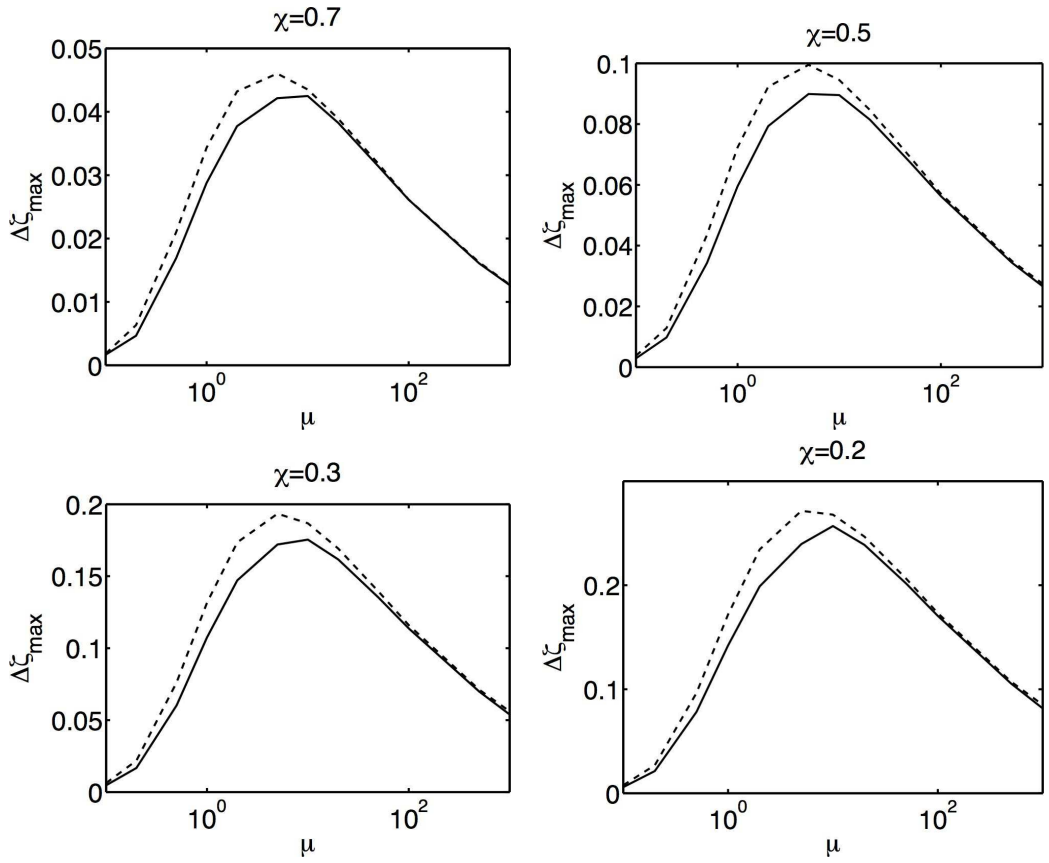

Figure 6.10: The maximum deviation from steady state for a drop in B for the well-mixed (– –) vs stratified (–) models for various values of χ

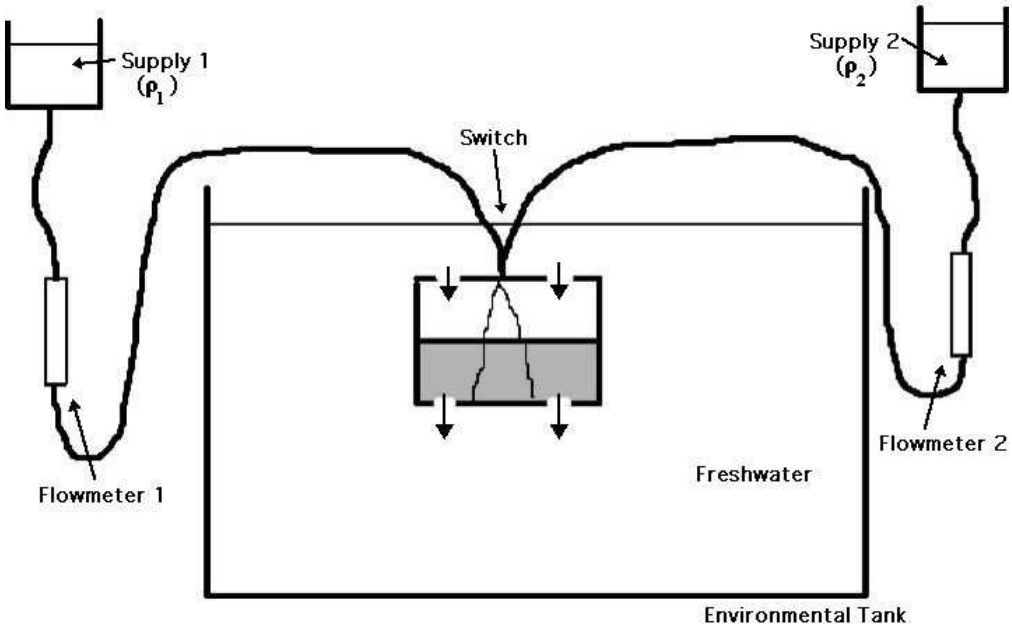

Figure 6.11: A schematic of the experiments, showing the ventilated box placed in the large environmental tank. The different buoyancy fluxes are obtained by switching between the two supply tanks.

6.6 Experiments

A sequence of experiments was conducted in order to compare the results to the models described in this paper. The room is represented by a plexiglass tank of dimensions 30x30x40 cm, which is submerged in a larger tank that represents the atmosphere (2.4x1.2x1.2 m). The large environmental tank is filled with fresh water. Rather than using heat to change the buoyancy of the fluid we used salt added to water (see Linden 1999 for details). Several holes are drilled into the top and bottom of the smaller tank to provide vents to connect the tank to the exterior. Two plume sources, based on the design of Dr Paul Cooper (see Hunt, Cooper & Linden 2000) are placed at the centre of the top of the tank. Since the source in the experiments injects negatively buoyant fluid from the top of the tank it represents an inverted form of the model described so far.

Two supply tanks, each with fluid of different density can feed one of the plume sources. We switch between the two supplies thus generating a step up or down in source buoyancy flux. Food dye was added to each batch of salt water with a different colour so as to distinguish between the two cases.

From one side of the large tank the apparatus was lit uniformly while recording from the other side using a digital monochrome ccd camera. By measuring the light intensity of the recorded images using the image analysis software, DigImage (see Cenedese and Dalziel (1998)), the interface can be detected as a jump from the light intensity associated with zero dye to that associated with the buoyant layer. Since in practice, the interface is not completely sharp due to finite Peclet number and small disturbances that may exist, a horizontal average, excluding the plume region, of each time frame was taken. The interface is then taken as the point of steepest gradient in light intensity, which is consistent with the method used by Kaye and Hunt (2004).

Since the plume sources generate non ideal plumes, virtual origin corrections were calculated with the formulas developed by Hunt and Kaye (2001) and

[1] close to 5

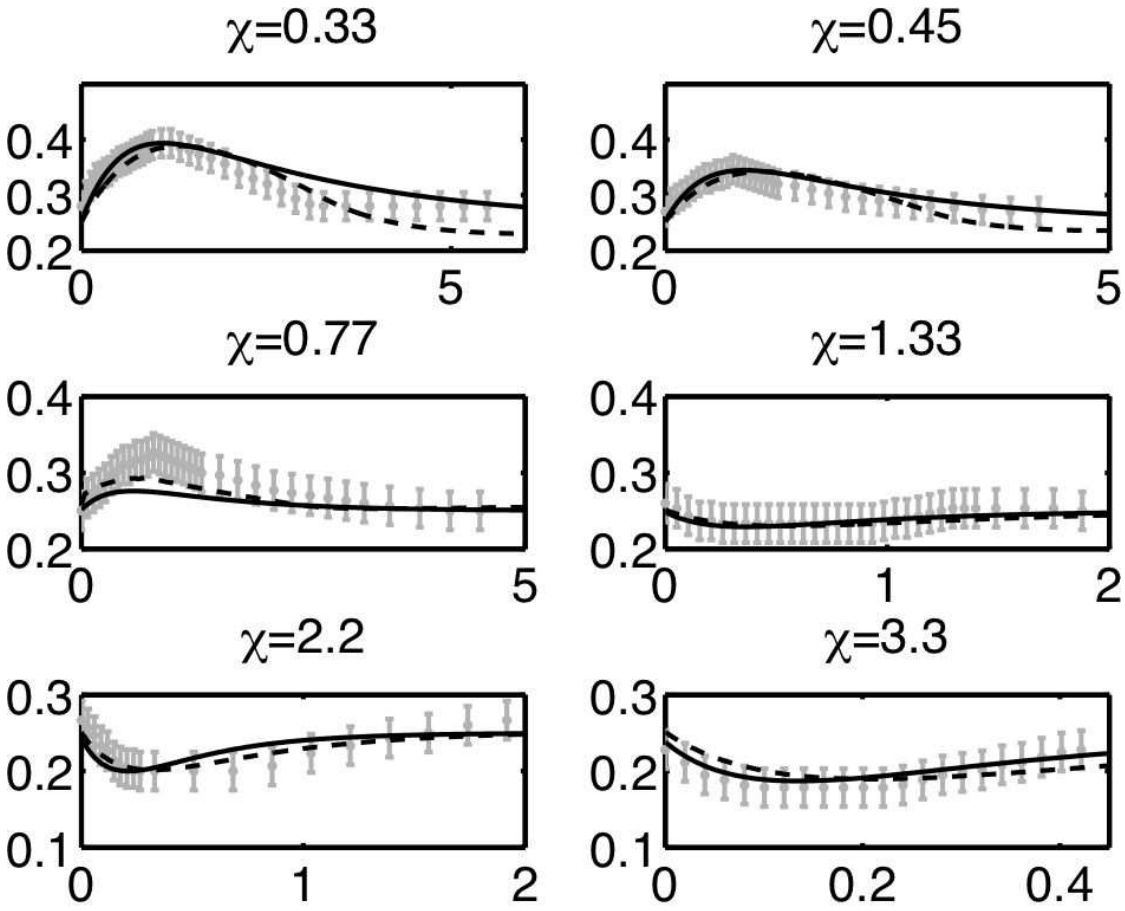

Figure 6.12: Interface Height vs time for various values of χ at $\zeta = 0.25$. Well Mixed (–), Stratified (- -), Experiment(•). The error bars on the experimental data correspond to typical interface thicknesses

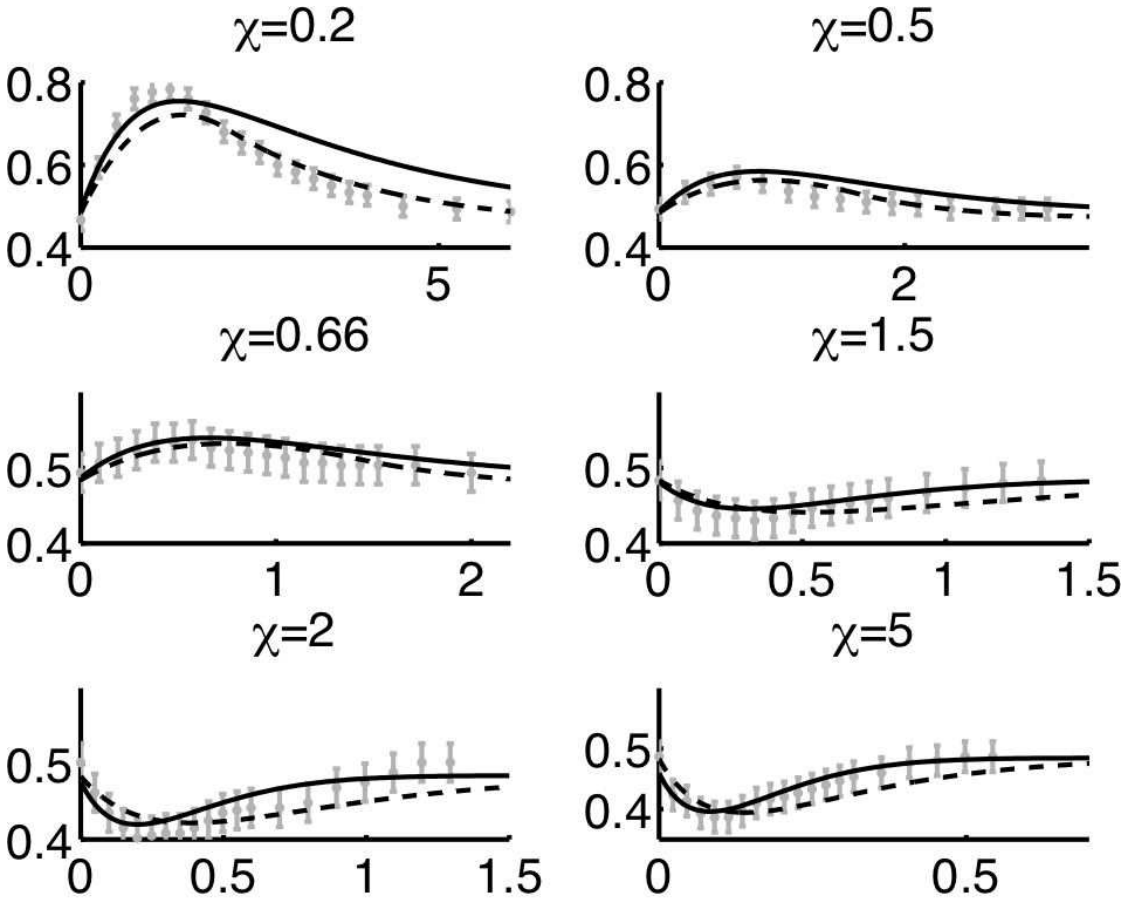

Figure 6.13: Interface Height vs time for various values of χ at $\zeta = 0.5$. Well Mixed (–), Stratified (- -), Experiment(•). The error bars on the experimental data correspond to typical interface thicknesses

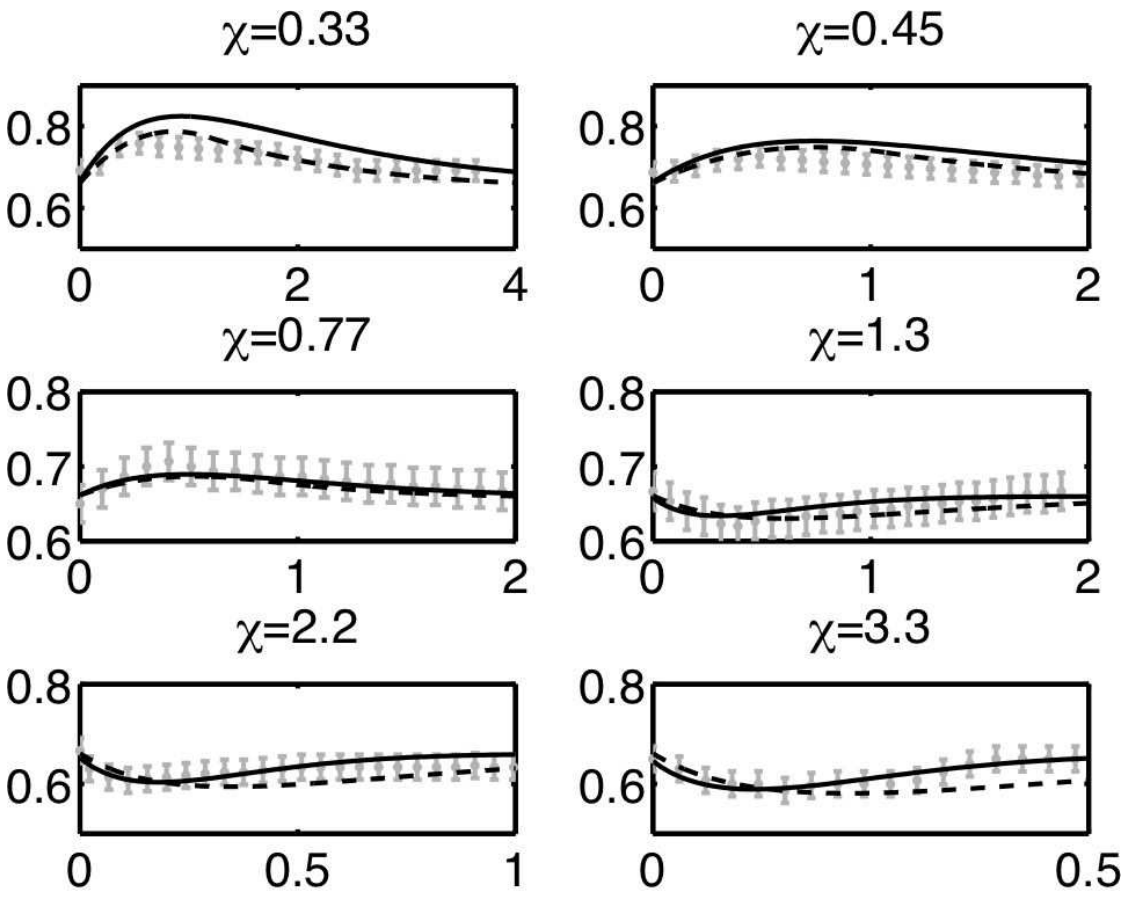

Figure 6.14: Interface Height vs time for various values of χ at $\zeta = 0.66$. Well Mixed (–), Stratified (- -), Experiment(•). The error bars on the experimental data correspond to typical interface thicknesses

then adjusted so that, for each experiment, both plume sources resulted in the same steady interface height.

Figures 6.12-6.14 display the results of these experiments. In all cases the agreement between theory and experiments is good. As predicted in §4, values of $\chi < 1$ imply that the Germeles model will reach steady state before the well mixed model. Conversely for $\chi > 1$ the well mixed model adjusts more quickly. Since in the experiments we neither obtain perfect stratification nor perfect mixing we expect the experimental curves to lie somewhere between the two models, which is, broadly speaking, what we observe.

A measure we use to compare the models to experiments is the prediction of the maximum deviation from the steady state interface (i.e. $\zeta_m - \zeta_{ss}$). Most of the values predicted by the well mixed and stratified models are within $\pm$ 15 % of the experimental values. Larger discrepancies are observed for the $\zeta_{ss} = 0.66$ case and small χ, where the well mixed model overpredicts the overshoot by close to 50%. This is probably because when there is a decrease in source buoyancy flux there is typically little mixing in the upper layer, particularly so for values of $\chi < 0.5$ as shown by Bower (2005). When the plume reaches its level of zero relative buoyancy it becomes a fountain, continues to rise and then falls back before spreading horizontally. Smaller values of $\chi < 1$ (i.e. larger differences in source buoyancy flux) mean that the fountain will have less momentum, rise a smaller height into the region above the level of zero buoyancy and thus cause less mixing, invalidating the well-mixed assumption for the upper layer.

Another region where the differences between theory and experiment were large (between 10 and 40% for both the Germeles and well-mixed models) is when the value of χ is closest to 1 (i.e. $\chi = 0.77$ and $\chi = 1.33$). This is due to the fact that the deviations of the interface from its steady state value tend to be so small as to be close to or even less than the actual thickness of experimental interface as shown by the error bars in figures 12-14. In these experiments the thickness of the interface is typically $4 - 10\%$ of the total height of the box. This makes it difficult

to pinpoint/define the precise location of the interface during the transient.

Outside these two regions the average error for the well-mixed model was 8.25% with a standard deviation of 4.5%. Excluding only the intermediate values of χ the average error for the Germeles model was 7.8% with a standard deviation of 4%. These values display the good agreement between models and experiments.

Another measure we can use is the time it takes for the interface to return to its steady state value. For $\chi < 1$ the Germeles model predicts this time well - within $\pm 11\%$. However, the well-mixed model performs poorly, overpredicting the time to steady state by as much as 100% for the $\chi = 0.2$ case. Similarly for $\chi > 1$ the well-mixed model predicts this time well - within $\pm 9.5\%$. However, the Germeles model performs poorly the larger χ gets, overpredicting the time to steady state by 80% for the $\chi = 0.33$ case.

It appears that the well mixed model works better at predicting the interface location when there is an increase in source buoyancy flux, particularly for larger values of χ. This is because when buoyancy is increased, larger values of χ lead to larger volume flow rates and momentum fluxes, causing more mixing in the upper layer, thus strengthening the well mixed approximation. Similarly the Germeles model works best for decreases in buoyancy flux, particularly for smaller values of χ. The reason for this is the lack of mixing that occurs when the plume becomes a fountain as described previously.

6.7 Summary and Conclusions

In this paper we considered a naturally ventilated space containing an isolated source of buoyancy. We developed a mathematical model based on two well-mixed layers and tracked the interface height and buoyancy of the upper layer. The initial descent of the interface height to its steady state value for this model had been previously discussed by Kaye & Hunt 2004. We focused our attention on the affects of a sudden change in buoyancy. We observed a rise and fall back to its

steady height of the interface for a decrease in source buoyancy flux. Similarly, we observed a drop and corresponding rise when the source buoyancy flux is increased. After the jump/drop the interface always settles back to the initial steady state height, agreeing with Linden et al. (1990)'s observation that the steady interface height is independent of the source buoyancy flux.

We then changed the focus to the assumption that the upper layer is always well mixed. By considering a model that captures stratification (the Germeles model) we compared the predicted deviations of the interface in an attempt to find out what information we lose with this well-mixed assumption. We found that over a wide range of parameters there is very little difference between the two models in terms of predicting the height of the interface. There is a difference in the readjustment timescale depending on whether the heat load is increased or decreased. The stratified system returns to steady state more quickly when there is a decrease in source buoyancy flux, while the well-mixed model will predict a faster time for an increase.

A set of laboratory experiments were conducted to validate our models. In all cases both the well-mixed and Germeles models agreed well with the experiments. Since in the experiments there is neither perfect mixing nor idealised stratification, we expected the interface to lie between the two models, which is generally what was observed. Consequently, since it is both easier and computationally cheaper, we suggest that the well-mixed model is adequate for most practical applications. However, it should not be used in situations where the fine detail of the stratification may be of interest.

In conclusion, we would like to point out that natural displacement ventilation offers several very appealing features, the most obvious of which is probably the potential of reducing energy consumption. In addition we draw attention to some of the other beneficial features.

1. Natural ventilation is a self controlling system. As Linden et al. (1990) showed the steady state interface location is independent of the strength of

heat source. As the amount of heat from sources is increased the flow rate through the space automatically increases. Consequently, a complicated and expensive control system is not required.

2. While we studied both the cases where there is a increase or decrease in source buoyancy flux, from a practical perspective the increasing buoyancy flux scenario is far more interesting. First, most realistic concerns typically arise in situations where there is an increase in the heat load into a room. Second, since in the situation where B is decreased the interface rises and never falls back below the steady height, there is really little need for concern as long as the steady interface height is designed to be at an appropriate level above occupants. Therefore, as long as steady state conditions satisfy any imposed requirements, these requirements will also be satisfied during any transients when the heat load is decreased.

3. Not only is natural ventilation self controlling, but additionally the timescale associated with readjustment acts in a favourable manner too. In §3 we showed that the larger the increase in source buoyancy flux is, the faster the interface returns to the steady state height. Therefore, in situations where the heat load is increased, there will be a transient during which the interface height can fall into the 'occupied' level. However, the duration of this transient will be shorter that the timescale of the system defined in (6.14) and will, in fact, be shorter the larger the jump in heat load is.

4. As mentioned, the only situation which really poses any concern is an increase in heat load. Reassuringly, the amplitude of the deviation from steady state is typically small for situations where this occurs. In §4 we showed that the maximum deviation for $\chi = 10$, which corresponds to a 1000 fold increase in source buoyancy flux, is less than 10% of the total height of the room. Therefore any descent of the interface into the occupied layer will not only readjust quickly, but also not penetrate very far.

The text in chapter 6, in part, has been submitted for publication in *Energy and Buildings* (D Bolster, A Maillard & PF Linden). I was the primary researcher on this project.

7

Transients in Natural Ventilation 2 - Time varying Source of Buoyancy

7.1 Abstract

We examine the transient behaviour of a naturally ventilated space with a periodically time varying heat source. The buoyancy driven flow is modelled using the 'emptying filling box' model developed by Linden et al. (1990). The space we consider has an isolated source of buoyancy, modelled as a plume, at the middle of the floor. The room is connected to the exterior via openings at the top and bottom of the box. Pressure differences between the exterior and interior that arise due to the buoyancy in the box generate a natural ventilation flow that leads to a two-layer flow with buoyant (warm) fluid in the upper layer and ambient fluid in the lower 'occupied' layer. During the flow's transient evolution, the upper layer has a non-uniform stratification within it, which we study using a simple numerical model. A series of analogue, small-scale laboratory experiments were also conducted in order to validate the numerical predictions. The time-varying stratification that evolves in the space leads to time-varying flow rates through

the space. Based on the numerical and experimental observations we identify four important flow rates associated with such a space and illustrate which of these flow rates dominate based on the strength and oscillation period associated with the thermal source.

7.2 Introduction

In the previous chapter we considered a flow in the emptying filling box, where the source buoyancy flux is switched from one value to another. The work presented in this chapter is intended to consider the related and important problem where there is a source whose buoyancy flux does not merely switch from one value to another, but oscillates between two values at some frequency. We model situations where the heat load is changing (e.g. equipment being turned on and off, people walking in and out of a room, etc.).

The following model considers the case where the initial source buoyancy flux is high. Then for some reason (e.g. machinery being turned on and off, people moving in and out of the space etc) the source buoyancy flux is reduced. We consider situations where the source buoyancy flux jumps between two values at various frequencies. In our model we look at the case where the natural ventilation interface (determined by the geometry of the room alone) is at about half the height of the room, because this seems most applicable to reality and also allows for the best visualization. As a control case we consider the situation where the buoyancy flux corresponds to the average of the upper and lower values. We are particularly interested in two aspects of the flow. Firstly, we wish to consider the transient response of the layer depth and flow rates to the variation in the source conditions. Secondly, we wish to identify how much the time-averaged flow rate through the room is affected by varying the source buoyancy flux.

The structure of the paper is as follows: In §7.3 the details of the model are described. In section §7.4 the numerical scheme is described and results for var-

ious conditions are presented. §7.5 discusses analogue experiments and compares the experimental measurements to the results of the numerical model. Section §7.6 discusses the application of the model to a real-life ventilation scenario.

7.3 Model Description

7.3.1 Plume Model

To model an isolated source of buoyancy, we utilize the classical plume model of MTT56, under the Boussinesq approximations discussed in chapter 3.

$$\frac{dQ}{dz} = 2\alpha M^{\frac{1}{2}}, \qquad M\frac{dM}{dz} = FQ, \qquad \frac{dF}{dz} = \frac{g}{\rho_0}\frac{d\rho_a}{dz}Q, \tag{7.1}$$

where πQ is the volume flux, πM is the momentum flux, πF is the buoyancy flux and α is the entrainment coefficient:

In (7.1) the quantities are averaged over a sufficiently long time scale to capture the mean properties of the inevitable turbulent fluctuations. However, we are interested in the response of the system to a time variation in the source conditions over times longer than these characteristic turbulent time scales. In general, the fluxes Q, M and F are functions of both z and t. In many cases the steady plume equations may be used under a quasi steady approximation (see Conroy et al. (2005) for a detailed discussion of the appropriate scalings required for this quasi-steady approximation to be be valid).

Boundary Conditions

The simplest situation is a so called 'point source' plume, which is a source of buoyancy where $Q(0,t) = M(0,t) = 0$ and $F(0,t)$ is fixed. We generalize this to the situation where $F(z=0,t)$ is

$$F(0,t) = \left(\frac{F_h + F_l}{2}\right) + \left(\frac{F_h - F_l}{2}\right) sgn(\sin(2\pi\Omega t)). \tag{7.2}$$

i.e. F(z=0) can take one of two values, F_h or F_l and it jumps between these two values with a frequency Ω. Let us define $\bar{F} = \frac{F_h+F_l}{2}$, the average source buoyancy flux and $\chi = \frac{F_h}{F_l} < 1$, the ratio of buoyancy fluxes.

To study the whole space, the vertical ambient density profile needs to be determined. We again consider the 'emptying filling box' flow, shown schematically in Figure 7.1. We are specifically interested in the response of the 'emptying filling-box' flow to this sudden change in source conditions, and so we do not consider the subtleties of the plume flow adjustment directly after switching from one source condition to the other. For typical conditions the plume transients occur on a much faster time scale than the time scale associated with the boundary condition (see Scase et al. (2006) for a detailed discussion of this situation).

The BT69 Filling Box Model

For the ambient, we follow the approach of Baines and Turner (1969) and Linden et al. (1990) (See Chapter 3). Volume conservation states

$$w_a A = -\pi(Q - Q_{out}), \tag{7.3}$$

where w_a is the vertical velocity outside the plume and πQ_{out} is the volume flow rate leaving the box through the upper vent. If the flow is of a sufficiently large scale for advection to dominate diffusion, the conservation of mass equation become:

$$\frac{\partial \rho_a}{\partial t} - \frac{\pi(Q - Q_{out})}{A}\frac{\partial \rho_a}{\partial z} = 0. \tag{7.4}$$

To close the system we must determine Q_{out}. Assuming that the source has no volume flux, conservation of volume implies that $Q_{out} = Q_{in}$, where πQ_{in} is the volume flow rate into the space. Assuming that the pressure distribution in the space is hydrostatic and that Bernoulli's equation applies it is straightforward to show that:

$$Q_{in} = Q_{out} = \frac{1}{\pi} A_* \sqrt{I_c};\ A_*^2 = \frac{A_{top}^2 A_{bot}^2}{\frac{1}{2}(A_{top}^2 + A_{bot}^2)};\ I_c = \int_h^H g' dz, \tag{7.5}$$

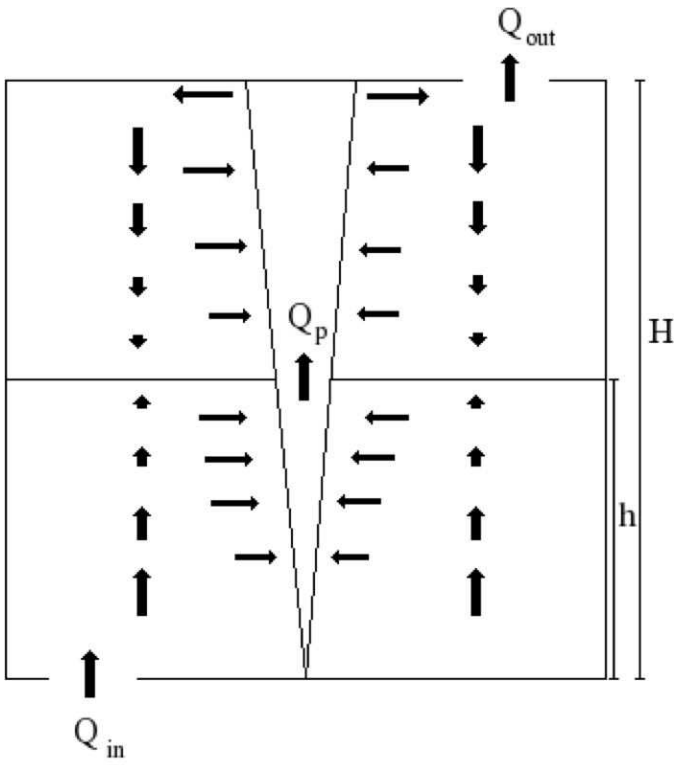

Figure 7.1: Illustration of the idealised flow in a natural ventilated space

where discharge coefficients have been absorbed into the opening areas for clarity. I_c quantifies the effect of the total buoyancy in the room on the hydrostatic pressure, while A_* is the effective opening area. (See Linden et al. (1990) and Woods et al. (2003) for a detailed derivation.) At steady state the upper layer is well mixed, with $I_c = g'_\infty(H - h_\infty)$, where g'_∞ is the reduced gravity of the fluid entering the buoyant layer via the plume.

Using the well-known similarity solution for the volume and momentum fluxes in an unstratified fluid (Morton et al. (1956))

$$F(z) = F_s, \qquad Q(z) = \frac{6\alpha}{5}\left(\frac{9\alpha}{10}F_s\right)^{\frac{1}{3}} z^{\frac{5}{3}}, \qquad M(z) = \left(\frac{9\alpha}{10}F_s\right)^{\frac{2}{3}} z^{\frac{4}{3}}, \tag{7.6}$$

we choose to scale the system with the mean source buoyancy flux defined previously ($\bar{F} = \frac{F_h + F_l}{2}$) and the room depth H. Therefore, we define the notional volume and momentum fluxes Q_h and M_h as well as a reduced gravity g'_H

$$Q_h = \frac{6\alpha}{5}\left(\frac{9\alpha}{10}\bar{F}\right)^{\frac{1}{3}} H^{\frac{5}{3}} \quad M_h = \left(\frac{9\alpha}{10}\bar{F}\right)^{\frac{2}{3}} H^{\frac{4}{3}} \quad g'_H = \left[\frac{6\alpha}{5}\left(\frac{9\alpha}{10}\right)^{\frac{1}{3}} H^{\frac{5}{3}}\right]^{-1} \bar{F}^{\frac{2}{3}}. \tag{7.7}$$

As the characteristic time scale, we will choose the filling box time scale T_f defined as

$$T_f = \frac{AH}{\pi Q_h}. \tag{7.8}$$

This is the time scale over which a source would completely fill a room in the absence of ventilation. Using these quantities we then scale the system variables as

$$z = H\zeta,\ C = \frac{\rho_{a0} - \rho}{\rho_0},\ Q = Q_h q,\ M = M_h m, \tag{7.9}$$

$$F = \bar{F} f,\ t = T_f \tau,\ A_v = \frac{\pi Q_h}{\sqrt{g'_H H}} a_v,\ w = \frac{H}{T_f} w^*. \tag{7.10}$$

With the above non-dimensionalization the plume equations become

$$\frac{dq}{d\zeta} = \frac{5}{3}p^{1/4}; \qquad \frac{dm}{d\zeta} = \frac{4}{3}\frac{fq}{m}; \qquad \frac{df}{d\zeta} = \frac{q}{q_s}\frac{dC_a}{d\zeta}, \tag{7.11}$$

where C_a is the ambient concentration and $q_s = -\frac{\bar{F}}{Q_h g}$. The boundary conditions become

$$f(0) = 1 + \left(\frac{\chi - 1}{\chi + 1}\right) sgn(\sin(\hat{\Omega}\tau)),\ \hat{\Omega} = \frac{2\pi\Omega}{T_f}, \tag{7.12}$$

where $\hat{\Omega}$ is the dimensionless source frenquency. The evolution equation for the room concentration becomes

$$\frac{\partial C}{\partial \tau} - (q - q_{out})\frac{\partial C}{\partial z} = 0, \tag{7.13}$$

where

$$q_{out} = a_v \sqrt{\int_0^1 C d\zeta} = a_v \sqrt{E}. \tag{7.14}$$

7.4 Numerical Model - Germeles algorithm

We solve this system of equations using a modification of the method originally developed by Germeles (1975) as described in chapter 3.

7.5 Experiments

Instead of discussing the properties of the solutions to this system of equations in isolation it is more useful to compare the predictions of the model to a sequence of analogue experiments. We used various brine solutions to model density variations in a plexiglas tank of dimensions 30x40x30 cm, which was submerged within a larger tank (2.4x1.2x1.2m) filled with fresh water, representing the external ambient in the model. Several holes were drilled in the top and bottom of the smaller tank to represent the openings in the model. Two plume sources were drilled into the centre of the top of the tank so that at all heights the cross-sectional area of the plume is much less than that of the room. For the sake of ease the source injected negatively buoyant (heavier) fluid from the top of the tank and so represents an inverted form of our model. The plume source follows a design by Dr. Paul Cooper (see Hunt et al. (2000) for details) in order to create as close to a turbulent top-hat profile on exit as possible. Due to the small magnitude

of the density differences (of the order of a few percent) the so-called Boussinesq approximation is valid, and so the inversion of the flow geometry has no dynamical significance, as density variations only affect the buoyancy force, and have no inertial effect.

Two supply tanks, each with fluid of different density fed one of the plume sources. We could therefore switch easily between the two supplies thus generating a step up or down in source buoyancy. For each experiment red food dye was added to a batch of brine. From this batch the two dense fluid supplies were made. Therefore the fluid injected into the smaller tank has the same relative dilution of food dye corresponding to the same fluid density, irrespective of which source supplies it. From one side of the large tank we lit the apparatus uniformly while recording from the other side using a digital monochrome ccd camera. We then measured the light intensity of the recorded images using the image analysis software, DigImage (see Cenedese and Dalziel (1998)). This light intensity can then be correlated to the density of the fluid. This is done by periodically drawing a variety of samples from the tank and measuring their density and the associated light intensity.

As discussed in the introduction, in the experiments it is necessary to inject a finite volume flux through the source. It is straightforward to modify the simple model presented above to allow for using the concept of effective or virtual origin(see Caulfield (1991) and Hunt and Kaye (2001) for details). As shown in Woods Caulfield and Phillips (2003) the height of the interface depends strongly only on the value of the virtual origin. In order to have the same natural ventilation interface associated with both the supplies of salt water we ensure that they have the same virtual origin by forcing the parameter Γ, originally defined by Morton (1959), to have the same value for both sources, where

$$\Gamma = \frac{5\sqrt{\pi}Q_0^2 B_0}{4\alpha M_0^{\frac{5}{2}}}. \tag{7.15}$$

The plume source has a fixed radius b_s and the source momentum flux is assumed to

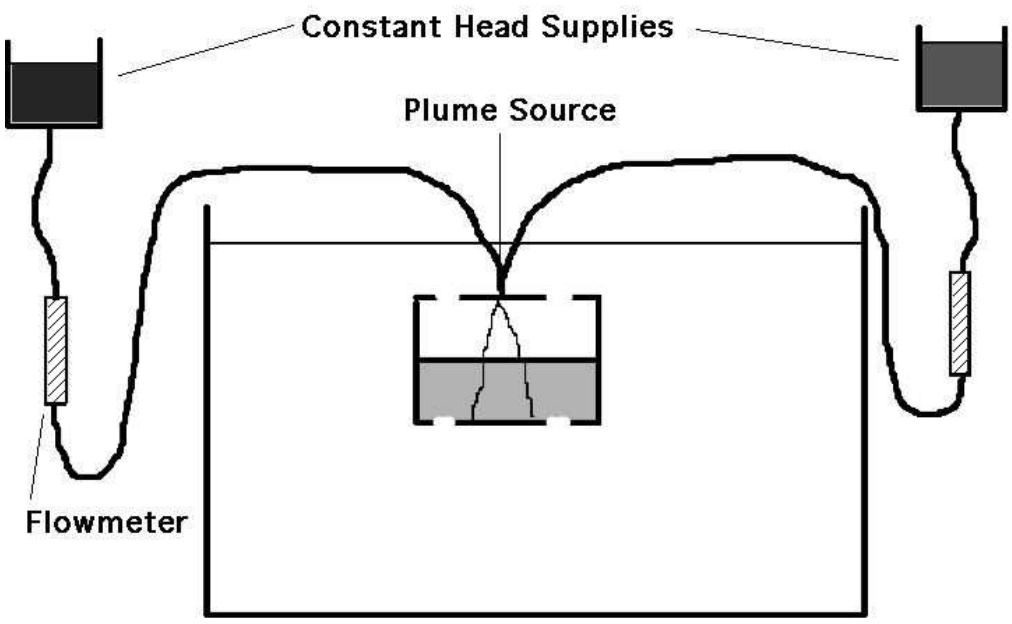

Figure 7.2: Experimental Setup

be proportional to $\frac{Q_0^2}{b_s^2}$. Therefore, for a given ratio of buoyancy fluxes, two plumes have the same virtual origin, and thus the same steady state interface height, if

$$\frac{g_l'}{g_u'} = \chi^{\frac{2}{3}}, \qquad \frac{Q_l}{Q_u} = \chi^{\frac{1}{3}}. \tag{7.16}$$

We conducted 12 experiments, with three different periods (labelled 'L', 'M' and 'S' for 'long', 'medium' and 'short' period respectively) and four different values of χ listed in Table 1. In each case it was apparent that the matching process described in (7.16) worked well and led to close agreement in steady-state interface locations. These experiments span a broad range of the relevant parameter ranges, and so it is natural to discuss the properties of our model system in terms of these parameters, simultaneously illustrating how accurately the model fits the experimental data.

Table 7.1: Description of Experimental Parameters

Experiment Number	χ	**Length of Period**	$\hat{\Omega}$
$L30$	30	$5T_f$	0.2
$M30$	30	$0.9T_f$	1.11
$S30$	30	$0.45T_f$	2.22
$L10$	10	$5T_f$	0.2
$M10$	10	$0.9T_f$	1.11
$S10$	10	$0.45T_f$	2.22
$L5$	5	$5T_f$	0.2
$M5$	5	$0.9T_f$	1.11
$S5$	5	$0.45T_f$	2.22
$L2$	2	$5T_f$	0.2
$M2$	2	$0.9T_f$	1.11
$S2$	2	$0.45T_f$	2.22

7.6 Results

In figures 7.3 and 7.4, we show the time varying ambient concentration profiles from experiment L30 from the heating (increased source buoyancy flux) and cooling (reduced source buoyancy flux) stages respectively. They are shown here to illustrate the three-layer structure that develops during the transient evolution of the flow. We have an upper highly buoyant layer associated with the increased source buoyancy flux, a middle layer of intermediate density layer associated with the reduced source buoyancy flux and a lower layer of ambient density. It is clear that the numerical model captures the essential features of the flow well. The interfaces between the various layers change significantly with time, and so in figures 5-8 we plot as a function of time the location of the two dominant interfaces, h_r and h_s (i.e. the heights defining the lower limits of the buoyant layers associated with the reduced buoyancy flux source (plotted with a thick line) and the increased buoyancy flux (plotted with a thin line). Overall we observe a good agreement between model and our theory.

We first need to consider the validity of the intrusion assumption. We assume that the plume will spread instantaneously at the level of zero buoyancy and

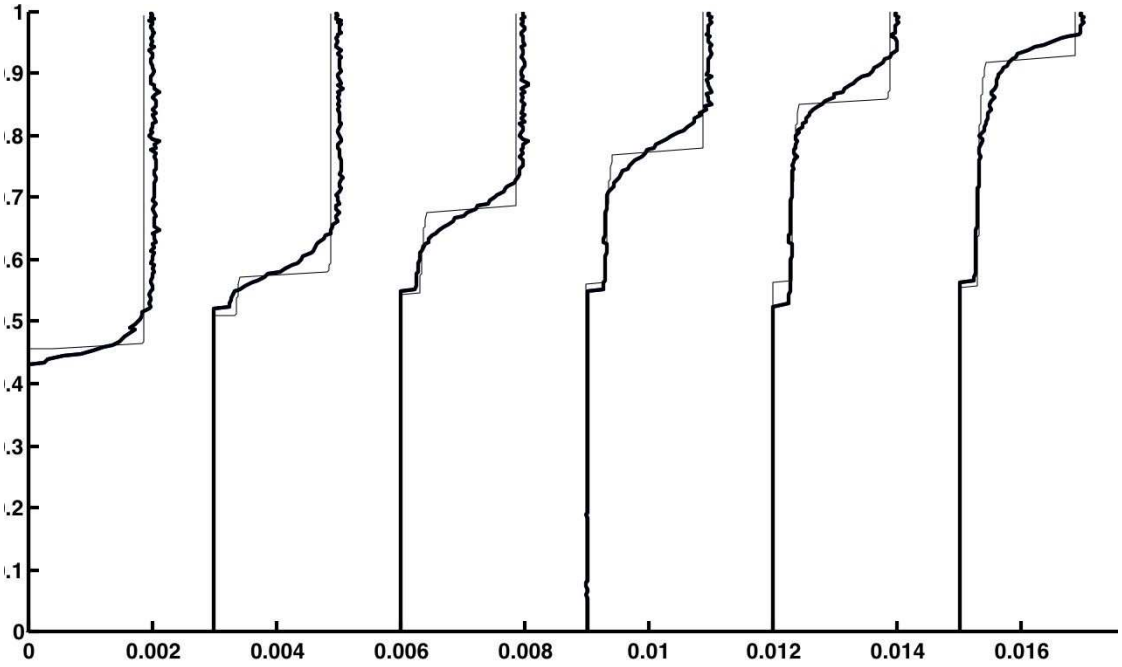

Figure 7.3: Density Profiles during the Cooling Stage in Experiment L30

that no penetration through this layer takes place. This should affect the location of the upper interface in the experiments. Looking at the results in Figures 7.5 - 7.8 we see that we get very good agreement between theory and experiment when the parameter χ is sufficiently large (i.e. $\chi > 10$)). This is unsurprising because a larger value of χ means a larger difference in source buoyancy fluxes. The larger the difference the harder it should be for the reduced buoyancy flux plume to penetrate into the upper layer, which is of course associated with the increased buoyancy flux plume. However, while there is definitely some erosion into the upper layer for the experiments with smaller values of χ (i.e. 5 and 2) it should be noted that the error is not huge (on the order of 10-15 percent) and that the qualitative description is good. We also considered the behavior of a more complicated model (based on the Bloomfield and Kerr (2000) model) that captured the fountain dynamics above the level of zero buoyancy. This involves solving six more equations, and we found that the predicted improvements are not sufficiently large to justify the

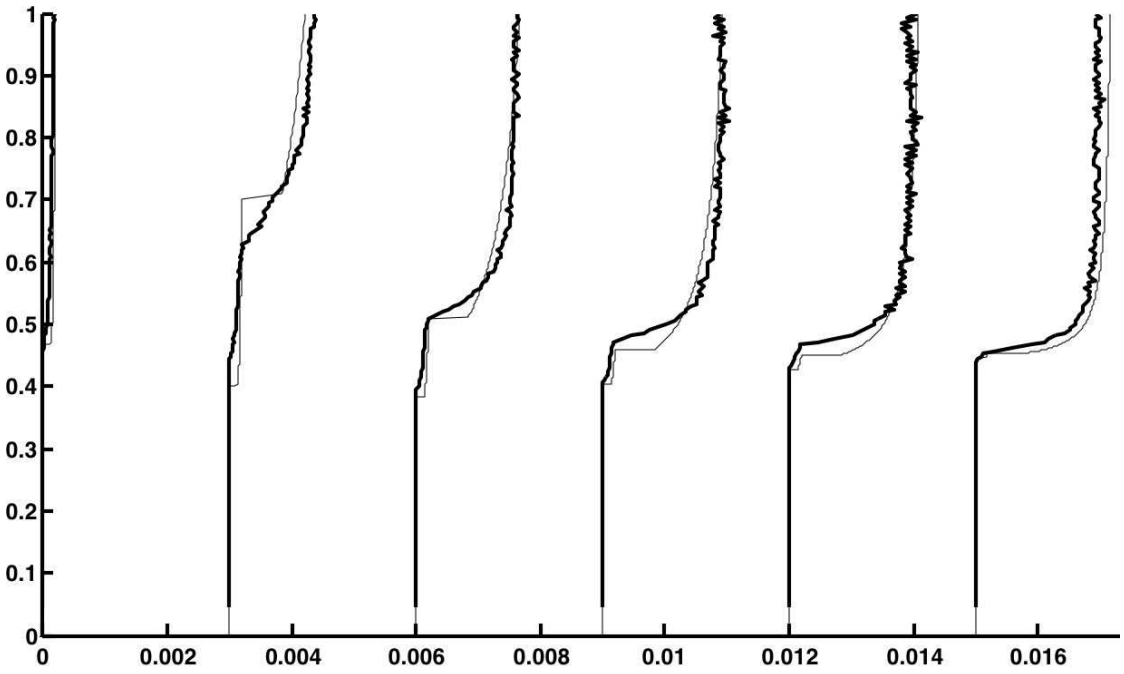

Figure 7.4: Density Profiles in the Heating Stage in Experiment L30. The thick line corresponds to the experimental data. The lighter line corresponds to the model

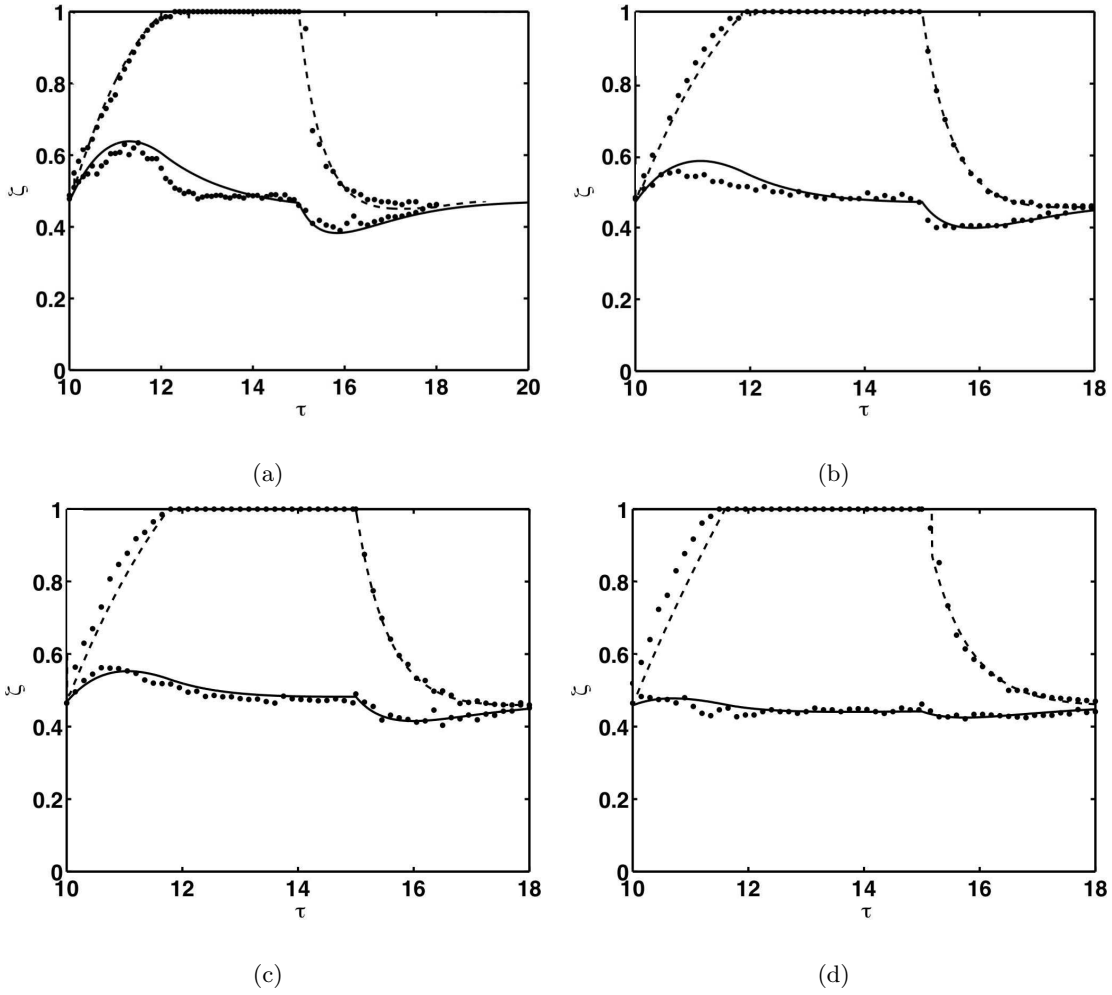

Figure 7.5: Interface Heights for the L Experiments, where the forcing period is $5T_f$. h_R is plotted with a solid line (–). h_I is plotted with the dashed line (- -). Experimental Results represented by the dots (·). (a) $\chi = 30$, (b) $\chi = 10$, (c) $\chi = 5$ and (d) $\chi = 2$

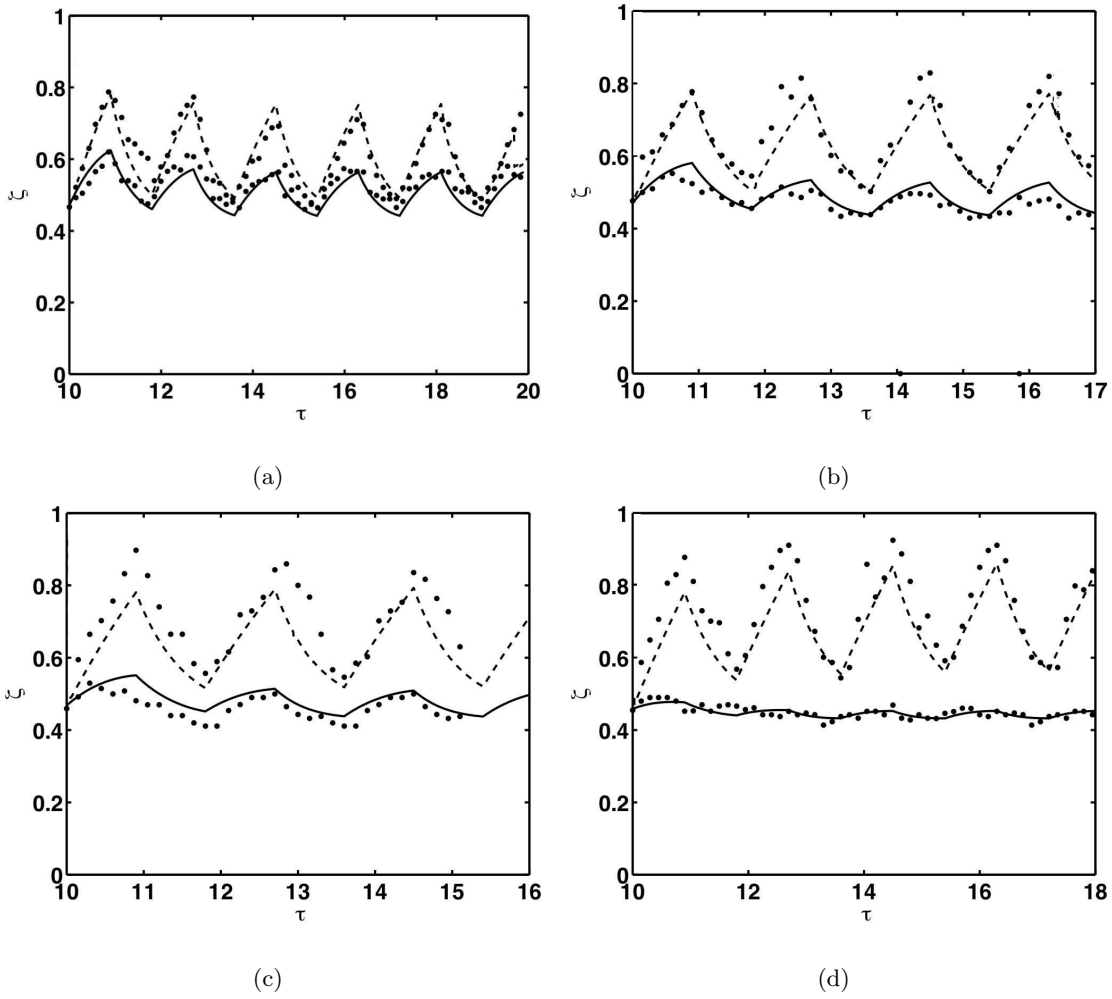

Figure 7.6: Interface Heights for the M Experiments, where the forcing period is $0.9T_f$. h_R is plotted with a solid line (–). h_I is plotted with the dashed line (- -). Experimental Results represented by the dots ($\cdot$). (a) $\chi = 30$, (b) $\chi = 10$, (c) $\chi = 5$ and (d) $\chi = 2$

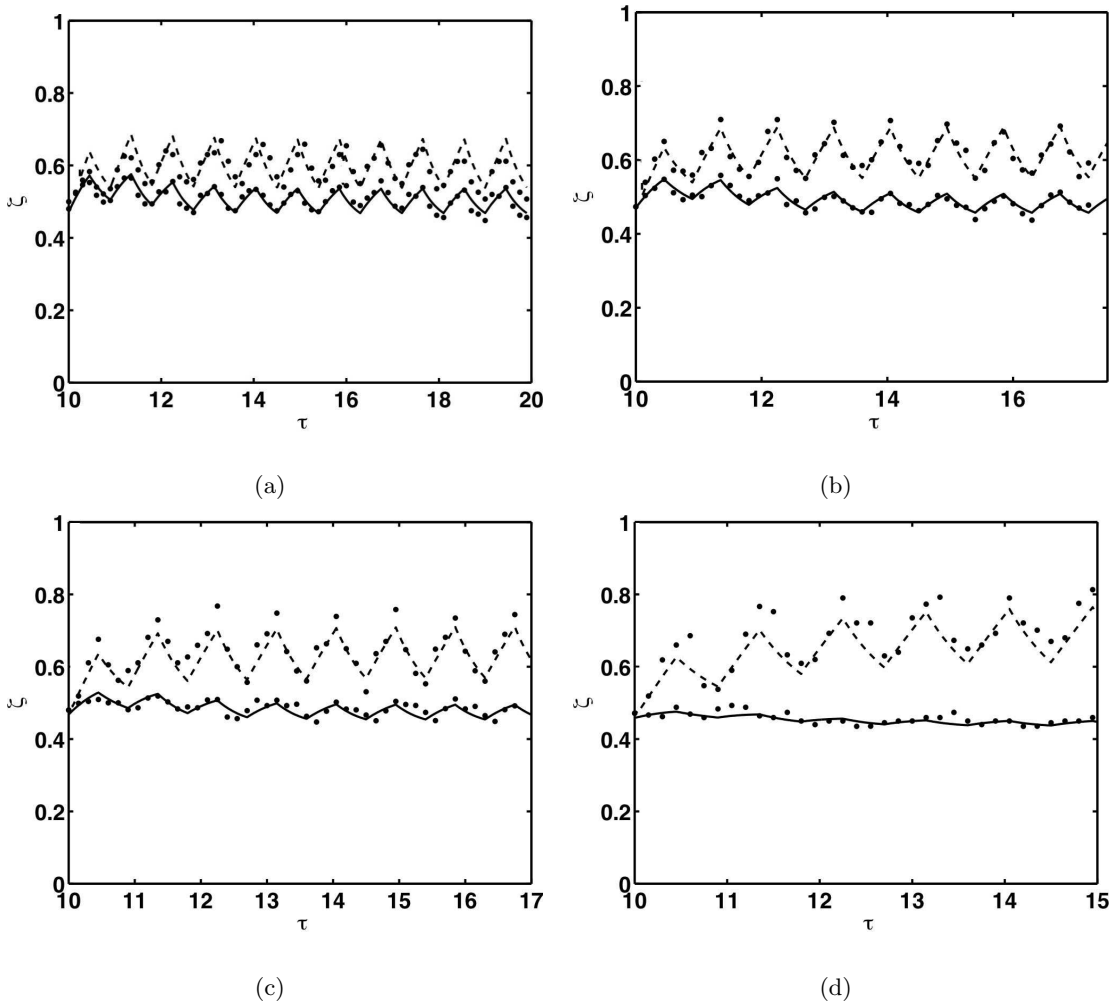

Figure 7.7: Interface Heights for the S Experiments, where the forcing period is $0.45T_f$. h_R is plotted with a solid line (–). h_I is plotted with the dashed line (- -). Experimental Results represented by the dots (·). (a) $\chi = 30$, (b) $\chi = 10$, (c) $\chi = 5$ and (d) $\chi = 2$

extra computational effort.

Certain characteristics of the flow captured both experimentally and numerically, are worthy of note. When T_f is large (as shown in figure 7.5) the flow essentially approaches close to steady state for both the increased and reduced source buoyancy fluxes. Moreover, in each case, the transient approach to this steady state is strongly affected by the presence in the chamber of a buoyant layer associated with the previous source buoyancy flux. Initially, since the source buoyancy flux is reduced, the new buoyancy layer intrudes underneath the old (more) buoyant layer, which drains through the upper opening. Since the plume arriving at the interface has a reduced buoyancy flux, it also has a substantially reduced volume flux than before as can be seen from the similarity solution due to Morton et al. (1956) given in (7.6) ($Q \sim F^{\frac{1}{3}}$). Therefore, the outflow through the upper opening (essentially driven by the hydrostatic pressure difference associated with the initial buoyant layer) is larger than the arriving plume volume flux and so the total depth of the buoyancy layers decreases initially (see Bower (2005) for a detailed discussion of this). As is apparent in figure 5a this transient excursion can be quite substantial when χ is small and hence the source buoyancy flux is substantially reduced. Then the upper buoyant layer typically drains away over approximately two filling box times for the particular interface location ($\zeta = 0.5$) we have chosen. This is consistent with the time scale analysis of Kaye & Hunt (2004) as this is the natural draining time for such a layer.

Subsequently, when the source buoyancy flux reverts to its larger value, the converse happens. The plume 'punches through' to the ceiling, and the old layer is eroded through entrainment. Also the volume flux of the plume arriving at the lower interface has now increased to a value larger than before, which was in balance with the outflow through the upper opening. Therefore, the total depth of the buoyant layers increases, analogously to the transient overshoot observed by Kaye & Hunt (2004) and Bower (2005). This overshoot is clearly observable, although it is typically smaller in amplitude than the reduction in depth observed

when the source buoyancy flux is reduced. Nevertheless, it is apparent that in this stage of the cycle, the intermediate layer is also eroded (this time by entrainment by the more buoyant plume as it punches through and fills the room from the top) over a time scale of approximately two filling box times.

For smaller periods of variation in the source buoyancy flux (as shown in figure 7.6 and 7.7) the upper layer associated with the plume fluid with increased source buoyancy flux, never completely drains away, but there is still a clear oscillation in the location of the interfaces, whose amplitude naturally decreases as $\chi \to 1$. All these aspects are well captured by the experimental data. The combined effect of the oscillations and the presence of the intermediate layer means that the reduced gravity of the upper layer inevitably changes from its initial value as the plume fluid associated with the increased source of buoyancy flux entrains fluid from the intermediate layer and travels varying distances before arrival in the upper layer. This variation in the density distribution and depth of the upper layer causes a slow adjustment in the mean depth of the upper layer (most apparent in flow where χ is close to 1, i.e. figure 7.7 (d), when such small variations are still significant). Nevertheless, in general the flows always eventually evolve into a regime where which two buoyant layers oscillate around a constant mean value.

Of course of most interest to flow ventilation is the extent to which oscillation in the source conditions affects the ventilation flow through the chamber. In figure 8a-c we plot the numerically calculated flow rates of the various choices of parameters shown in Table 7.1. Each panel is for a different value of T_f as this proves to be the most natural way to group the results. There are four important steady state flow rates that should be compared with these calculations namely

$$q_{\bar{f}} = \bar{f}^{\frac{1}{3}}\zeta^{\frac{5}{3}}, \qquad q_I = f_h\zeta^{\frac{5}{3}}, \qquad q_R = f_l\zeta^{\frac{5}{3}}, \qquad \bar{q} = \frac{1}{2}\bigg(q_I + q_R\bigg). \tag{7.17}$$

In these expressions, $q_{\bar{f}}$ is the steady state flow rate associated with average of the upper and lower buoyancy fluxes, q_I is the steady state flow rate associated with the increased buoyancy flux, q_R is the steady state flow rate associated with the

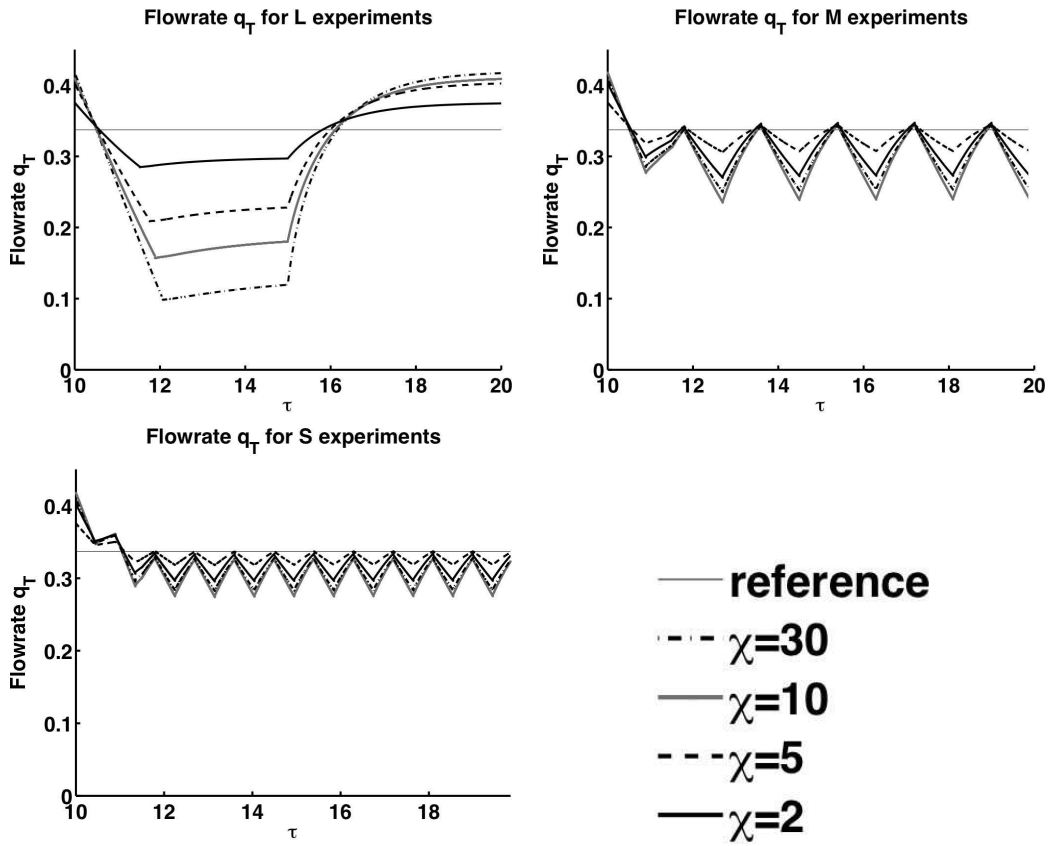

Figure 7.8: Numerically Predicted Flowrates through the Room for the L,M and S experiments

reduced buoyancy flux and $\bar{q}$ is the average of the the upper and lower flowrates, while ζ is the steady state interface location.

We expect the actual flow rate always to lie in the range $q_l < q_t < q_h$. Furthermore, over sufficiently long time intervals, the heat load of the actual sources corresponds to the load associated with a source with mean buoyancy flux $\bar{f}$, and so the associated volume flow rate $q_{\bar{f}}$ is the most natural control value. Scaling the other flow rates with $q_{\bar{f}}$ (essentially removing the dependence on the depth of the buoyancy layers) we obtain

$$\frac{q_u}{q_{\bar{f}}} = \frac{2^{\frac{1}{3}}}{(1+\chi)^{\frac{1}{3}}} \quad \frac{q_l}{q_{\bar{f}}} = \frac{(2\chi)^{\frac{1}{3}}}{(1+\chi)^{\frac{1}{3}}} \quad \frac{\bar{q}}{q_{\bar{f}}} = \frac{1+\chi^{\frac{1}{3}}}{2^{\frac{2}{3}}(1+\chi)^{|\frac{1}{3}}}. \tag{7.18}$$

From these expressions, we can show straightforwardly that $q_l < \bar{q} < q_{\bar{f}} < q_h$. From figure 8a-d, it is apparent that, unsurprisingly, the flow rate q_t varies with the period of the oscillation of the source conditions, and the amplitude of this variation decreases as $\chi \to 1$. In all cases the flow rate is less than $\bar{q_f}$, although the mismatch decreases as the frequency of variation increases. For smaller frequency (i.e. figure 7.8 a) the mean flow rate over a whole cycle is closer to $\bar{q}$, as the flow spends significant periods in each state. However, this agreement is not exact, due to the clear asymmetry between situations when the buoyancy flux is respectively reduced and increased. When the buoyancy flux is reduced, the flow drops rapidly (due primarily to the simple draining of the upper layer) whereas when the buoyancy flux is increased, due to the inevitable entrainment of the intermediate layer fluid by the more buoyant plume as it 'punches through', the flow rate adjusts more slowly and smoothly to higher values.

In figure 7.9, we illustrate the effect of this asymmetry by plotting the mean flow rates for each of the experiments as a function of χ against the various average flow rates. It is clear that in general the flow rates lie between $\bar{q}$ and $q_{\bar{f}}$, although for the experiments with $T_f = 5$, the mean flow rate can be slightly less than $\bar{q}$. However, as T_f decreases $q_T \to q_{\bar{f}}$ from below as expected and in all cases both q_h and q_l are poor estimators of the actual average flow rate through the

room.

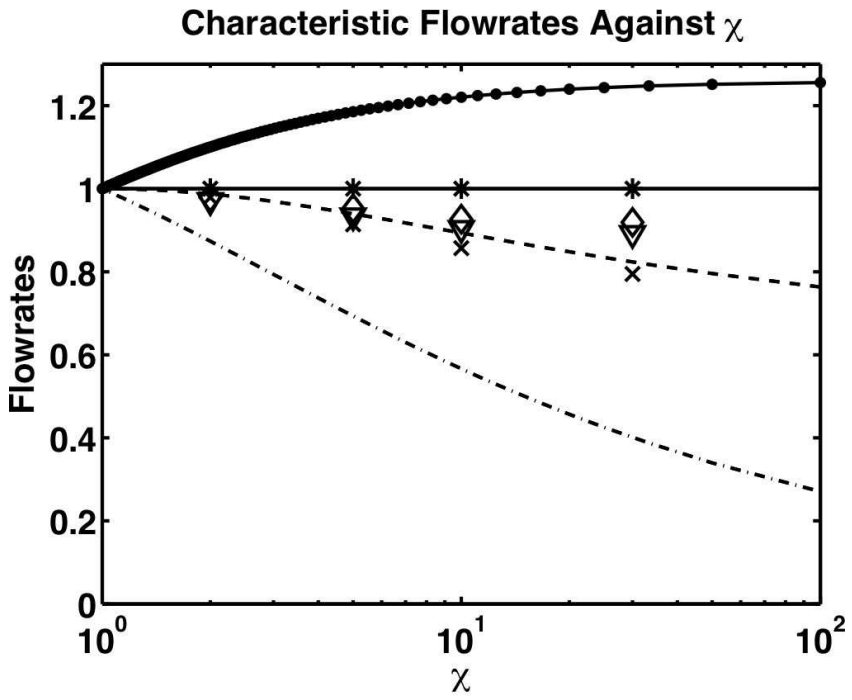

Figure 7.9: Plot of the Four Characteristic Normalized Flow Rates for various values of χ – $\bar{q}_f(-)$, $q_T(\bullet)$, $\bar{q}$(- -) and $q_L(-\cdot)$. Compared to the average Flowrates from Experiments. $*$=reference case, $\times = L$, $\triangle = M$, $\diamond = S$

7.7 Discussion and application

It is obviously important to understand how this analysis relates to real applications, and in particular the characteristic values of the various parameters for real buildings. First let us consider the parameter χ. When $\chi = 1$ this corresponds to the situation where there are no changes in buoyancy (i.e. when a room has reached steady state), which simply recovers the Linden et al. (1990) solution and corresponds to a room which has been occupied for a sufficiently long time with no changes in any of the heat sources in it. When $\chi = 0$ we have a scenario where a heat source is continuously being turned on and off. Small values of χ could correspond to a lecture hall which groups of people enter and exit at

regular intervals or a metropolitan train station, which doesn't have a continuous, but rather a discrete and at least quasi-periodic, flux of people through it. Intermediate values of χ would represent an office space where people are regularly entering or leaving and computers or other pieces of equipment are continuously being turned on and off.

In order to find where on figure 7.9 a specific space lies one must determine the appropriate filling box time scale, defined by (7.8). For example if we consider an office space of cross-sectional area 300 m^2 and height 3 m with a maximum of 100 and average of 85 heat sources (people and equipment moving in and out each contributing 100 Watts or 0.0028 $m^4 s^{-1}$ to the source buoyancy flux) we get $T_f \simeq 23$ minutes and $\chi = 0.7$. For this particular case we can see from figure 9 that there is no significant variation in the average flow rate through the space for high or low frequency changes in source buoyancy flux and so it is not a concern.

However, if we consider a similarly sized space that has a larger variation in source buoyancy, such as a metropolitan transit station where people enter, wait for a train to arrive and leave at essentially periodic intervals, we can have much smaller values of χ. If we assume a similar maximum occupancy as the office, $\bar{F}_0$ will also be smaller. Therefore T_f will be larger, although due to the dependence of the volume flux on the one-third power of the buoyancy flux, probably not hugely so. For example, if we take maximum occupancy at 100 people and minimum at 5 people we have $\chi = 0.05$ and $T_f \simeq 27$ minutes. Now if we look at figure 7.9 we see that we can have a variation of up to 20 % depending on the frequency at which people enter and leave, which will depend on the frequency of trains.

For example, during rush hour times, trains can arrive and leave in opposite directions as frequently as every two minutes, which corresponds to a characteristic change time of approximately $T_f/30$. At other, quieter times this system can have a much lower arrival and departure frequency, closer to the filling box time. At the quieter times the appropriate average flow rate through the system should be $\bar{q}$. However, during the rush hour times it is not immediately obvious what the

average flow rate through the system will be. It will lie somewhere between $\bar{q}$ and $q_{\bar{f}}$, approaching $q_{\bar{f}}$ asymptotically as the forcing frequency is increased.

Other examples of spaces that would take on large values of χ include theatres, cinemas, classrooms and lecture halls, where large numbers of people enter and exit the given space periodically. In all of these cases though the period of occupancy is several times larger than the filling time scale. Therefore, the most appropriate flow rate to assume would be $\bar{q}$. Spaces such as corridors and hallways can have high values of χ and small occupancy times and flow rates closer to $q_{\bar{f}}$ may be appropriate. From figure 7.9 it should be evident that $\bar{q}$ is always less than $q_{\bar{f}}$. Therefore, $\bar{q}$ can be thought of as a worst case scenario and as long as it satisfies any minimum air supply standards, these minimum standards will always be met, regardless of the period that the system is being forced at. From a conservative perspective this is the flow rate that should be assumed by design engineers.

7.8 Conclusions

We have presented a numerical model, based on the Germeles algorithm, to study the transient response of a naturally ventilated space with a periodically time varying heat source. Two dimensionless parameters govern the behaviour of the system. These are $\chi = \frac{F_h}{F_l}$, the ratio of upper to lower source buoyancy fluxes associated with the source and $\hat{\Omega}$, the dimensionless forcing frequency of the source defined by (7.12).

The dynamics associated with changes in source buoyancy are as follows. When the heat load in a naturally ventilated space is increased, the plume associated with that heat source will 'punch' all the way through to the top of the room and spread at the ceiling, filling the upper part of the room from the top. The previous stratification in the upper layer is eroded away by entrainment into the plume. Conversely, when the heat load is decreased, the plume will rise to its

level of zero buoyancy where it is decelerated. It will spread at this level, draining the most buoyant fluid above it out of the room. When the change in source buoyancy flux is small the plume may have enough momentum to penetrate into the more buoyant fluid and some erosion of this upper layer will occur by entrainment. However, for many cases, especially large decreases in source buoyancy flux, this entrainment is negligible and the dynamics are appropriately captured by neglecting it.

A series of small scale laboratory experiments was conducted in order to validate the model. We found that the agreement is very good, particularly when the change in source buoyancy flux is very large (i.e. χ large). Based on observations from our numerical and laboratory experiments we identified two characteristic average flow rates associated with the flow, which based on real space values of the dimensionless parameters χ and $\hat{\Omega}$ can be used to estimate the average flow rate through that space.

For small changes in source buoyancy flux (i.e. χ close to 1) the average flow rate through the system does not vary much regardless of the frequency with which the forcing varies. However, for large changes in source buoyancy flux differences of around 20% (for $\chi = 20$)or larger can exist depending on the frequency of forcing. The higher the forcing frequency is, the larger the average flow rate. In the infinite frequency limit the system approaches a flow rate corresponding to a steady source with a source buoyancy flux equal to the average of the lower and upper buoyancy fluxes. The variation in average flow rates stems from the non-linear relationship of the plume volume flow rate with source buoyancy flux (i.e. $Q \sim B_s^{\frac{1}{3}}$). Therefore, in spaces where large variations in thermal loading occur, it is important to consider the frequency of this forcing in order to estimate an accurate average flow rate through the space.

The text in chapter 7, in part, has been submitted for publication in *Building Services Engineering Research & Technology* (D Bolster & CP Caulfield). I was the primary researcher on this project.

8

Contaminants in Coastal Aquifers

8.1 Abstract

The Henry formulation, which couples subsurface flow and salt transport via a variable-density flow formulation, can be used to evaluate the extent of sea water intrusion into coastal aquifers. The coupling gives rise to nontrivial flow patterns that are very different from those observed in inland aquifers. We investigate the influence of these flow patterns on the transport of conservative contaminants in a coastal aquifer. The flow is characterized by two dimensionless parameters: the Péclet number, which compares the relative effects of advective and dispersive transport mechanisms, and a coupling parameter, which describes the importance of the salt water boundary on the flow. We focus our attention on two regimes—low and intermediate Péclet number flows. Two transport scenarios are solved analytically by means of a perturbation analysis. The first, a natural attenuation scenario, describes the flushing of a contaminant from a coastal aquifer by clean fresh water, while the second, a contaminant spill scenario, considers an isolated point source.

8.2 Introduction

Contamination of freshwater bodies by salt water poses one of the most significant environmental challenges. Within the past few decades, the water quality in many of the coastal aquifers across the world has rapidly degraded. Overexploitation of the groundwater basins has led to the drops of water tables and seawater intrusion into the aquifers. In many countries, e.g., Cyprus, Mexico, Oman and Israel, hundreds of wells along the coastline had to be shut down. A common source of this salt water is the sea, although naturally occurring brines, landfill leachate and irrigation practices can also result in contamination. The scenario we consider in this study is when sea water intrudes into a coastal aquifer, which poses significant environmental and economical challenges around the world, because even very small proportions of seawater render freshwater unpotable. Facing a shortage of suitable drinking water, many arid coastal countries have had either to look for alternative sources, such as imported water, or to implement costly technological solutions, such as desalination.

While salt as a source of contamination of coastal aquifers has received considerable attention, other threats to the quality of the groundwater have been studied less systematically. Results from an E.U.-sponsored project entitled BORE MED (Boron contamination of water resources in the Mediterranean region: distribution, sources, social impact and remediation) show that Boron contamination in coastal aquifers poses a potential threat to the future use of many Mediterranean groundwater basins as a source of drinking and irrigation water (Vengosh et al. (2004)). Not only might Boron render potential drinking water unpotable, but it may also make it unsuitable for irrigation since elevated Boron concentrations are known to cause certain crop failure.

Every summer, coastal communities from Maine to California are forced to temporarily close some of their most popular beaches because of unsafe levels of bacteria in the water. Typically, these sudden bacterial blooms disappear, only

to return without warning later in the season. In many cases, health officials are unable to pinpoint the cause of the contamination, leading frustrated beachgoers to blame everything from inadequate sewage treatment plants to overwhelmed storm drain systems, while ignoring the possibility of groundwater contamination in the beach aquifer itself. The studies by Boehm et al. (2004, 2006) indicate that a large fraction of this contamination may actually be coming from coastal groundwater.

Across the world, in coastal regions with heavy mining communities, deterioration of coastal aquifers is reaching serious proportions and their viability is currently threatened. For example, according to the Minister of Water Affairs & Forestry of South Africa, the Cape Flats aquifer, a part of the important coastal aquifer system in South Africa, which underlies large mining developments, fits into this category of rapidly deteriorating water sources. These are but a few examples. Others include contamination by heavy metals, groundwater nutrients, fertilizers etc.

Modeling of contaminant transport in coastal aquifers is complicated by the influence of an intruding seawater wedge on the velocity field within the aquifer. Increased salinity at the seaward boundary distorts the velocity field from a simple cross flow and introduces vertical velocities along with velocity gradients. Regardless of application, there is a scarcity of analytical solutions to advective-dispersion equation with a variable velocity fields. Such solutions are mostly limited to either steady-state transport or simplified flow conditions or both (e.g., Tartakovsky and Federico (1997)).

For seawater intrusion, the velocity fields can be computed with two alternative paradigms. The first postulates the existence of a sharp interface separating the fresh and salt water. This assumption allows the use of potential theory to derive analytical solutions for the location of this interface (e.g., Bear and Dagan (1964); Huppert and Woods (1995); Naji et al. (1998); Kacimov and Obnosov (2001)). Since the sharp interface paradigm ignores a transition zone between the fresh and salt water, these and other similar results are strictly valid for advection-

dominated systems.

The second paradigm explicitly accounts for the existence of a transitional zone. The model consists of a variable density (Darcy) flow equation coupled with the advection-diffusion equation for the transport of salt. Even for the simplest geometries of a flow domain, this coupling makes it difficult to obtain analytical solutions, which are essential for the testing and validation of numerical codes. To the best of our knowledge, the Henry (1964) formulation of variable density flow in coastal aquifers provides the only mathematical setting for which analytical solutions are available. Consequently, Henry's problem is one of the most widely used benchmarking problems. Henry's quasi-analytical solution to this problem is based on a Galerkin projection and results in infinite series, whose slow convergence rates require the extensive use of numerics. Numerical errors that are inherent in these computations might compromise the usefulness of Henry's solution for benchmarking.

Simpson and Clement (2003) hypothesized that under certain conditions the Henry problem can be simplified by replacing the full coupling of the governing equations with a pseudo coupling that is applied via the boundary conditions (i.e. by assuming that the spatial variability of the water density has negligible effect). Dentz et al. (2006) tested this hypothesis by deriving perturbation-based analytical solutions for the fully and pseudo coupled systems and testing their accuracy and robustness numerically. They showed that for many cases it is indeed sufficient to only implement the coupling via the boundary conditions, which is the approach we adopt in this study.

In this paper we are concerned with the transport of passive contaminants in a coastal aquifer. The problem is formulated in section 8.3 and its dimensional analysis is presented in section 8.4. Sections 8.5 and 8.6 contain the analyses of two different contamination scenarios corresponding to natural attenuation and isolated sources, respectively.

8.3 Formulation of Henry Problem for Contaminant Transport

Consider flow and contaminant transport in a confined coastal aquifer in which the diffused seawater wedge is in equilibrium with the freshwater flow field (Fig. 8.1a). The aquifer is also assumed to be homogeneous and isotropic, with constant hydraulic conductivity and porosity. Following Henry (1964), we idealize this problem by treating the flow domain as a rectangle shown in Fig. 8.1b.

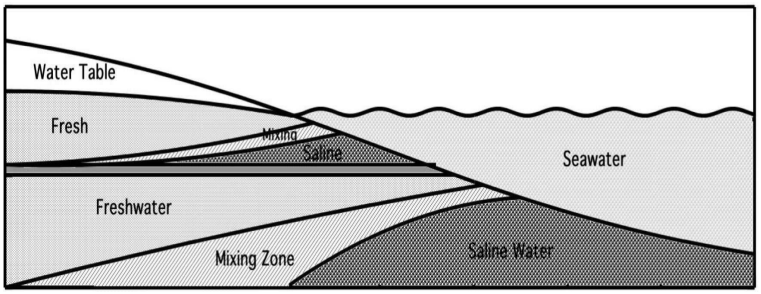

(a)

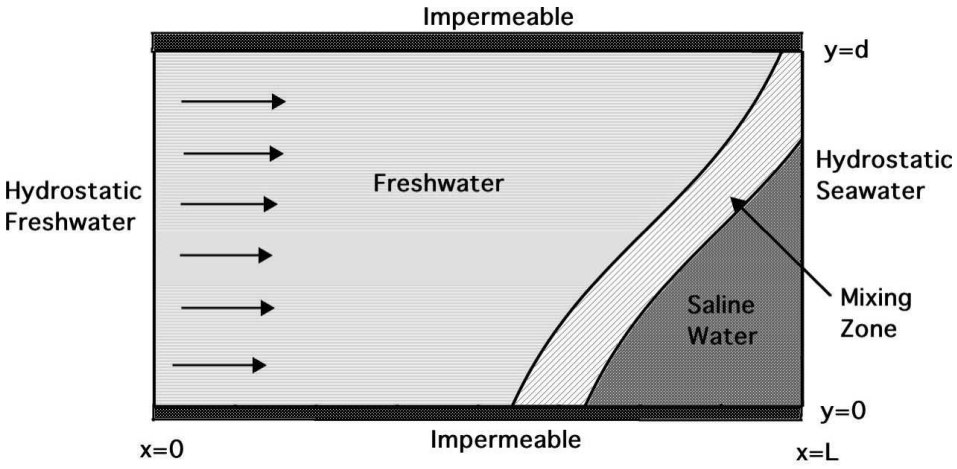

(b)

Figure 8.1: (a) A schematic representation of a coastal aquifer system and (b) its mathematical conceptualization by Henry (1964).

Henry's formulation of the corresponding two-dimensional flow problem

is based on mass conservation and a modified Darcy equation written in terms of freshwater head $h(\mathbf{x})$,

$$\nabla \cdot \mathbf{q} = 0, \qquad \mathbf{q} = -K\nabla\left(h + y\epsilon\frac{c}{c_s}\right), \qquad \epsilon \equiv \frac{\rho_s - \rho_f}{\rho_f}, \tag{8.1}$$

where $\mathbf{q}$ is the fluid flux; K is the hydraulic conductivity; c and c_s are the concentrations of salt in groundwater and sea water, respectively; and ρ_f and ρ_s are the fresh and sea water densities, respectively. The equivalent freshwater head h is defined as

$$h = \frac{p}{\rho_f g} + y, \tag{8.2}$$

where p is water pressure, g is the gravitational acceleration constant, and y is the vertical coordinate. These equations are subject to the boundary conditions

$$h(x = 0, y) = h_0, \qquad h(x = L, y) = d + \epsilon(d - y) \tag{8.3}$$

$$\frac{\partial h}{\partial y}(x, y = 0) = -\epsilon\frac{c(x, y = 0)}{c_s}, \qquad \frac{\partial h}{\partial y}(x, y = d) = -\epsilon\frac{c(x, y = d)}{c_s}. \tag{8.4}$$

The concentration of salt in groundwater, $c(\mathbf{x})$, satisfies a steady advection-diffusion equation

$$K\nabla h \cdot \nabla c + K\frac{c}{c_s}\frac{\partial c}{\partial y} + \omega D\nabla^2 c = 0, \tag{8.5}$$

where ω is the porosity of the medium and D is the effective (average) dispersion coefficient for salt which, in Henry's formulation, is assumed to be constant throughout the entire domain. The boundary conditions for salt transport are freshwater at the inlet boundary, saline water at the outlet boundary and impermeable conditions on the top and bottom of the aquifer. This corresponds to

$$c(x = 0, y) = 0, \qquad c(x = L, y) = c_s \tag{8.6}$$

$$\frac{\partial c}{\partial y}(x, y = 0) = 0, \qquad \frac{\partial c}{\partial y}(x, y = d) = 0. \tag{8.7}$$

Additionally, consider the migration of a conservative contaminant in the velocity field $\mathbf{u} = \mathbf{q}/\omega$ given by a solution of the Henry problem (8.1) – (8.5). The

concentration of this contaminant, $\gamma(\mathbf{x}, t)$, satisfies a transient advection-diffusion equation

$$\frac{\partial \gamma}{\partial t} + \mathbf{u} \cdot \nabla \gamma = D_L \frac{\partial^2 \gamma}{\partial x^2} + D_T \frac{\partial^2 \gamma}{\partial y^2}. \tag{8.8}$$

In the spirit of Henry's formulation, the longitudinal (D_L) and transverse (D_T) dispersion coefficients are assumed to be constant. Kalejaiye and Cardoso (2005) showed that this is a legitimate assumption for flows where the Rayleigh number is less than 1000, which holds for all models presented in this paper. We formally define this Rayleigh number, Ra, in the following section on dimensionless analysis. Introducing $D_\gamma \equiv D_L$ and $D_T = \beta D_\gamma$, we rewrite (8.8) as

$$\frac{\partial \gamma}{\partial t} + \mathbf{u} \cdot \nabla \gamma = D_\gamma \left(\frac{\partial^2 \gamma}{\partial x^2} + \beta \frac{\partial^2 \gamma}{\partial y^2} \right). \tag{8.9}$$

Depending on a pollutant, D_γ might or might not coincide with the dispersion coefficient for salt, D. To simplify the subsequent presentation, we assume that these two dispersion coefficients are of the same order, $D_\gamma \sim \mathcal{O}(D)$. The specification of initial and boundary conditions for (8.8) describes a particular contamination scenario, among which we consider two.

The first represents natural attenuation of a contaminated coastal aquifer, a setting in which seaward flow of fresh water flushes out a contaminant that is initially distributed uniformly throughout an aquifer. In addition to its practical significance, this problem allows one to identify regions where contamination is most persistent and to elucidate the effects of seawater intrusion on contaminant transport in coastal aquifers. In particular, our analysis can be used to address important logistical questions, such as: How does the sea boundary affect the clean up process? What are the long-term consequences of contamination? How does contaminant fate and migration in coastal aquifers differ from those in inland confined aquifers?

The second scenario models the spread of a contaminant released from an isolated spill conceptualized here as a point source. Common examples include contaminants leaking from a septic tank, a leak from a pipe or a small spill pool.

Due to the linearity of the transport equation, understanding the problem associated with a single source is equivalent to understanding that of any number of point and/or distributed sources.

8.4 Dimensional Analysis

Following Dentz et al. (2006), we introduce dimensionless parameters

$$\xi = \frac{x}{L}, \quad \eta = \frac{y}{L}, \quad \zeta = \frac{d}{L}, \quad \tau = \frac{\kappa \Delta h_0}{L^2} t, \quad C = \frac{c}{c_s}, \quad \Gamma = \frac{\gamma}{\gamma_0}, \tag{8.10}$$

$$H = \frac{h-d}{\Delta h_0}, \quad \mathbf{U} = \frac{\mathbf{u}L}{K\Delta h_0}, \quad Pe = \frac{K\Delta h_0}{\theta D}, \quad Pe_\gamma = \frac{K\Delta h_0}{\theta D_\gamma}, \quad \alpha = \frac{\epsilon L}{\Delta h_0} \tag{8.11}$$

where γ_0 is a problem specific reference contaminant concentration. The governing equations (8.1) – (8.8) are recast in the dimensionless form

$$\nabla^2 H = -\alpha \frac{\partial C}{\partial \eta}, \qquad \mathbf{U} = -\nabla H - \mathbf{e_3} \alpha C, \tag{8.12}$$

$$\nabla H \cdot \nabla C + \alpha C \frac{\partial C}{\partial \xi} + \frac{1}{Pe} \nabla^2 C = 0, \tag{8.13}$$

and

$$\frac{\partial \Gamma}{\partial \tau} + \mathbf{u} \cdot \nabla \Gamma = \frac{1}{Pe_\gamma} \left(\frac{\partial^2 \Gamma}{\partial \xi^2} + \beta \frac{\partial^2 \Gamma}{\partial \eta^2} \right). \tag{8.14}$$

The gradients in (8.12)-(8.13) are nondimensional (i.e.$\nabla = [\frac{\partial}{\partial \xi} \ \frac{\partial}{\partial \eta}]$) as are all gradients from here on in. These equations are subject to the boundary conditions

$$H(0, \eta) = 1, \qquad H(1, \eta) = \alpha(\zeta - \eta), \tag{8.15}$$

and

$$\frac{\partial H}{\partial \eta}(\xi, 0) = -\alpha C(\xi, 0), \qquad \frac{\partial H}{\partial \eta}(\xi, 0) = -\alpha C(\xi, 0). \tag{8.16}$$

It now becomes apparent that flow and transport are governed by three dimensionless parameters Pe, Pe_γ, and α. The Péclet numbers Pe and Pe_γ compare the relative importance of advection and dispersion mechanisms for the transport of salt and contaminant, respectively. The coupling parameter α accounts for density variation between the seawater and fresh water and quantifies the effects of

gravity and the salt water boundary on the flow field. Specifically, $\alpha = 0$ corresponds to a uniform horizontal flow; as α increases, gravity effects introduce vertical velocities and modify horizontal ones. The Rayleigh number as defined by Kalejaiye and Cardoso (2005) is the product of α and Pe (i.e. Ra=αPe).

Contaminant transport under the high Péclet number regimes is dominated by advection. Since diffusion is neglible, contaminant is carried along the flow streamlines, so that its migration is described by solutions to the flow problem. Our analysis deals with the remaining two Péclet number regimes: low and intermediate. Since typical Péclet numbers for coastal aquifers fall within the range $\mathcal{O}(10^{-2}) \leq Pe \leq \mathcal{O}(10^{5})$ (T. Nishikawa of USGS, personal communication), these two Péclet number regimes are of practical significance.

8.5 Natural Attenuation of Contaminated Coastal Aquifers

Consider the following simplified problem of natural attenuation of coastal aquifers. Suppose that at time $t = 0$ an aquifer is uniformly contaminated by, say, industrial or agricultural pollutants, whose concentration is γ_{in}. Then the sources of contamination are eliminated, and fresh water flowing towards the sea begins to remove the contaminants from the aquifer.

An analytical solution for this idealized scenario, which is based on the assumption that the contaminant is distributed uniformly throughout the aquifer, can be used as a benchmark for numerical analyses of more realistic natural attenuation scenarios. Additionally, the technique of allowing a uniformly distributed contaminant to be drained from the ambient environment—the so-called "step down" method—is routinely used to understand the fundamental physics of the transport phenomenon (Kaye and Hunt (2006); Bolster and Linden (2007)).

Our goal is to describe the seaward migration of contaminants and to identify regions where the contamination remains persistent. For this case the reference density defined in the nondimensionalisation in (8.10) is $\gamma_0 = \gamma_{in}$. Contaminant

transport is described by (8.14) subject to the initial and boundary conditions

$$\Gamma(\xi,\eta,0)=1,\quad \frac{\partial\Gamma}{\partial\eta}(\xi,0,\tau)=\frac{\partial\Gamma}{\partial\eta}(\xi,\zeta,\tau)=0,\quad \Gamma(0,\eta,\tau)=\Gamma(1,\eta,\tau)=0. \tag{8.17}$$

The last boundary condition implies that the sea acts as an infinite reservoir that dilutes and immediately carries off the contaminant.

8.5.1 Intermediate Péclet Number

The velocity distribution $\mathbf{U}$ in (8.14) can be obtained analytically via a perturbation expansion of hydraulic head H and other system states in the coupling parameter α Dentz et al. (2006),

$$H^{IP}(\xi)=\sum_{k=0}^{\infty}\alpha^k H_k^{IP}(\xi),\qquad \mathbf{U}^{IP}(\xi)=\sum_{k=0}^{\infty}\alpha^k \mathbf{U}_k^{IP}(\xi). \tag{8.18}$$

The convergence of these series requires that α be small, an assumption whose validity is discussed in Dentz et al. (2006). If one further assumes that the pseudo-coupled model is valid as well, then the terms in the expansion (8.18) are

$$H_0^{IP}=1-\xi,\qquad H_1^{IP}=\eta_B(\xi),\qquad H_i^{IP}\equiv 0. \tag{8.19}$$

where

$$\eta_B=\frac{\xi\zeta}{2}+\sum_{l=1}^{\infty}a_l\cos\left(\frac{l\pi\eta}{\zeta}\right)\frac{\sinh(l\pi\xi/\zeta)}{\sinh(l\pi/\zeta)}\quad\text{and}\quad a_l=2\zeta\frac{1-(-1)^l}{l^2\pi^2}. \tag{8.20}$$

It is worthwhile to recall that the second assumption implies that flow and salt transport are coupled only through the boundary conditions. The numerical and analytical studies Simpson and Clement (2003); Dentz et al. (2006) demonstrated that this assumption remains accurate over a wide range of flow conditions.

Substituting (8.19) – (8.20) into (8.12) and (8.18), we obtain a solution for the velocity field $\mathbf{U}=(U,V)^T$

$$U_0^{IP}=1,\qquad U_1^{IP}=\frac{\zeta}{2}-\sum_{l=1}^{\infty}l\pi a_l\cos\left(\frac{l\pi\eta}{\zeta}\right)\frac{\cosh(l\pi\xi/\zeta)}{\sinh(l\pi/\zeta)}, \tag{8.21}$$

and

$$V_0^{IP} = 0, \qquad V_1^{IP} = \sum_{l=1}^{\infty} l\pi a_l \sin\left(\frac{l\pi\eta}{\zeta}\right) \frac{\sinh(l\pi\xi/\zeta)}{\sinh(l\pi/\zeta)}. \tag{8.22}$$

Both $U_i^{IP} \equiv 0$ and $V_i^{IP} \equiv 0$ for $i \geq 2$.

In analogy to (8.18), we look for a solution of the contaminant transport problem (8.14) and (8.17) in the form of an infinite series in the powers of α,

$$\Gamma^{IP} = \sum_{k=0}^{\infty} \alpha^k \Gamma_k^{IP}. \tag{8.23}$$

The leading term in this expansion satisfies

$$\frac{\partial \Gamma_0^{IP}}{\partial \tau} + \frac{\partial \Gamma_0^{IP}}{\partial \xi} = \frac{1}{Pe_\gamma}\left(\frac{\partial^2 \Gamma_0^{IP}}{\partial \xi^2} + \beta \frac{\partial^2 \Gamma_0^{IP}}{\partial \eta^2}\right) \tag{8.24}$$

subject to initial condition $\Gamma_0^{IP}(x, y, t = 0) = 1$ and the boundary conditions (8.17). The corresponding solution is

$$\Gamma_0^{IP} = 8\pi \mathrm{e}^{\frac{Pe}{2}(\xi - \frac{t}{2})} \sum_{n=0}^{\infty} a_n \sin(n\pi\xi) \mathrm{e}^{-\frac{\pi^2 n^2 t}{Pe}}, \qquad a_n = n \frac{1 - (-1)^n \mathrm{e}^{-Pe/2}}{Pe^2 + 4n^2\pi^2}. \tag{8.25}$$

The first-order term Γ_1^{IP} in the expansion (8.23) satisfies

$$\frac{\partial \Gamma_1^{IP}}{\partial \tau} + \frac{\partial \Gamma_1^{IP}}{\partial \xi} = \frac{1}{Pe_\gamma}\left(\frac{\partial^2 \Gamma_1^{IP}}{\partial \xi^2} + \beta \frac{\partial^2 \Gamma_1^{IP}}{\partial \eta^2}\right) - U_1^{IP} \frac{\partial \Gamma_0^{IP}}{\partial \xi} \tag{8.26}$$

subject to the homogeneous initial and boundary conditions. A coordinate transformation

$$\hat{\eta} = \eta/\sqrt{\beta} \tag{8.27}$$

maps (8.26) onto an isotropic advection-diffusion equation

$$\frac{\partial \Gamma_1^{IP}}{\partial \tau} + \frac{\partial \Gamma_1^{IP}}{\partial \xi} = \frac{1}{Pe_\gamma}\left(\frac{\partial^2 \Gamma_1^{IP}}{\partial \xi^2} + \frac{\partial^2 \Gamma_1^{IP}}{\partial \hat{\eta}^2}\right) - U_1^{IP}(\xi, \hat{\eta}) \frac{\partial \Gamma_0^{IP}}{\partial \xi}. \tag{8.28}$$

Let

$$\begin{aligned} G(x, y; \xi, \zeta; \tau) =& \frac{4}{\zeta}\left[\sum_{p=1}^{\infty} \sin(p\pi x) \sin(p\pi\xi) \exp\left(-\frac{\pi^2 p^2}{Pe}\tau\right)\right] \\ & \times \left[\frac{1}{2} + \sum_{m=1}^{\infty} \cos\left(\frac{m\pi y}{\zeta}\right) \cos\left(\frac{m\pi\eta}{\zeta}\right) \exp\left(-\frac{\pi^2 m^2}{Pe\zeta^2}\tau\right)\right] \end{aligned} \tag{8.29}$$

denote the Greens function for an isotropic diffusion equation subject to the appropriate homogeneous initial and boundary conditions. Then a solution of (8.28) can be written as

$$\Gamma_1^{IP} = -\int_0^{\tau}\int_0^{1}\int_0^{\hat{\zeta}} G(\xi,\hat{\eta},\xi_1,\hat{\eta}_1,\tau-t)U_1^{IP}(\xi_1,\hat{\eta}_1)\frac{\partial\Gamma_0^{IP}(\xi_1,\hat{\eta}_1,t)}{\partial\xi} \mathrm{e}^{-\frac{Pe}{2}(\xi_1-\frac{t}{2})}\mathrm{d}\hat{\eta}_1\mathrm{d}\xi_1\mathrm{d}t, \tag{8.30}$$

which can be written in the original coordinate system (ξ,η) as

$$\Gamma_1^{IP} = -\int_0^{\tau}\int_0^{1}\int_0^{\hat{\zeta}} G(\xi,\eta,\xi_1,\hat{\eta}_1,\tau-t)U_1^{IP}(\xi_1,\hat{\eta}_1)\frac{\partial\Gamma_0^{IP}(\xi_1,\hat{\eta}_1,t)}{\partial\xi} \mathrm{e}^{-\frac{Pe}{2}(\xi_1-\frac{t}{2})}\mathrm{d}\hat{\eta}_1\mathrm{d}\xi_1\mathrm{d}t. \tag{8.31}$$

This solution can be evaluated either analytically or numerically. The former approach consists of evaluating the quadratures analytically and is given in terms of infinite series. These series converge at least exponentially, and hence can be truncated after a few terms. (We do not reproduce this expression here due to its length.) The numerical evaluation consists of computing the quadratures with an adaptive recursive Simpson's method. Both methods produced identical results and required approximately the same computational time.

To validate the proposed approach and to test its accuracy, we compare the first-order perturbation solution $\Gamma^{IP} \approx \Gamma_0^{IP} + \alpha\Gamma_1^{IP}$ with a numerical (finite difference) solution of the contaminant transport problem (8.14) and (8.17). Fig. 8.2 displays this comparison for $Pe = 10$ and two values of α, (a) $\alpha = 0.5$ and (b) $\alpha = 1$. The two solutions agree very well for the $\alpha = 0.5$ case. The agreement is still good for $\alpha = 1$, although small differences between the perturbation and numerical solutions are more evident.

The effects of the coupling parameter α on contaminant transport are elucidated in Fig. 8.3, which shows concentration profiles for $Pe = 10$, $\beta = 1$, and several values of α. We also considered different values of $\beta = D_T/D_L \in [0.1, 1]$ and found their effects on contaminant distributions to be negligible. This is because

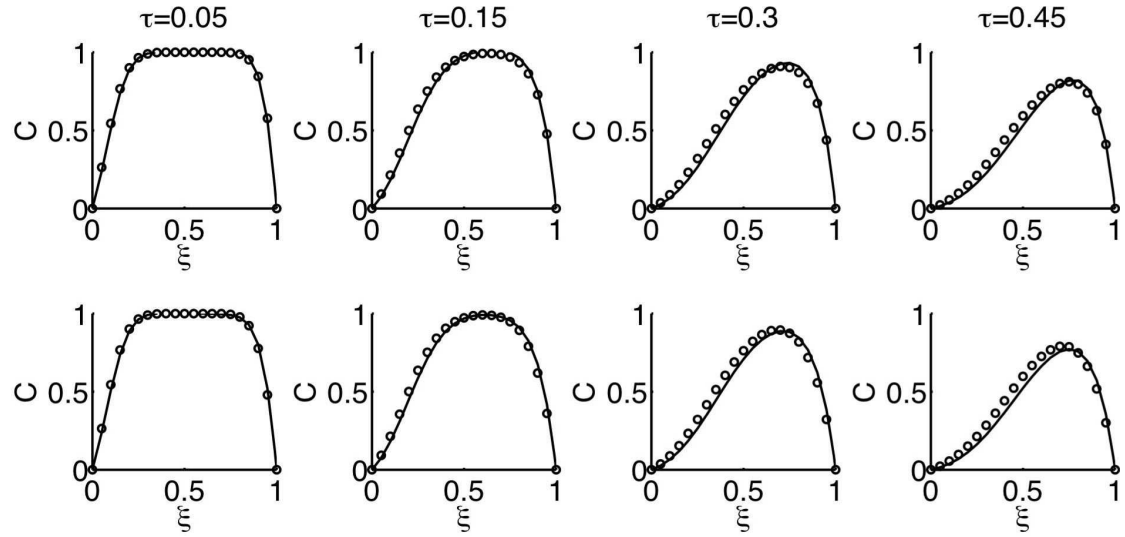

(a)

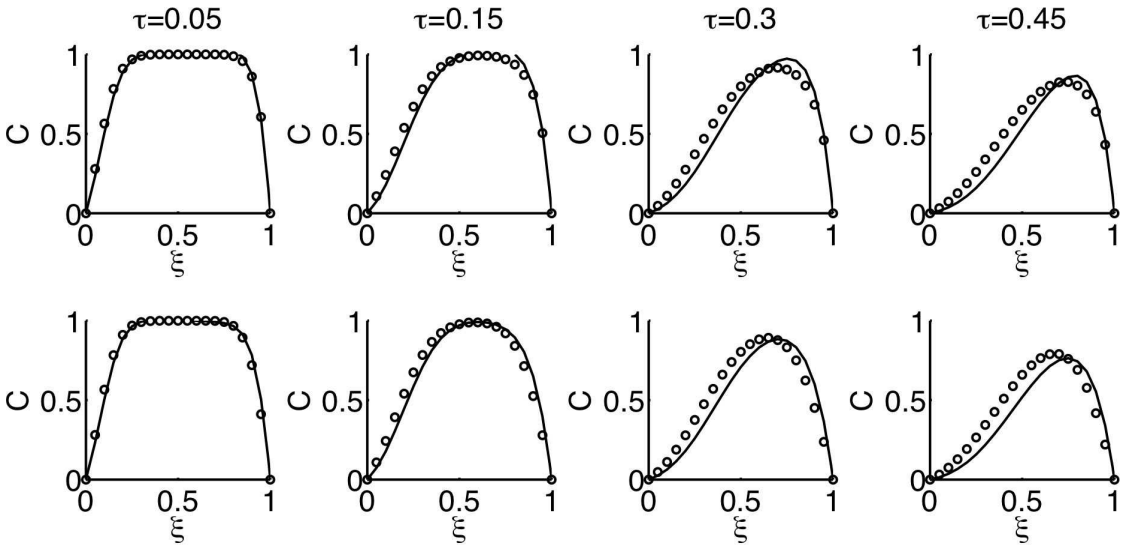

(b)

Figure 8.2: Temporal snapshots of contaminant concentration distributions of the natural attenuation problem with $Pe = 10$ and (a) $\alpha = 0.5$, (b) $\alpha = 1$ at two heights ($\eta = 0.1$ (top row) and $\eta = 0.4$ (bottom row)) across the width of the aquifer provided by the perturbation (solid line) and numerical (dots) solutions .

the vertical component of the concentration gradient in this transport regime is very small.

The effects of the coupling parameter α are strongest in the region adjacent to the sea, and diminish further inland. The increase in α leads to a redistribution of contaminant relative to the case where no seawater intrusion occurs. The contaminant concentration is highest in the upper coastal side of the domain and decreases slightly in the lower right part. This behavior is due to the fact that the region of outflow is diminished because of the presence of the intruding sea water. (It does not imply that the contaminant concentration increases as it approaches the seaward boundary.) Similarly, less contaminant is present in the lower right region, because uncontaminated seawater enters and flushes this region. This has important implications for the fate of a contaminant, as discussed in detail in section 8.6.

8.5.2 Small Péclet Number

Small Péclet numbers correspond to either high dispersion or small mass fluxes. Both scenarios can occur in coastal aquifers, in which tidal fluctuations increase the effective dispersion coefficients and natural hydraulic gradients are small. Analytical solutions to the flow problem can now be obtained via perturbation expansions in small Pe Dentz et al. (2006),

$$H^{SP} = \sum_{n=0}^{\infty} Pe^n H_n^{SP}, \quad \mathbf{U}^{SP} = \sum_{n=0}^{\infty} Pe^n \mathbf{U}_n^{SP}. \tag{8.32}$$

The leading terms in these expansions are given by

$$H_0^{SP} = 1 - \xi + \alpha\xi(\zeta - \eta), \qquad \mathbf{U}_0^{SP} = U_0^{SP}(\eta)\mathbf{e}_\xi \equiv [1 + \alpha(\eta - \zeta)]\,\mathbf{e}_\xi, \tag{8.33}$$

where $\mathbf{e}_\xi$ is the unit vector along the ξ-axis of the coordinate system. Inserting (8.33) into (8.14) and rescaling time with the diffusive timescale $t = \tau L/D_\gamma$, we obtain an equation

$$\frac{\partial \Gamma}{\partial \tau} + PeU_0^{SP}(\eta)\frac{\partial \Gamma}{\partial \xi} - \left(\frac{\partial^2 \Gamma}{\partial \xi^2} + \beta\frac{\partial^2 \Gamma}{\partial \eta^2}\right) = 0, \tag{8.34}$$

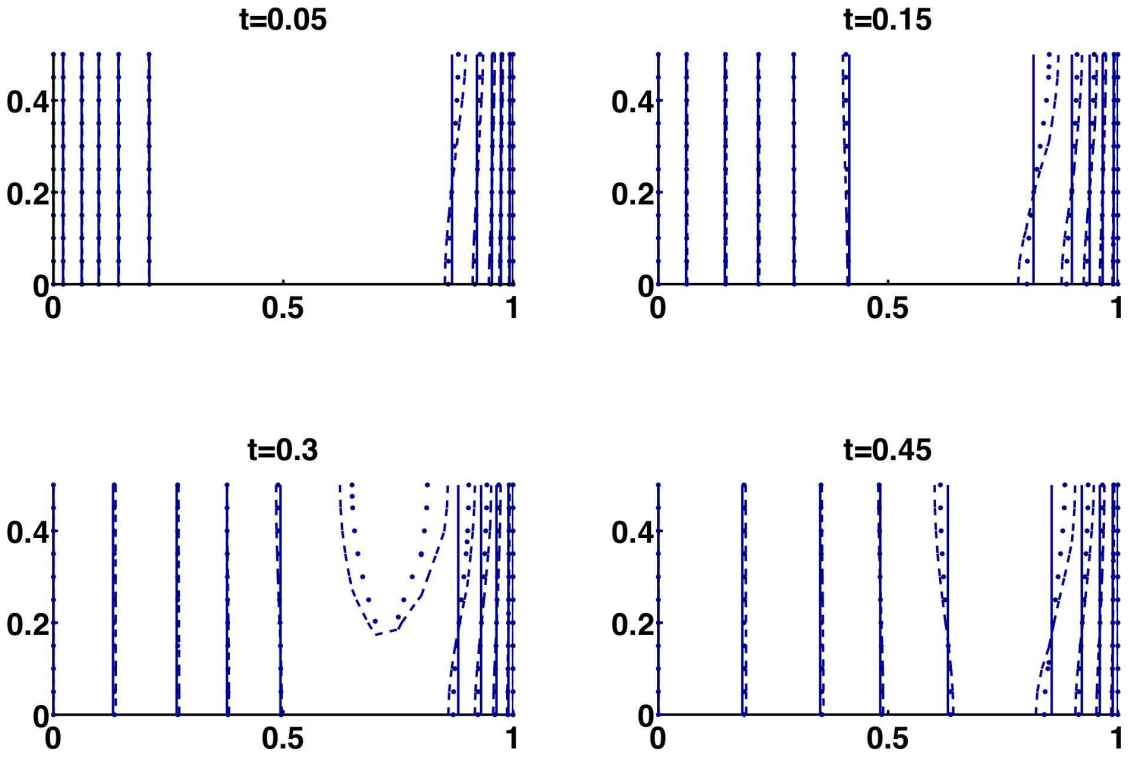

Figure 8.3: Temporal snapshots of contaminant concentration distributions provided by the perturbation (solid line) solution of the natural attenuation problem with $Pe = 10$ and $\alpha = 0$ (solid lines), $\alpha = 0.5$ (dots) and $\alpha = 1$ (dashed lines).

which describes contaminant transport in linear shear flow.

We look for a solution of the transport equation (8.34) subject to the initial and boundary conditions (8.17) in the form of an infinite series in the powers of Pe,

$$\Gamma^{SP} = \sum_{k=0}^{\infty} Pe_{\gamma}^{k} \Gamma_{k}^{SP}. \tag{8.35}$$

The leading term in this expansion satisfies

$$\frac{\partial \Gamma_0^{SP}}{\partial \tau} = \frac{\partial^2 \Gamma_0^{SP}}{\partial \xi^2} + \beta \frac{\partial^2 \Gamma_0^{SP}}{\partial \eta^2} \tag{8.36}$$

subject to initial condition $\Gamma_0^{SP}(\xi, \eta, \tau = 0) = 1$ and the boundary conditions (8.17). The corresponding solution is

$$\Gamma_0^{SP} = 2 \sum_{n=1}^{\infty} \left[\frac{1 - (-1)^n}{n\pi} \right] \sin(n\pi\xi) \mathrm{e}^{-\pi^2 n^2 t}. \tag{8.37}$$

The first-order term in the expansion (8.35) satisfies

$$\frac{\partial \Gamma_1^{SP}}{\partial \tau} = \frac{\partial^2 \Gamma_1^{SP}}{\partial \xi^2} + \beta \frac{\partial^2 \Gamma_1^{SP}}{\partial \eta^2} - U_0^{SP} \frac{\partial \Gamma_0^{SP}}{\partial \xi} \tag{8.38}$$

subject to the homogeneous initial and boundary conditions. Using the coordinate transformation (8.27), we obtain a solution of this equation,

$$\Gamma_1^{SP} = -\int_0^{\tau} \int_0^1 \int_0^{\hat{\xi}} G(\xi, \hat{\eta}; \xi_1, \hat{\eta_1}; \tau - t) U_0^{SP}(\hat{\eta_1}) \frac{\partial \Gamma_0^{SP}(\xi_1, \hat{\eta_1}, \tau)}{\partial x} \mathrm{d}\hat{\eta_1} \mathrm{d}\xi_1 \mathrm{d}t. \tag{8.39}$$

Fig. 8.4 shows a good agreement between the first-order perturbation solution $\Gamma^{SP} \approx \Gamma_0^{SP} + Pe\Gamma_1^{SP}$ and a finite difference solution of the contaminant transport problem (8.14) and (8.17) with $Pe = 0.5$, $\beta = 1$ and $\alpha = 2$. A careful examination of the solution reveals that concentration isolines within the flow domain are slightly tilted, which is a result of the shear flow (8.33). For $\alpha = 2$ the first-order correction is small, and so is the influence of the sea boundary.

Fig. 8.5 demonstrates the effects of the coupling parameter α on contaminant transport with $Pe = 0.5$ and $\beta = 1$. Similar to the intermediate Péclet number regime, we found that β has a minimal effect as the dominant direction

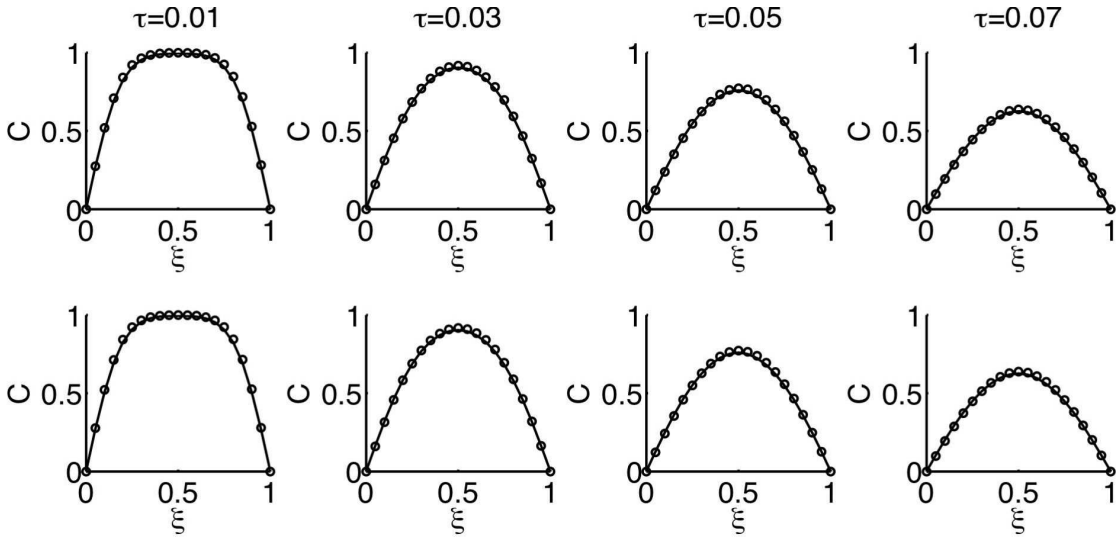

Figure 8.4: Temporal snapshots of contaminant concentration distributions at two heights ($\eta = 0.1$ and $\eta = 0.4$ across the width of the aquifer provided by the perturbation (solid line) and numerical (dots) solutions of the natural attenuation problem with $\alpha = 2$ and $Pe = 0.5$.

of transport is in the longitudinal direction. The effects of the saltwater boundary are quite insignificant, with the difference between the solutions corresponding to $\alpha = 0$ and $\alpha = 4$ being minute. At $\alpha = 20$ one can see some tilting of the isolines, but even so it is not all that significant. The relatively small influence of the sea boundary (as quantified by the coupling parameter α large) on contaminant transport process can be explained by the fact that, for small Péclet numbers, transport is dominated by diffusion. Since the sea boundary influences the velocity field and, thus, advective transport, its overall effects on the small-Péclet-number transport is insignificant.

8.6 Point-Source Contamination of Coastal Aquifers

Consider the migration of a pollutant introduced into an initially uncontaminated coastal aquifer by an isolated point source of unit strength (a delta

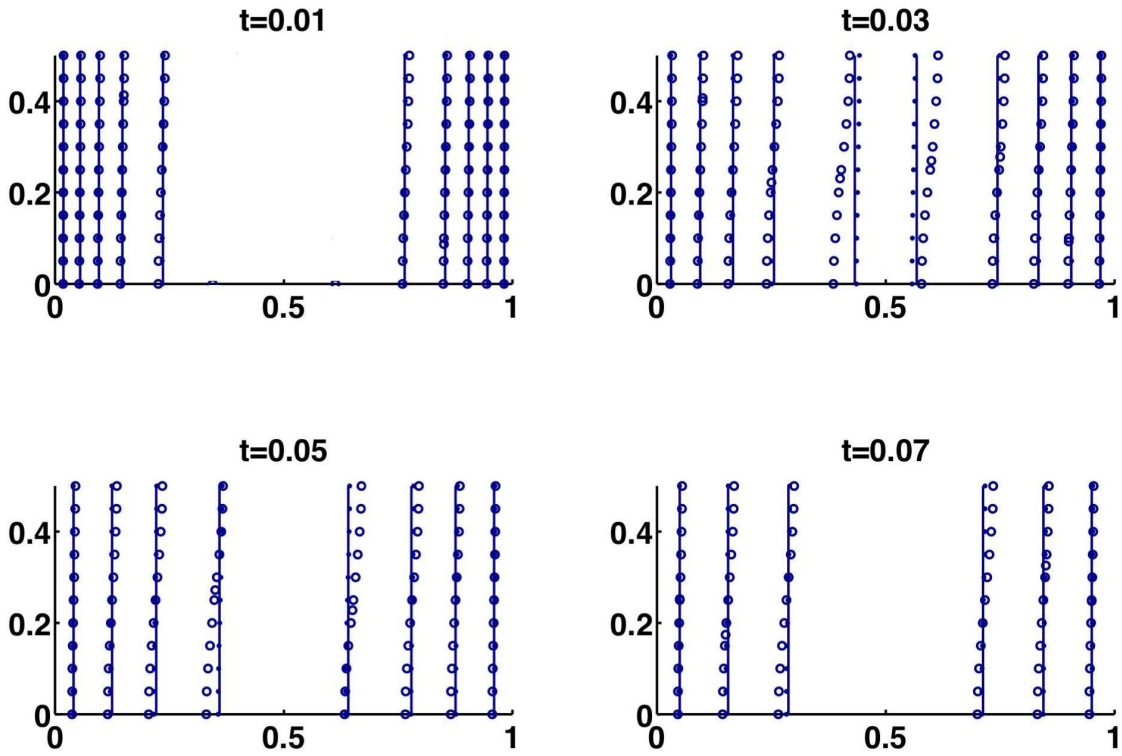

Figure 8.5: Temporal snapshots of contaminant concentration distributions provided by the perturbation (solid line) solution of Natural Attenuation Problem with $Pe = 0.5$ and $\alpha = 0$ (solid lines), $\alpha = 4.0$ (dots) and $\alpha = 20.0$ (circles).

function) located at a point (ξ', η'). This problem, which corresponds to a leak from a storage tank or a pipe, a small spill pool, etc., is described by

$$\frac{\partial \Gamma}{\partial \tau} + \mathbf{U} \cdot \nabla \Gamma = \frac{1}{Pe_\gamma} \nabla^2 \Gamma + \delta(\xi - \xi')\delta(\eta - \eta') \tag{8.40}$$

subject to the initial and boundary conditions

$$\Gamma(\xi, \eta, 0) = 0, \quad \frac{\partial \Gamma}{\partial \eta}(\xi, 0, \tau) = \frac{\partial \Gamma}{\partial \eta}(\xi, \zeta, \tau) = 0, \quad \Gamma(0, \eta, \tau) = \Gamma(1, \eta, \tau) = 0. \tag{8.41}$$

Depending on the flow regime, the velocity $\mathbf{U}$ is given by either (8.21) – (8.22) or (8.33). Note that due to the linearity of the transport equation (8.40), the solutions obtained in this section can be utilized—by means of a superposition—to describe contaminant migration from multiple point and/or distributed sources.

8.6.1 Intermediate Péclet number

We represent a solution of the contaminant transport problem (8.40) – (8.41) as an infinite series in the powers of α (8.23). The leading term in this expansion satisfies

$$\frac{\partial \Gamma_0^{IP}}{\partial \tau} + U_0^{IP} \frac{\partial \Gamma_0^{IP}}{\partial \xi} = \frac{1}{Pe} \left(\frac{\partial^2 \Gamma_0^{IP}}{\partial \xi^2} + \beta \frac{\partial^2 \Gamma_0^{IP}}{\partial \eta^2} \right) + \delta(\xi - \xi')\delta(\eta - \eta') \tag{8.42}$$

subject to the initial and boundary conditions (8.41). The corresponding solution is

$$\begin{aligned} \Gamma_0^{IP} =& \frac{2}{\hat{\zeta}} \mathrm{e}^{Pe(\xi - \xi')/2} \sum_{n=1}^{\infty} \frac{\sin(n\pi\xi)\sin(n\pi\xi')}{Pe/4 + \pi^2 n^2/Pe} \left[1 - \mathrm{e}^{-(Pe/4 + \pi^2 n^2/Pe)t} \right] \\ &+ \frac{4}{\hat{\zeta}} \mathrm{e}^{Pe(\xi - \xi')/2} \sum_{n,m=1}^{\infty} \frac{\sin(n\pi\xi)\sin(n\pi\xi')\cos(m\pi\eta/\zeta)\cos(m\pi\eta'/\zeta)}{Pe/4 + \pi^2(n^2 + m^2/\hat{\zeta}^2)/Pe} \\ &\left[1 - \mathrm{e}^{-(\frac{Pe}{4} + \frac{\pi^2(n^2 + m^2/\hat{\zeta}^2)}{Pe})t} \right]. \end{aligned} \tag{8.43}$$

The first-order term satisfies

$$\frac{\partial \Gamma_1^{IP}}{\partial \tau} + \frac{\partial \Gamma_1^{IP}}{\partial \xi} = \frac{1}{Pe} \left(\frac{\partial^2 \Gamma_1^{IP}}{\partial \xi^2} + \beta \frac{\partial^2 \Gamma_1^{IP}}{\partial \eta^2} \right) - U_1^{IP} \frac{\partial \Gamma_0^{IP}}{\partial \xi} - V_1^{IP} \frac{\partial \Gamma_0^{IP}}{\partial \eta} \tag{8.44}$$

subject to the initial and boundary conditions (8.41). The corresponding solution is

$$\Gamma_1^{IP} = -\int_0^{\tau}\int_0^{1}\int_0^{\hat{\zeta}} G(\xi,\eta;\xi_1,\hat{\eta_1};\tau-t)\phi(\xi_1,\hat{\eta}_1,t)\mathrm{d}\hat{\eta}\mathrm{d}\xi\mathrm{d}t, \tag{8.45}$$

where

$$\phi(\xi,\hat{\eta},\tau) = -\left[U_1(\xi,\hat{\eta})\frac{\partial\Gamma_0^{IP}}{\partial\xi}(\xi,\hat{\eta}) + V_1(\xi,\hat{\eta})\beta^{\frac{1}{2}}\frac{\partial\Gamma_0^{IP}}{\partial\eta}(\xi,\hat{\eta})\right]\mathrm{e}^{-\frac{Pe}{2}(\xi-\frac{\tau}{2})}. \tag{8.46}$$

The integrals in (8.45) were evaluated both analytically and numerically, with the two approaches leading to the identical results.

Fig. 8.6 shows the steady-state contaminant distributions corresponding to three alternative spill locations, three values of α and two values of $\beta = D_T/D_L$. (Recall that $\alpha = 0$ corresponds to the fully decoupled flow model, and that the influence of the seawater boundary on flow and transport patterns increases with the value of α.) Regardless of the location of the spill, the value of α affects the contaminant concentration along the seaward (right) boundary. Its influence diminishes with the distance from the sea.

An important feature of both the natural attenuation and point spill problems is that as α increases the contaminant concentration decreases in the lower right section of the aquifer and increases in its upper right section. This is evident in both the isotropic and anisotropic cases. This behavior appears to be a universal characteristic of contaminant transport in coastal aquifers that reflects the dominant flow patterns. At the bottom of the seaward boundary there is an influx of uncontaminated (salty) water, which causes the decrease in contaminant in that region of the aquifer. However, this intruding sea water diverts the fresh-water flow inside the aquifer upwards, thus causing the increase in concentration at the upper seaward boundary.

This general finding about the influence of the sea boundary—the elevated concentrations in the upper seaward regions of coastal aquifer—remains valid for aquifer systems that are more realistic than the one conceptualized by Henry's problem, including the aquifer system depicted in Fig. 8.1. For example, it helps

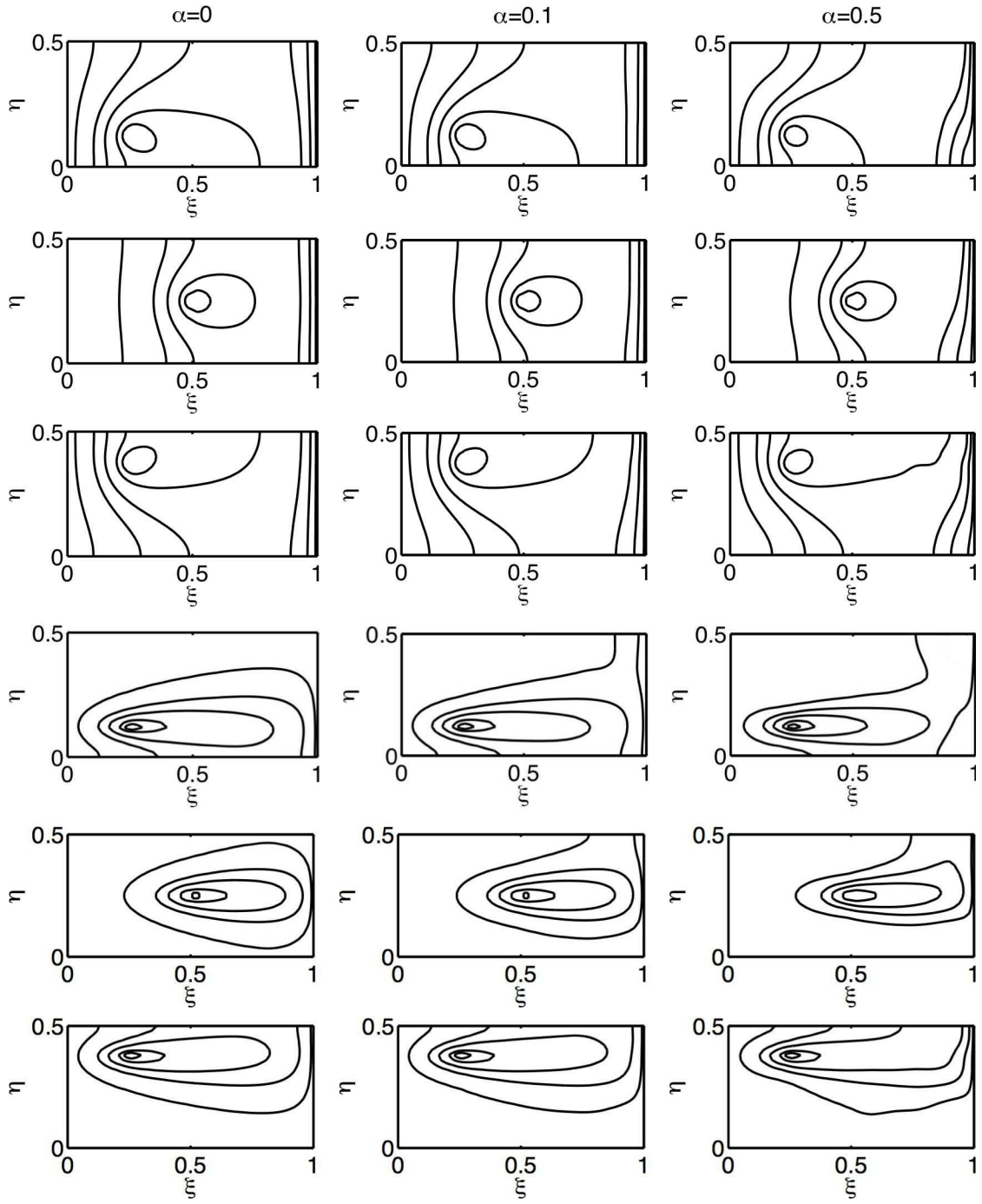

Figure 8.6: Concentration isolines corresponding to three locations of the spill, three values of the coupling parameter α and two values of the anisotropy ratio β. The top three rows correspond to $\beta = 1$ and the bottom three are for $\beta = 0.1$ From top to bottom, the three spill locations (ξ, η) are at $(0.25, 0.125)$, $(0.5, 0.5)$ and $(0.25, 0.375)$ respectively.

to explain the higher than expected contaminant concentrations in the surf zone observed by Boehm et al. (2004, 2006), and crop failures in the fields that are adjacent to the sea and are irrigated with (contaminated) water from unconfined aquifers.

8.6.2 Small Péclet Number

A solution of the contaminant transport problem (8.40) – (8.41) can be represented by expansion (8.35). The leading term in this expansion satisfies

$$\frac{\partial \Gamma_0^{SP}}{\partial \tau} = \left(\frac{\partial^2 \Gamma_0^{SP}}{\partial \xi^2} + \beta \frac{\partial^2 \Gamma_0^{SP}}{\partial \eta^2} \right) + \delta(\xi - \xi')\delta(\eta - \eta') \tag{8.47}$$

subject to the initial and boundary conditions (8.41). The corresponding solution is

$$\begin{aligned} \Gamma_0^{SP} =& \frac{2}{\pi^2 \hat{\zeta}} \sum_{n=1}^{\infty} \frac{1}{n^2} \sin(n\pi\xi) \sin(n\pi\xi') \left(1 - e^{-\pi^2 n^2 t}\right) \\ &+ \frac{4}{\pi^2 \hat{\zeta}} \sum_{n,m=1}^{\infty} \frac{n^2}{n^2 + m^2/\hat{\zeta}^2} \cos(n\pi\xi) \sin(n\pi\xi') \\ &\cos\left(\frac{m\pi\eta}{\zeta}\right) \cos\left(\frac{m\pi\eta'}{\zeta}\right) \left[1 - \mathrm{e}^{-\pi^2 (n^2 + \frac{m^2}{\hat{\zeta}^2}) t}\right]. \end{aligned} \tag{8.48}$$

The first-order term satisfies

$$\frac{\partial \Gamma_1^{SP}}{\partial \tau} = \left(\frac{\partial^2 \Gamma_1^{SP}}{\partial \xi^2} + \beta \frac{\partial^2 \Gamma_1^{SP}}{\partial \eta^2} \right) - U_0^{SP} \frac{\partial \Gamma_0^{SP}}{\partial \xi} \tag{8.49}$$

subject to the initial and boundary conditions (8.41). The corresponding solution is

$$\Gamma_1^{SP} = -\int_0^{\tau} \int_0^1 \int_0^{\hat{\zeta}} G(\xi, \eta; \xi_1, \hat{\eta}_1; \tau - t) U_0^{SP}(\xi_1, \hat{\eta}_1) \frac{\partial \Gamma_0^{SP}(\xi_1, \hat{\eta}_1, \tau)}{\partial \xi} \mathrm{d}\hat{\eta}_1 \mathrm{d}\xi_1 \mathrm{d}t. \tag{8.50}$$

Fig. 8.7 depicts the steady-state limit of the perturbation solution $\Gamma^{SP} \approx \Gamma_0^{SP} + Pe\Gamma_1^{SP}$ for $Pe = 0.5$, several values of α and two values of the anisotropy coefficient β. As in the natural attenuation problem, the sea boundary does not have significant influence on the contaminant transport, although the influence is more pronounced. This suggests that, for large times, advection plays a more prominent

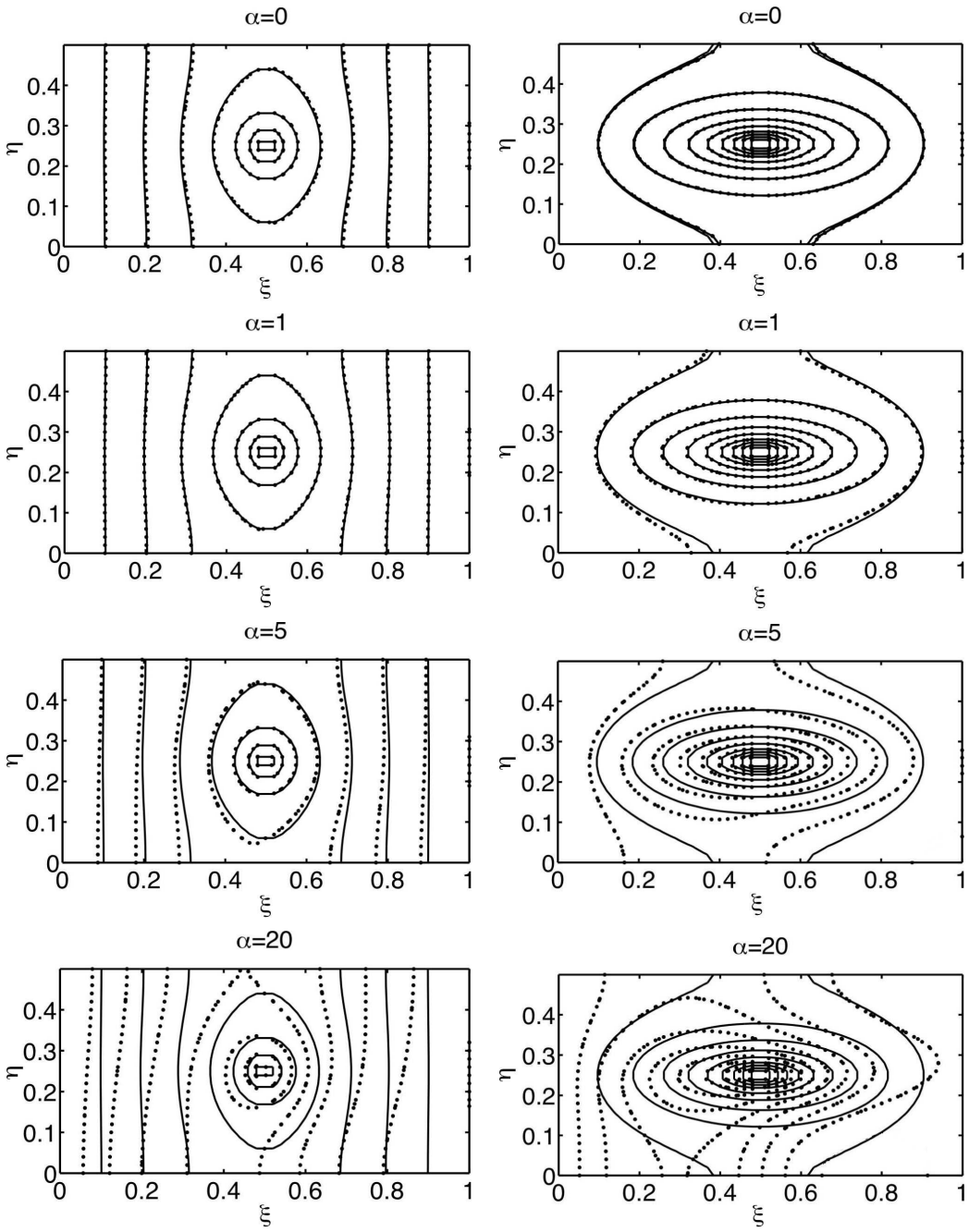

Figure 8.7: Steady-state concentration isolines for a localized spill at low Péclet numbers, four values of the coupling parameter α and two values of the anisotropy coefficient (Left column is $\beta = 1$. Right column is $\beta = 0.1$) . The dark lines correspond to purely diffusive transport ($Pe = 0$), and the lighter lines correspond to diffusion-dominated transport with $Pe = 0.5$.

role in the spread of contaminant than in its natural attenuation. However, for this effect to become noticeable, α has to be made so large as to render its practical realizability minimal. Additionally, the effects of advection are more noticeable for the anisotropic case. This is not surprising since the effect of anisotropy is to suppress dispersion in the transverse direction, thus increasing advective influence.

8.7 Summary and Conclusions

We employed the Henry formulation and perturbation analyses to derive analytical solutions describing contaminant migration in coastal aquifers. We showed that flow and transport in coastal aquifers can be characterized by two dimensionless parameters, the Péclet number Pe and a coupling parameter α. The former compares advective and dispersive mechanisms of transport, while the latter quantifies the density effects and the influence of the saltwater boundary on the flow field. The analytical solutions derived describe natural attenuation of, and contaminant spill in, coastal aquifers for intermediate and low Péclet numbers. Our analysis leads to the following major conclusions.

1. The saltwater boundary significantly affects contaminant transport in the intermediate Péclet number (advection-diffusion) regime. Its influence on transport in the small Péclet number (diffusion dominated) regime is significantly smaller. This is to be expected, since the main effect of the saltwater boundary is to modify the velocity field, i.e., the advective mechanism of transport.

2. For the sea boundary to affect transport patters in the low Péclet number regime, the coupling parameter α must be very large. For real coastal aquifers it is highly unlikely that this situation will occur.

3. Although the Henry formulation is a simplified model of coastal aquifers, it provides a useful physical insight into transport mechanisms affecting the

spread of contaminants in such systems. The saltwater intrusion forces contaminant transport towards the upper seaward boundary, thus causing elevated contaminant discharge into the surf zone at beach areas.

4. Our analytical solutions also provide insight for management decisions that must be made regarding the use of coastal aquifers for irrigation and drinking water purposes. In particular, they can provide guidelines for the viability of natural attenuation of contaminated coastal aquifers after the sources of contamination have been eliminated.

The text in chapter 8, in part, has been accepted for publication in the *Advances in Water Resources*, ('Analytical Models of Contaminant Transport in Coastal Aquifers') 2007 (D Bolster, DM Tartakovsky & M Dentz). I was the primary researcher on this project.

9

Summary and Conclusions

The research presented in this thesis can broadly be categorised in three sections, which are summarised here.

9.1 Contaminants and Low Energy Displacement Ventilation

The adoption of energy-efficient ventilation systems requires that they also provide an acceptable level of IAQ and comfort. The introduction of outside air, either through filters or simply by opening a window introduces outside pollutants. Additionally, internal pollutants are generated and need to be extracted from the building.

The success of alternative ventilation strategies depends on our ability to predict the internal environment and to assess the IAQ and comfort, as well as determining the potential energy savings. The purpose of this work was to expand our capabilities to model particulate distributions and transport within energy-efficient buildings, so that designers and engineers can have confidence that the buildings will perform appropriately. The research presented here provides models that can be used for design guidance, as well as to accurately assess these low energy ventilation strategies.

9.1.1 Project Outcomes

1. Validated models to predict contaminant distribution in a space with a heat source and temperature stratification for passive and particulate contaminants.

2. Data sets from small-scale experiments of the dispersion of a passive scalar and settling particles.

3. Data sets from full-scale room experiments.

4. Simplified models that can be used as a basis for design guidance.

9.1.2 Conclusions

Displacement ventilation systems are very promising from an energy perspective and should be adopted for this reason. However, one must carefully consider the purpose of the room being ventilated as well as the typical contaminants types and size distributions that may exist in this room. Caution must be taken when choosing the optimum ventilation strategies. Depending on the size of contaminants and location of the sources certain low-energy systems can outperform traditional systems in removing contaminants. However, there are also many scenarios where the traditional system exposes occupants to lower levels. For example, if the primary source of contamination comes from the occupants in the space, then displacement systems minimize exposure compared to traditional mixing ventilation systems. However, if the source of contamination is external, then exposure is typically worse for the low energy systems.

Studying only the average amount of contaminant in a space can be very misleading as displacement ventilation can lead to non trivial vertical gradients in the contaminant field. Thus, while the average concentration in a space may be below acceptable standards, specific locations may be well above these and thus expose occupants to undesirable levels of contaminants.

Low energy ventilation systems can expose people to higher levels of contaminants, because the contaminant transport mechanisms do not exploit the same features. The energy efficiency of most systems comes from extraction of the warmest air. However, there is no physical reason why the location of the warmest air must coincide with the highest levels of contaminant.

While this study sets some important groundwork for the study of passive and particulate contaminants in low-energy ventilation systems it is by no means complete. There are many possible directions for future work, which are not restricted to, but include transient effects, further full scale studies, case studies, extensions to other low energy ventilation systems, further physics, health effects studies, uncertainty analysis, and socio-economic studies.

9.2 Transients in Natural ventilation

Natural ventilation, when possible, is highly appealing due to the fact that it requires zero energy input. Most current models for natural ventilation only consider steady states. However, typical heat sources in buildings are transient in their nature. Therefore understanding the influence of these transients is important for effective designs. In this thesis two studies of transients in natural displacement ventilation have been presented. The first considers sudden changes in heat sources and the response of the natural ventilation system to this change. The second study considers the influence of heat sources that vary periodically in time.

9.2.1 Project Outcomes

1. Validated models to predict flow rates and temperature distribution within a naturally ventilated space with a time varying heat source.

2. Data sets from small-scale experiments for sudden and periodically time varying heat sources.

3. Simplified models that can be used as a basis for design guidance.

9.2.2 Conclusions

Natural displacement ventilation offers several very appealing features, the most obvious of which is the potential of reducing energy consumption. In these studies we have identified several others.

Most mechanical ventilation systems require expensive and complicated control systems that can often fail. Natural ventilation is a self controlling system. The steady state interface location dividing the cool occupied lower layer and the warm upper layer is independent of the strength of heat source. As the amount of heat from sources is increased the flow rate through the space automatically increases. Consequently, no expensive control system is required.

Not only is it self controlling, but additionally the natural response of a naturally ventilated space to sudden changes in heat loads acts in a favorable manner. Decreases in heat loads do not typically cause concern. However, increases in heat loads can potentially cause problems. A naturally ventilated space automatically 'fights' this increase in two manners. First, while the interface will descend when there is an increase in source buoyancy flux, this descent will be small, no matter how large the increase is. Therefore, a well designed system can avoid penetration of the upper layer to the occupied space. Secondly, the time for the descent of the interface becomes smaller and smaller the larger the increase in source buoyancy flux. As such, even if penetration of this interface into the occupied space does occur, it will not last very long.

When considering heat sources that vary periodically in time it is important to identify the average flow rates through a space. When the changes in heat load are small, the average flow rate through the system does not vary much regardless of the frequency with which the forcing varies. However, when large variations in heat loading occur differences of around 20% (for $\chi = 20$) or larger can exist depending on the frequency of forcing. The higher the forcing frequency is, the larger the average flow rate. In the infinite frequency limit the system approaches a flow rate corresponding to a steady source with a source buoyancy

flux equal to the average of the lower and upper buoyancy fluxes. The variation in average flow rate stems from the nonlinear relationship of the plume volume flow rate with source buoyancy flux. Therefore, in spaces where large variations in thermal loading occur, it is important to consider the frequency of this forcing in order to estimate an accurate average flow rate through the space.

9.3 Coastal Intrusions

Within recent history, the water quality in many of the coastal aquifers across the world has rapidly degraded. Over-exploitation of the groundwater basins has led to the drops of water tables and seawater intrusion into the aquifers. Facing a shortage of suitable drinking water, many arid coastal countries have had either to look for alternative sources, such as imported water, or to implement costly technological solutions, such as desalination. While salt as a source of contamination of coastal aquifers has received considerable attention, other threats to the quality of the groundwater have been studied less systematically. Results from various projects show that other contaminants in coastal aquifers pose a potential threat to the future use of many groundwater basins across the world.

We employed the Henry formulation to derive analytical solutions describing contaminant migration in coastal aquifers. The flow and transport in coastal aquifers can be characterized by two dimensionless parameters, the Peclet number Pe and a coupling parameter α. The former compares advective and dispersive mechanisms of transport, while the latter quantifies the density effects and the influence of the saltwater boundary on the flow field. We considered two common contamination scenarios, natural attenuation of a contaminated aquifer and a contaminant spill within an aquifer.

9.3.1 Project Outcomes

1. Models to predict and better understand the transport of contaminants within a coastal aquifer.

9.3.2 Conclusions

Although the Henry formulation is a simplified model of coastal aquifers, it provides a useful physical insight into transport mechanisms affecting the spread of contaminants in such systems. Intruding saltwater can significantly affect the transport of a contaminant in a coastal aquifer in the intermediate Péclet number (advection-diffusion) regime. However, for small Péclet number scenarios (diffusion dominated) its influence is far less. This happens because the influence of the saltwater boundary is to modify the velocity field, not the diffusive properties, within the aquifer. When the saltwater intrusion plays a role on transport, it forces contaminant towards the upper seaward boundary, thus causing elevated contaminant discharge into the surf zone at beach areas.

Our analytical solutions also provide insight for management decisions that must be made regarding the use of coastal aquifers for irrigation and drinking water purposes. In particular, they can provide guidelines for the viability of natural attenuation of contaminated coastal aquifers after the sources of contamination have been eliminated.

Appendix A

Particulate Models - Point Source Strength Definition

A point source in the plume in the lower layer can be thought of as an additional source into the upper layer.

$$\frac{dP}{dz} = \frac{5}{3z}\Big(K - P\Big), \qquad z < h \tag{A.1}$$

which implies that if we have a source of strength $\hat{K}_s$ at a height z_s in the lower layer, the concentration being injected into the upper layer by the plume is

$$P(z = h) = K_l + \hat{K}_s\left(\frac{z_s}{h}\right)^{\frac{5}{3}} = K_l + K_s \tag{A.2}$$

Therefore the conservation equations can be written as

$$\frac{dK_l}{dt} = -\left(\frac{Q_p + Q_{fall}}{Sh}\right)K_l + \frac{Q_{fall}}{Sh}K_u + \frac{Q_{in}}{Sh}K_{in}, \tag{A.3}$$

$$\frac{dK_u}{dt} = \frac{Q_p}{S(H-h)}\Big(K_l + K_s\Big) - \left(\frac{Q_{fall} + Q_p}{S(H-h)}\right)K_u. \tag{A.4}$$

In order to compare equivalent systems the conservation equation for the well mixed room should include a source of the same strength leading to

$$\frac{dK_{wm}}{dt} = \frac{Q_{in}(K_{in} + K_s)}{SH} - \frac{Q_{in} + Q_{fall}}{SH} \tag{A.5}$$

Appendix B

Concentration of Germeles Layer at Top of Room for Particulate Contaminantss

When a new layer forms at the top of the room it has $\Big(Q_p(z=H)\Big)\Delta t$ fluid being supplied to it by the plume and $\Big(Q_{out}\Big)\Delta t$ being extracted by the vent. The size of the new layer, due to gravitational settling is $\Big(Q_p(z=H)+Q_f-Q_{out}\Big)\Delta t$. Therefore, assuming perfect mixing in this new layer the concentration of this new layer will be

$$C=\frac{Q_p}{Q_p+Q_f}P(z=H), \tag{B.1}$$

which can readily be shown to be

$$C=\frac{1}{1+\frac{3\alpha\zeta}{5-2\zeta}}P(z=H), \tag{B.2}$$

Appendix C

Particulate Contaminants Model (c) - Analytical Solution

For a well mixed lower layer the conservation equations for the upper and lower layer are slightly modified. In nondimensional form they are

$$\frac{d\bar{c}_l}{d\tau} = \frac{\alpha}{\zeta}\Big(c_u(\zeta = \zeta_h) - \bar{c}_l\Big) - \frac{1}{\zeta}\bar{c}_l \tag{C.1}$$

$$\frac{d\bar{c}_u}{d\tau} = \frac{\alpha}{1-\zeta_h}\Big(- c_u(\zeta = \zeta_h)\Big) + \frac{1}{1-\zeta_h}\Big(\bar{c}_l - c_u(\zeta = 1)\Big) \tag{C.2}$$

In order to close this system of equations we must find analytical expressions for $c_u(\zeta = \zeta_h, t)$ and $c_u(\zeta = 1, t)$ and these are not neccesarily immediately obvious. Because diffusion is being neglected due to high Peclet numbers the method of characteristics can be used to determine the concentration of contaminant in the upper layer at the interface height. It will be the same concentration as was at the top of the room a period τ_{desc} earlier, where we define τ_{desc} as the time taken for a front to travel from the top of the room to the interface. It can be shown that

$$\tau_{desc} = \frac{3}{5}\zeta_h \ln\left(\frac{1-(1-\frac{3}{5}\alpha)\zeta_h}{\zeta-(1-\frac{3}{5}\alpha)\zeta_h}\right) \tag{C.3}$$

Therefore, we are now only left with the task of finding the concentration at the top of the room in order to close this system of equations. Assuming that when the plume strikes the ceiling it spreads instantaneously across the entire area of the ceiling we can equate the background concentration to that of the plume at the top of the room. This can be shown to be

$$c_u(\zeta = 1, t) = p_u(\zeta = 1, t) = \frac{5(1-\zeta_h)\bar{c}_u(t) + 3\bar{c}_l(t)\zeta_h}{5 - 2\zeta_h}\left(\frac{1}{1 + \frac{3\alpha\zeta}{5-2\zeta}}\right) \tag{C.4}$$

and

$$c_u(\zeta_h, t) = c_u(1, t - \tau_{desc}) = \frac{5(1-\zeta_h)\bar{c}_u(t - \tau_{desc}) + 3\zeta_h\bar{c}_l(t - \tau_{desc})}{5 - 2\zeta_h}\left(\frac{1}{1 + \frac{3\alpha\zeta}{5-2\zeta}}\right) \tag{C.5}$$

The solutions to the conservation equations for this system can now be written as

$$\bar{c}_l(t) = \left(\int_\tau^t \frac{\alpha}{\zeta_h} c_u(\zeta = \zeta_h, \tau') e^{(\frac{\alpha+1}{\zeta})\tau'} d\tau'\right) e^{-\frac{(\alpha+1)}{\zeta}t} + C_{l0} e^{-\frac{(\alpha+1)}{\zeta}(t-\tau)} \tag{C.6}$$

$$\bar{c}_u(t) = \left(\frac{1}{(1-\zeta)A_1}\int_\tau^t \left(-\alpha A_1 c_u(\zeta) + A_2\bar{c}_l(\tau')\right) e^{\frac{5(1-\zeta)}{A_1}\tau'} d\tau'\right) e^{\frac{-5(1-\zeta)}{A_1}t} + C_{u0} e^{\frac{5(1-\zeta)}{A_1}(\tau - t)} \tag{C.7}$$

where C_{l0} and C_{u0} are the initial conditions for concentration in the lower and upper layers respectively.

where $A_1 = 5 - 2\zeta + 3\alpha\zeta$ and $A_2 = 5 - 10\zeta + 3\alpha\zeta + 5\zeta^2 - 3\alpha\zeta^2$.

By dividing the solution into time intervals of length τ_{desc} these solutions can be computed analytically. Alternatively these integrals could be computed numerically easily enough. During the first period (i.e. $0 < t < \tau_{desc}$) it is important to note that $c_u(\zeta_h) = 1$, the initial concentration in the room.

$\underline{\mathbf{0 < t < \tau_{desc}}}$ $(n = 0)$

$$\bar{c}_l^0 = \frac{C_{l0}\alpha}{\alpha + 1} + C_{l0}\left(1 - \frac{\alpha}{\alpha + 1}\right) e^{-\frac{\alpha+1}{\zeta}t} \tag{C.8}$$

$$\bar{c}_u^0 = C_{u0} e^{\frac{-5(1-\zeta)}{A_1}t} + B_1\left(1 - e^{\frac{-5(1-\zeta)t}{A_1}}\right) + B_2\left(e^{-\frac{1+\alpha}{A_1}} - e^{-\frac{5(1-\zeta)}{A_1}t}\right) \tag{C.9}$$

where $B_1 = \frac{A_1}{5(1-\zeta)}\left(\frac{-\alpha A_1 C_{l0} + \frac{C_{l0}\alpha}{1+\alpha} A_2}{(1-\zeta)A_1} e^{\frac{5(1-\zeta)}{A_1}t}\right)$ and $B_2 = \frac{-A_1\zeta A_2 C_{lo}(1-\frac{\alpha}{1+\alpha})}{\alpha A_1 + A_1 - 5\zeta + 5\zeta^2}$
In general for each time period n=m ($m\tau_d < t < (m+1)\tau_d$) the solution can be written as a series

$$\bar{c}_l^m(t) = \Gamma_{l0}^m + \sum_{n=1}^{k^m} \Gamma_{ln}^m e^{f_p^m t} \tag{C.10}$$

$$\bar{c}_u^m(t) = \Gamma_{u0}^m + \sum_{p=1}^{l^m} \Gamma_{up}^m e^{g_p^m t} \tag{C.11}$$

where Γ_{ln}, Γ_{up}, f_p and g_p are constants that can be evaluated from the previous time period

$$\begin{aligned}\bar{c}_l^m(t) = \bar{c}_l^{m-1}(t = m\tau_d) e^{-\frac{\alpha+1}{\zeta}(t-m\tau_d)} + \frac{\alpha}{\zeta} e^{-\frac{\alpha+1}{\zeta}t}\Bigg[\frac{(\Gamma_{u0}^{m-1} + \Gamma_{l0}^{m-1})\zeta}{\alpha+1}\left(e^{\frac{\alpha+1}{\zeta}t} - e^{\frac{\alpha+1}{\zeta}(m\tau_d)}\right) \\ + \sum_{p=1}^{l^{m-1}} \frac{\Gamma_{up}^{m-1}\zeta}{g_p^{m-1}\zeta + \alpha + 1}\left(e^{\left(\frac{g_p^{m-1}\zeta+\alpha+1}{\zeta}\right)\left(t - g_p^{m-1}\tau_d\right)} - e^{\left(\frac{g_p^{m-1}\zeta+\alpha+1}{\zeta}\right)\left(m\tau_d - g_p^{m-1}\tau_d\right)}\right) \\ + \sum_{n=1}^{k^{m-1}} \frac{\Gamma_{ln}^{m-1}\zeta}{f_n^{m-1}\zeta + \alpha + 1}\left(e^{\left(\frac{f_n^{m-1}\zeta+\alpha+1}{\zeta}\right)\left(t - f_n^{m-1}\tau_d\right)} - e^{\left(\frac{f_n^{m-1}\zeta+\alpha+1}{\zeta}\right)\left(m\tau_d - f_n^{m-1}\tau_d\right)}\right)\Bigg]\end{aligned} \tag{C.12}$$

which can be written in the form of equation (C.10). Additionally, for the upper layer

$$\bar{c}_u^m(t) = \bar{c}_u^{m-1}(t = t - m\tau_d)e^{-\frac{5}{5-2\zeta}(t-\tau)} + \left(\Gamma_{l0}^m - \alpha\Gamma_{u0}^{m-1} - \frac{3\alpha\zeta}{5(1-\zeta)}\Gamma_{u0}^{m-1}\right)$$
$$\left(1 - e^{-\frac{5}{5-2\zeta}(t-m\tau_d)}\right) + e^{-\frac{5}{5-2\zeta}t}\Bigg[- 5\alpha \sum_{p=1}^{l^{m-1}} \frac{\Gamma_{up}^{m-1}}{5 + 5g_p^{m-1} - 2g_p^{m-1}}$$
$$\left(e^{\frac{5+5g_p^{m-1}-2g_p^{m-1}}{5-2\zeta}t + \frac{2g_p^{m-1}-5g_p^{m-1}}{5-2\zeta}\tau_d} - e^{\frac{(5g_p^{m-1}-2g_p^{m-1}\zeta)(m-1)+5m}{5-2\zeta}\tau_d}\right)$$
$$- \frac{3\alpha\zeta}{5(1-\zeta)} \sum_{n=1}^{k^{m-1}} \frac{\Gamma_{ln}^{m-1}}{5 + 5f_n^{m-1} - 2f_n^{m-1}}$$
$$\left(e^{\frac{5+5f_n^{m-1}-2f_n^{m-1}}{5-2\zeta}t + \frac{2f_n^{m-1}-5f_n^{m-1}}{5-2\zeta}\tau_d} - e^{\frac{(5f_n^{m-1}-2f_n^{m-1}\zeta)(m-1)+5m}{5-2\zeta}\tau_d}\right)\Bigg]$$
$$+ \sum_{n=1}^{k^m} \frac{5}{5 + 5f_n^m - 2\zeta f_n^m}\left(e^{\frac{5f_n^m - 2\zeta f_n^m}{5-2\zeta}t} - e^{\frac{5f_n^m - 2\zeta f_n^m}{5-2\zeta}m\tau_d - \frac{5}{5-2\zeta}(t-m\tau_d)}\right).$$

(C.13)

Bibliography

WD Baines and JS Turner. Turbulent buoyant convection from a source in a confined region. *J. Fluid Mech.*, 37:51–80, 1969.

AV Baughman, AJ Gadgil, and WW Nazaroff. Mixing of a point source pollutant by natural convection flow within a room. *Indoor Air*, 4:114–122, 1994.

J. Bear and G. Dagan. Some exact solutions of interface problems by means of the hodograph method. *J. Geophys. Res.*, 69:1563 – 1572, 1964.

P Blondeau, V Iordache, O Poupard, D Genin, and F Allard. Relationship between outdoor and indoor air quality in eight french schools. *Indoor Air*, 15:2–12, 2005.

L Bloomfield and R Kerr. A theoretical model of a turbulent fountain. *J. Fluid Mech.*, 424:197–216, 2000.

AB Boehm, GG Shellenbarger, and A Paytan. Groundwater discharge: potential association with fecal indicator bacteria in the surf zone. *Environ Sci Technol.*, 38(13):3558–3566, 2004.

AB Boehm, A Paytan, GG Shellenbarger, and KA Davis. Composition and flux of groundwater from a california beach aquifer: Implications for nutrient supply to the surf zone. *Continental Shelf Research*, 26:269–282, 2006.

DT Bolster and PF Linden. Contaminated ventilated filling boxes. *Journal of Fluid Mechanics*, Under Review, 2007.

D Bower. *Transient Phenomena in Natural Ventilation:theory and Experiment.* PhD thesis, University of Cambridge, 2005.

SSS Cardoso and AW Woods. Mixing by a turbulent plume in a confined stratified region. *J. Fluid Mech.*, 250:277–305, 1993.

CP Caulfield. *Stratification and Buoyancy in Geophysical Flows.* PhD thesis, University of Cambridge, 1991.

CP Caulfield and AW Woods. The mixing in a room by a localized finite-mass-flux source of buoyancy. *J. Fluid Mech.*, 471:33–50, 2002.

C Cenedese and SB Dalziel. Concentration and depth fields determined by the light transmitted through a dyed solution. *Proceedings of the 8th International Symposium on Flow Visulaization*, 8:Paper 061, 1998.

CJ Coffey and GR Hunt. Ventilation efficiency measures based on heat removal. *Building and Environment*, Submitted, 2005.

DT Conroy, SG Llewellyn Smith, and CP Caulfield. Evolution of a chemically reacting plume in a ventilated room. *J. Fluid Mech.*, 537:221–253, 2005.

M. Dentz, D. M. Tartakovsky, E. Abarca, A. Guadagnini, X. Sanchez-Vila, and J. Carrera. Variable density flow in porous media. *J. Fluid Mech.*, 561:209 – 235, 2006.

AC Drescher, C Lobascio, A Gadgil, and WW Nazarofif. Mixing of a point-source indoor pollutant by forced convection. *Indoor Air*, 5:204–214, 1995.

HE Feustel. Comisan international multizone air-flow and contaminant transport model. *Energy and Buildings*, 30:3–18, 1999.

AE Germeles. Forced plumes and mixing of liquids in tanks. *J. Fluid Mech.*, 71: 601–623, 1975.

H R Henry. Effects of dispersion on salt encroachment in coastal aquifers. Technical Report Water Supply Pap. 1613-C, U. S. Geol. Surv., 1964.

S Holmberg and Y Li. Modelling of the indoor environment particle dispersion and deposition. *Indoor Air*, 8:113–122, 1998.

GR Hunt and NG Kaye. Virtual origin correction of lazy turbulent plumes. *J. Fluid Mech.*, 435:377–396, 2001.

GR Hunt, P Cooper, and PF Linden. Thermal stratification produced by jets and plumes in enclosed spaces. In H. B. Awbi, editor, *Proc. Roomvent 2000 - 7th International Conference on Air Distribution in Rooms*, pages 191–198. Elsevier, New York, 2000.

HE Huppert and AW Woods. Gravity-driven flows in porous layers. *J. Fluid Mech.*, 292:55 – 69, 1995.

PL Jenkins, TJ Phillips, EJ Mulberg, and SP Hui. Activity patterns of californians: Use and proximity to indoor pollutant sources. *Atmos. Envir.*, 26A:2141–2148, 1992.

AR Kacimov and Yu V Obnosov. Analytical solution for a sharp interface problem in sea water intrusion into a coastal aquifer. *Proc. Royal Soc. London, Series A*, 457(2016):3023 – 3038, 2001.

BO Kalejaiye and SSS Cardoso. Specification of the dispersion coefficient in the modeling of gravity-driven flow in porous media. *Water Resources Research*, 41, 2005.

NB Kaye and GR Hunt. Time-dependent flows in an emptying filling box. *J. Fluid Mech.*, 520:135–156, 2004.

NB Kaye and GR Hunt. Pollutant flushing with natural displacement ventilation. *Building and Environment*, In Press, 2006.

NB Kaye and GR Hunt. Heat source modelling and natural ventilation efficiency. *Building and Environment*, 72(4):1624–1631, 2007.

PD Killworth and JS Turner. Plumes with time-varying buoyancy in a confined region. *Geophys. Astrophys. Fluid Dynamics*, 20:265–291, 1982.

NE Klepeis. Validity of the uniform mixing assumption: Determining human exposure to environmental tobacco smoke. *Environmental Health Perspectives*, S107:357–363, 1999.

M Kumagai. Turbulent buoyant convection from a source in a confined two-layered region. *J. Fluid Mech.*, 147:105–131, 1984.

ACK Lai and WW Nazaroff. Modeling indoor particle deposition from turbulent flow onto amooth surfaces. *Journal of Aerosol Science*, 31:463–476, 2000.

WE Lambert, JM Samet, and JD Spengler. Environmental tobacco smoke concentrations in no-smoking and smoking sections of restaurants. *American Journal of Public Health*, 83:1339–1341, 1993.

YJP Lin and PF Linden. Buoyancy-driven ventilation between two chambers. *J. Fluid Mech.*, 463:293–312, 2002.

PF Linden. The fluid mechanics of natural ventilation. *Ann. Rev. Fluid Mech.*, 31:201–238, 1999.

PF Linden, GF Lane-Serff, and DA Smeed. Emptying filling boxes: the fluid mechanics of natural ventilation. *J. Fluid Mech.*, 212:309–335, 1990.

Q Liu and PF Linden. The fluid dynamics of an underfloor air distribution system. *Journal of Fluid Mechanics*, 554:323–341, 2006.

BR Morton. Forced plumes. *J. Fluid Mech. A*, 234:1–23, 1959.

BR Morton, GI Taylor, and JS Turner. Turbulent gravitational convection from maintained and instantaneous sources. *Proc. Roy. Soc. A*, 234:1–23, 1956.

A. Naji, A. H.-D. Cheng, and D. Ouazar. Analytical stochastic solutions of salt-water/freshwater interface in coastal aquifers. *Stoch. Hydrol. Hydraul.*, 12:413 – 429, 1998.

MK Owen, DS Enaor, and LE Sparks. Airborne particle sizes and sources found in indoor air. *Atmospheric Environment*, 26A:164–174, 1992.

H Ozkaynak, PB Ryan, GA Allen, and WA Turner. Indoor air quality modeling: Compartmental approach with reactive chemistry. *Environ. Int*, 8:461–471, 1982.

CE Rodes, RM Kames, and RW Wiener. The significance and characteristics of the personal activity cloud on exposure assesment measurements for indoor contaminants. *Indoor Air*, 2:875–891, 1991a.

CE Rodes, RM Kames, and RW Wiener. The significance and characteristics of the personal activity cloud on exposure assesment measurements for indoor contaminants. *Indoor Air*, 2:875–891, 1991b.

M Sandberg and D Etheridge. *Building Ventilation: Theory and Measurement*. John Wiley & Sons, 1st edition, 1996.

Mat Santamouris. *Building Ventilation: The State Of The Art*. Earthscan / James & James, 2005.

MM Scase, CP Caulfield, SB Dalziel, and JCR Hunt. Time-dependent plumes and jets with decreasing source strengths. *Journal of Dluid Mechanics*, 563:443–461, 2006.

T Schneider, J Kildeso, and NO Breum. A two compartment model for determining the contribution of sources, surface deposition and resuspenion to air and surface dust concentration level in occupied spaces. *Building and Environment*, 34:583–595, 1999.

M. J. Simpson and T. P. Clement. Theoretical analysis of the worthiness of henry and elder problems as benchmarks of density-dependent groundwater flow models. *Adv. Water Resour.*, 26(1):17 – 31, 2003.

C Smith. Hospital operating theatre environment and the assessment of filters for use in associated ventilating plants. *Annals of Occupational Hygene.*, 17: 303–314, 1975.

DM Tartakovsky and V Di Federico. An analytical solution for contaminant transport in non-uniform flow. *Transport in Porous Media*, 27(1):85–97, 1997.

Avner Vengosh, Erika Weinthal, Wolfram Kloppmann, and the BOREMED team. Natural boron contamination in mediterranean groundwater. *Geotimes*, May: 20–25, 2004.

H Versteeg and W Malalasekra. *An Introduction to Computational Fluid Dynamics - THe Finiet Volume Method*. Prentice Hall, 1996.

AW Woods, CP Caulfield, and JC Phillips. Blocked natural ventilation: the effect of a source mass flux. *J. Fluid Mech.*, 495:119–133, 2003.

MG Worster and HE Huppert. Time-dependent density profiles in a filling box. *J. Fluid Mech.*, 132:457–466, 1983.

Z Zhang and Q Chen. Experimental meausurements and numerical simulations of particle transport and distribution in ventilated rooms. *Atmospheric Environment*, 40:3396–3408, 2006.

B Zhao, X Li, and Z Zhang. Numerical study of particle deposition in two differently ventilated rooms. *Indoor and Built Environmen*, 13:443–451, 2004a.

B Zhao, X Li, and Z Zhang. Numerical study of particle deposition in two differently ventilated rooms. *Indoor and Built Environment*, 13:443–451, 2004b.